DYNAMIC ASPECTS OF SPRAYS FOR

ABSORPTION APPLICATIONS

By

YASH SHARADCHANDRA TAMHANKAR

Bachelor of Engineering in Chemical Engineering
University of Pune
Pune, Maharashtra, India
2006

Master of Science in Chemical Engineering
Oklahoma State University
Stillwater, OK
2010

Submitted to the Faculty of the
Graduate College of the
Oklahoma State University
in partial fulfillment of
the requirements for
the Degree of
DOCTOR OF PHILOSOPHY
May, 2015

DYNAMIC ASPECTS OF SPRAYS FOR

ABSORPTION APPLICATIONS

Dissertation Approved:

Dr. Clint P. Aichele

Dissertation Adviser

Dr. James R. Whiteley

Dr. Tony Cai

Dr. Danielle Bellmer

ACKNOWLEDGEMENTS

Completing a PhD is much like climbing a mountain (since I have a read a lot on mountaineering recently). You identify a peak that has never been climbed before, learn and identify shortcomings in previous attempts on the mountain, build a better plan to scale the mountain by incorporating better routes and equipment, acclimate and fine tune the logistics involved in setting up multiple camps, and ultimately scale the mountain, camp by camp. A PhD involves the same steps. One performs a detailed literature review to identify areas that need to be researched, identify the shortcomings or limitations of previous works, develop a better plan by incorporating modern analytical tools and more robust, flexible equipment, perform trial runs to test and fine tune the experimental setup, ultimately perform the final experiments, collect and analyze data and then write up all the results.

Like climbing a mountain, completing a PhD cannot be accomplished without the contributions of many. First, I would like to acknowledge my advisors, Dr. Clint Aichele and Dr. Rob Whiteley for all their help, guidance and support. Dr. Aichele always encouraged me to keep making progress, make most of the networking opportunities available, and above all to analyze experimental data from various perspectives to derive logical conclusions. Dr. Whiteley has been instrumental in my development as a researcher and as an individual. His patience and guidance have greatly helped in finding answers to questions beyond research. Dr. Whiteley has been nothing short of a father figure to both me and Dr. Aichele. I will remember him as the voice of reason, logic and practicality.

Michael (Mike) Resetarits and Tony Cai have been instrumental in the successful completion of this work. Their insights, recommendations, and help guided the project in the right direction. Mike is the best presenter I have seen over the years. I yearn to be as good as him in the future. Dr. Dani Bellmer was always available and flexible to accommodate me in her busy schedule. Further, I would like to thank Professors Unde, Gadgil, Kamble, and Sathe from my undergraduate studies for stoking my interest in chemical engineering. Anil Muskawad from my days with Praj Industries has till date served as friend and a mentor.

I would like to acknowledge the support of all of Dr. Aichele and Dr. Whiteley's students (present and past). Above all, I would like to express my gratitude to Brett King. Every single data point in this dissertation was a team effort between me and Brett. I will never forget Brett's willingness to help at all times and his drive to learn new things. His strong work ethic is an example to all. I owe him more than just a beer!

I would like to thank Eileen Nelson for all her help and assistance in proofreading this dissertation. Carolyn Sanders was most patient in dealing with all the financial issues that came up in purchasing new equipment and setting up of the experimental facility. Shelley Potter was always available to help us with regards to any questions regarding safety. Shelley's infectious laugh brightened most days. I would also like to acknowledge the support and help of Shelley Taylor and Paula Kendrick. Justin Eubanks and Brenda Sorenson from the Environmental Health and Safety Office at Oklahoma State University worked with us to ensure proper disposal of solvents. Their support and time is greatly appreciated. Brandi Simmons (Laser Safety Officer at Oklahoma State University) always pro-actively reminded us of our laser compliance requirements and updates.

Many vendors greatly helped in completing our setup. I would like to acknowledge Chad Sipperley, and Will Bachalo from Artium Technologies for helping us set up the Phase Doppler Interferometry (PDI) and answering all our questions. Chad was most patient in training me on the PDI. David Flournoy and Ruben Martinez from Swagelok helped out in ordering the correct connectors for all our piping. David Flournoy's multiple visits to our lab to help us are greatly appreciated. Rob Shepherd from Alloy Stainless and Piping was always available with his recommendations on piping. Jessica Boyd from VWR was always prompt in putting our orders in for lab supplies and chemicals. Jim Finley at Glassworks manufactured most of the custom glass pieces. His recommendations and ideas greatly helped in coming up with robust designs. Mike Lucas (Physics Machine Shop, Oklahoma State University) quickly and efficiently turned around any custom fabrication needed.

The best part of being in Stillwater for the last six years has been the life-long friendships I have made. Cecely Jones was always around on the good, the bad and more importantly the ugly days. Her help, support and encouragement helped me stay the course. Driving around dirt roads will not be the same without Cecely. I cannot thank her enough for everything. I was fortunate to become close friends with Bridgette Lee. Hanging out with Bridgette was such a stress reliever. I learnt to laugh and enjoy life to the fullest due to her. Leigh Krause helped out a lot with the TIC analysis. She even helped me coach soccer to kids 6 years and under. Her kid-like energy brought a smile at all times. I will dearly miss our pancake breakfasts, mid-day coffee and donut breaks and late night chips and queso runs. Amey Kokane and Ariana Tarifa were pillars of support throughout. Shaunak Potdar, Yu Mizuki, Neha Bhadbhade, Prarthana Padbidri and Keri Fong always watched out for me. I would have been lost without them. Solomon Gebreyohannes and Sahith Doppalapudi were the best mates to take courses with.

Finally, I would like to thank my family members. My parents, Sharadchandra Tamhankar and Ketaki Tamhankar (Sharad and Kekutai) have always supported me in all my endeavors. Their consideration, support and patience are greatly appreciated. Both my parents took great pains to ensure that both me and my sister had a good education, food on the table, warm beds and above all love in our lives. My sister Manasi is my go-to person for most things in life. She has always provided sound advice, support and help. It was Manasi who encouraged me to apply to graduate schools in the US. She was always

confident that I would excel in a research-driven academic environment. I could not have asked for a better sibling. Manasi, this dissertation is dedicated to you. Thank you!

Acknowledgements reflect the views of the author and are not endorsed by committee members or Oklahoma State University.

Name: YASH S. TAMHANKAR

Date of Degree: MAY, 2015

Title of Study: DYNAMIC ASPECTS OF SPRAYS FOR ABSORPTION APPLICATIONS

Major Field: CHEMICAL ENGINEERING

Abstract: Spray columns show potential for absorption applications such as CO_2 capture because of the low gas phase pressure drop and resistivity to the corrosive action of amine solvents such as Monoethanolamine (MEA) due to the lack of internal hardware. Spray absorption data in terms of mass transfer coefficients is needed for robust design, whereas dropsize data and interfacial area data are required to improve the current understanding of spray absorption. The aim of this study was to measure spray absorption rates, drop size, and surface area for the CO_2-MEA system in a laboratory spray column. In specific, the study was conducted to elucidate the effect of increasing MEA concentration on spray absorption of CO_2. Further, the interfacial area inside the Spray column was ascertained by absorbing CO_2 in a low normality Sodium hydroxide (NaOH) solution as a measure of the spray efficiency. Absorption rates for the CO_2-MEA system were found to decrease with increasing inlet loading on one hand, and increase with L/G ratio, and MEA concentration on the other. Dropsize measurements were found to be practically independent of the inlet loading. A new methodology to compute planar area from dropsize measurements was developed. The computed planar surface areas were found to be comparable for the two MEA concentrations tested. Free MEA content was thus found to dominate the spray absorption process. Increasing MEA concentration for spray absorption of CO_2 may be a feasible option. Interfacial area measurements inside the spray column were found to be strongly dependent on the contactor height. The interfacial area in sprays was found comparable to packed columns at low gas-liquid contact heights. Data for both the CO_2-MEA and CO_2-NaOH system, points to a large degree of mass transfer in the region in the immediate vicinity of the nozzle tip. Short contact spray columns for absorption applications are thus recommended.

TABLE OF CONTENTS

LIST OF TABLES

Table Page

LIST OF FIGURES

Figure Page

NOMENCLATURE

A = area of concentric circular zone, m^2
A_C = column cross sectional area, m^2
a_e = interfacial area, m^2/m^3
A_{plume} = cross sectional area of spray plume, m^2
C = correction factor for drop count
C_{NaOH} = concentration of hydroxide solution, $kmol/m^3$
d = drop diameter, µm
$D_{CO2,l}$ = diffusivity of CO_2 in the liquid solvent, m^2/s
D_{32} = Sauter mean diameter, µm
F_A = fractional surface area
G = total gas rate, m^3
G_I = inert gas rate, kmol/min
h = Barett contributions to Henry's constant calculation, Lit/mol
$h_{Na}+$, $h_{OH}-$, h_{CO2}, h_{CO3}^{2-} = Barett contributions to Henry's constant calculation, Lit/mol
H_{CO2} = Henry's constant for CO_2 in solvent, m^3.atm/kmol
$H_{CO2\text{-}PM}$ = Henry's constant for CO_2 in solvent as defined by Pohorecki and Moniuk (1988), kmol/ m^3.atm
$H_{CO2,w\text{-}PM}$ = Henry's constant for CO_2 in water as defined by Pohorecki and Moniuk (1988), kmol/ m^3.atm
I = ionic strength of solution, mol/Lit
k_g' = local liquid side mass transfer coefficient in gas units, $kmol/m^2$.s.atm
$k_g a_e$ = local liquid volumetric mass transfer coefficient in gas units, $kmol/m^3$.min.atm
$K_G a_e$ = overall volumetric mass transfer coefficients, $kmol/m^3$.min.atm
$k_{OH}-$ = second order rate constant, $m^3/kmol.s$
$k^{\infty}_{OH}-$ = second order rate constant at infinite dilution, $m^3/kmol.s$
L = total liquid rate, Lit or m^3
L_{MEA} = MEA liquid rate, kmol/min
N_{CO2} = CO_2 flux, kmol/min
n = drop count or number of concentric circular zones
p_{CO2} = CO_2 partial pressure, atm
P_{SA} = planar surface area, m^2
R = gas constant, m^3.atm/kmol.K
S = surface area of all drops in a concentric circular zone, m^2
T = temperature, K
V = volume of solvent, m^3
V_{spray} = volume of solvent sprayed, m^3
$Y_{CO2,in}$ = CO_2 mole ratio in inlet gas
$Y_{CO2,out}$ = CO_2 mole ratio in outlet gas

Z = gas-liquid contact height or column height, m

Subscript
i = bin in dropsize measurement
in = gas inlet
j = 1, 2, 3….. = concentric circular zone number
lm = logarithmic
out = gas outlet

Superscript
* = equilibrium

Greek
α = loading, mol CO_2/mol MEA
α_{lean} = lean loading, mol CO_2/mol MEA
α_{rich} = rich loading, mol CO_2/mol MEA
Δ = difference

CHAPTER I

INTRODUCTION

I.1. Need for CO_2 capture

Reduction of CO_2 emissions from power plants to mitigate global warming has been under great focus in the last several years. As of 2013, energy related CO_2 emissions were estimated to be about 5396 million metric tons (USEIA 2014). About 70% of the power generated in the United States is from CO_2 emitting sources (USEIA 2011). Flue gas emitted by power plants is a significant source of CO_2. Of these power generation sources, coal-fired power plants account for 40% of the total power generated (USEIA 2011).

Carbon Capture & Sequestration (CCS) methods are widely propagated for reducing CO_2 emissions. Of the three major approaches for CCS (pre-combustion, oxy-combustion, and post combustion), post combustion CCS is considered the most advanced because of utilization of the mature aqueous amine absorption-stripping process (Rochelle, Chen *et.al.* 2011).

I.2. Aqueous amine absorption and stripping

Aqueous amine absorption-stripping of CO_2 from flue gas is the most developed and established technology for Post Combustion Carbon Capture and Storage (CCS) (Rochelle, Chen *et.al.* 2011; Oexmann and Kather 2009). Amine absorption-stripping has been widely used in the natural gas industry for removing CO_2 and H_2S (contaminants in raw gas) for more than 80 years (Kohl and Nielson 1997). The “tail end” nature of this technology allows it to be coupled with existing

power plants without major modifications (Dugas 2009; Van Wagener 2011). A typical flow sheet of the process is shown in Figure 1.1.

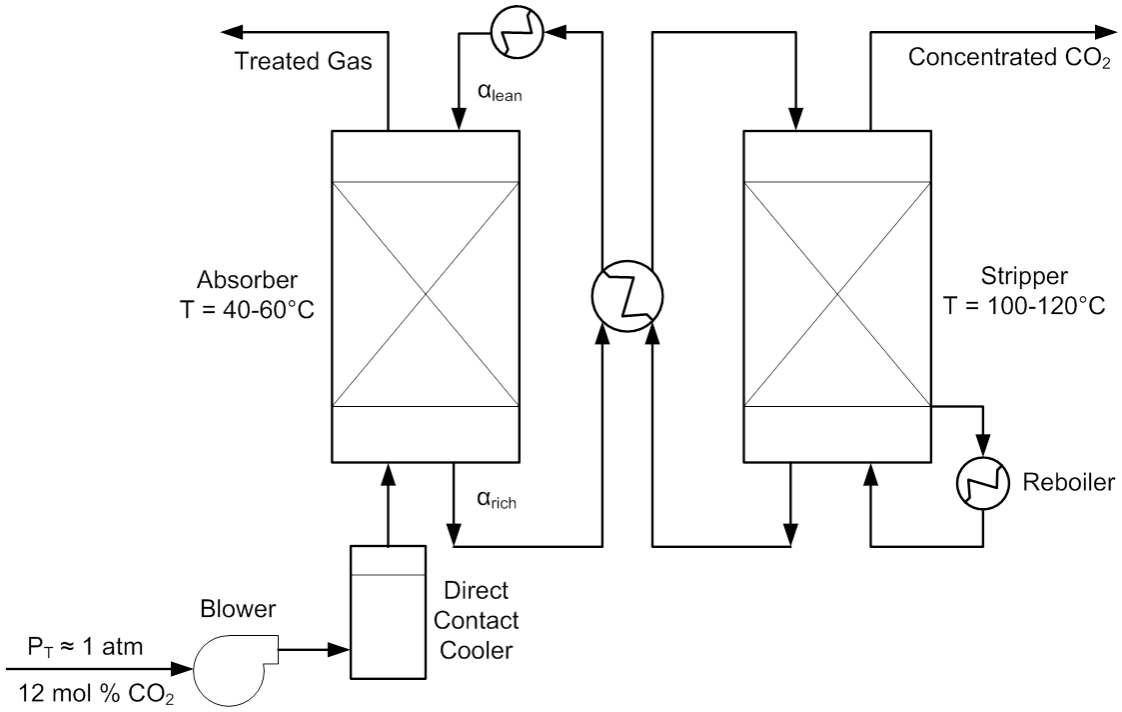

Figure 1.1. Aqueous amine absorption and stripping process

Flue gas with approximately 12 mol % CO_2 is introduced at the bottom of the absorber by means of a blower. The up-flowing gas contacts counter-currently with the down-flowing lean amine solution. CO_2 in the gas dissolves in the liquid solution and then reacts exothermally with the amine to form carbamates and bicarbonates. The mass transfer of CO_2 and subsequent reaction in the liquid, greatly reduce the bulk gas phase CO_2 concentration. The CO_2 rich amine is pumped from the bottom of the absorber to the top of the stripping column to recover the solvent, via the cross heat exchanger. The cross heat exchanger is used to heat the rich amine solution and cool the lean amine solution, respectively. The temperature in the stripper is maintained sufficiently high by means of a steam driven reboiler to reverse the reaction between CO_2 and amine. A condenser at the top of the stripper is used to separate the water vapor exiting along with the

liberated CO_2. The concentrated CO_2 stream emerging from the top of the stripping column can then be compressed and sequestered.

At present, 30 wt% MEA (7m MEA) is the preferred solvent for absorption-stripping of CO_2 in natural gas treatment. Compared to other aqueous amines, MEA exhibits the highest CO_2 pickup capacity (because of its low molecular weight) and the lowest relative cost (Kohl and Nielson 1997). Conversely, the high heat of reaction between MEA and CO_2 compared to other amines results in high regeneration costs (Oyenekan and Rochelle 2009; Kohl and Nielson 1997; Feng, Du *et.al.* 2010). Increasing solvent concentration results in greater CO_2 pickup and increased corrosivity (Rochelle 2009; Kohl and Nielson 1997; Abu-Zahra, Schneiders *et al.* 2007). Additionally, the viscosity increase expected with higher concentration MEA can significantly reduce the mass transfer rates (Kuntz 2006). The 30 wt% limit on the MEA concentration is a trade-off point ensuring high mass transfer rates, reasonable pick up capacity at an appreciable regeneration cost, and some corrosivity (with addition of anti-corrosive agents).

High operating and capital costs render the absorption-stripping process with 30 wt% MEA impractical at present for post combustion CCS (Oyenekan and Rochelle 2009). These high operating costs originate from the large energy required to regenerate the solvent and the high pressure drop associated with packed or tray-ed columns (Rochelle 2009; Tsai 2010). Unlike natural gas processing, flue gas from power plants is available at near atmospheric pressure. As a result, low pressure drop across the absorber becomes critical. Thus, there is a need to reduce the energy requirement of the process by either employing more efficient G-L contactors or solvents with greater CO_2 absorption capacities or both.

I.3. Spray technology

Spray columns are the simplest gas-liquid contacting device. In spray columns, the liquid is dispersed in form of drops and contacts the up-flowing gas as seen in Figure 1.2. Spray columns

are relatively inexpensive, fouling and corrosion resistant compared to packed columns (no internals) and have low gas side pressure drop (Mehta and Sharma 1970). Conversely, the lack of internals can result in significant gas phase back-mixing, thereby reducing efficiency (Mehta and Sharma 1970; Pinilla, Diaz *et.al.* 1984). Spray columns cannot provide a high number of transfer units and are only employed for easy separations (Rousseau 1987; Mycock, Mckenna *et.al.* 1995). Spray columns are extensively used in Flue Gas Desulfurization (FGD) units to remove SO_2 from gas streams (Kohl and Nielson 1997; Yeh and Rochelle 2003).

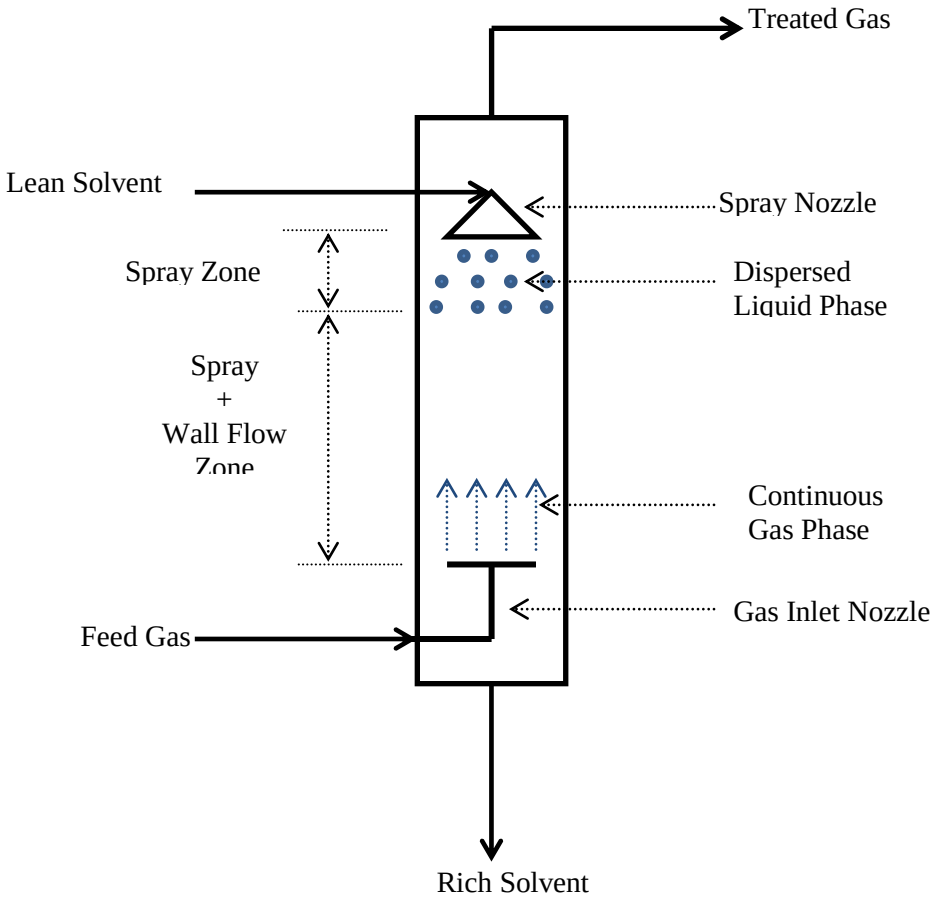

Figure 1.2. Spray column schematic

Spray columns show potential in absorbing CO_2 into MEA based on,

1. Low pressure drop compared to packed or tray-ed columns

2. Lack of internals

The low pressure drop associated with spray columns can significantly reduce the blower cost compared to structured packing. Preliminary calculations show a 60%-70% reduction in installed blower cost using spray columns. The correlation used to compute these estimates was specifically developed for post-combustion CCS using aqueous amines (Tsai 2010).

Additionally, the absence of internals makes spray columns less susceptible to corrosion. This permits the use of higher MEA concentrations; thereby reducing the recirculation rate and the regeneration duty. Zahra, Schneiders *et. al.* (2007) estimate a 12% reduction in reboiler duty using 11m MEA (40 wt %) instead of 7m MEA (30 wt %). It must be noted, that increasing solvent concentration results in greater oxidative degradation rates, increased corrosion, and increased cost for disposal (Dugas 2009; Van Wagener 2011). However, oxidative degradation of MEA in absence of dissolved metals (Fe & Cu used as corrosion inhibitors) is insignificant (Van Wagener 2011). Moreover, certain O_2 scavengers and inhibitors can significantly reduce oxidative degradation of MEA (Van Wagener 2011).

Thus, spray columns show sufficient promise in reducing the cost of the absorption-stripping process for post-combustion CCS to warrant further investigation.

I.4. Need for spray absorption rate measurements

Rate based modeling is the preferred technique for sizing columns used for an aqueous amine absorption-stripping process (Oyenekan and Rochelle 2009; Dugas 2009; Bandyopadhyay and Biswas 2012; Sardar and Sivasubramanian 1985). The enhancement in mass transfer due to the exothermic reaction and presence of additional acid gases in the inlet gas, results in poor and unreliable efficiency estimates (Weiland, Rawal *et.al.* 1982). Javed, Mahmud *et. al.* (2010) have presented a methodology to size spray columns based on system specific rate measurements.

Values of system specific, spray mass transfer coefficients is required to determine the height of a spray column.

Aqueous amine absorption-stripping has been practiced for over 80 years in the natural gas industry. Typically, raw natural gas enters the absorber at 200 psia or more (Maddox 1974). This high inlet gas pressure permits use of trays and packings, without substantial cost penalty. Only in recent years has the use of amine absorption-stripping process for post-combustion CCS been propagated. Low inlet flue gas pressure from power plants provides a strong incentive for using low pressure drop contactors such as spray columns. Hence spray absorption of CO_2 in MEA has not been extensively studied leading to a scarcity of system specific, spray absorption data.

I.5. Need for dropsize measurements

The absorption efficiency of sprays depends greatly on the surface area of drops. Secondary effects such as break-up, shattering, and coalescence can affect the spray absorption efficiency. Use of correlations to predict dropsize from nozzles can lead to unrealistic quantification of surface area. Vendor dropsize data is frequently extrapolated based on limited experimental measurements (Lipp 2013b). Further, almost all of the available experimental vendor data is for water. Thus, there is a need to experimentally measure dropsize from commercial nozzles for CO_2-MEA system. More significantly, there is a need to quantify the surface area from experimental dropsize measurements. Coupling of mass transfer rate data with dropsize data can help improve the understanding of spray absorption.

I.6. Need for interfacial area measurements

The interfacial area measurements inside spray columns can provide further insight into surface area effects. Interfacial area measurements provide a convenient means to ascertain the efficiency of spray contactors. Further, comparison of spray columns to packed columns can conveniently be made on an interfacial area basis. Comparing surface area values (based on dropsize

measurements) with interfacial area measurements, the contribution of drop saturation, and secondary effects can be deduced. Additionally, coupling of interfacial area measurements with surface area quantification can provide a basis to develop scalable interfacial area correlations.

I.7. Research goal and objectives

The primary research goal of this study is to provide insight into spray absorption. The practical goals of the study were to measure mass transfer rates for spray absorption of CO_2 in dispersed MEA, measure dropsize for CO_2-MEA system, and to provide an estimate for the spray efficiency. In order to meet the goals outlined above, the following objectives had to be met:

1. Build a spray column set-up capable of measuring mass transfer flux and dropsize measurements at multiple locations, for solvents used in CO_2 capture applications.
2. Develop analytical methods and operating procedures for all equipment and tests needed in measuring mass transfer coefficients, and drop size.
3. Develop a methodology to quantify surface area from experimental drop size measurements.
4. Evaluate the effect of MEA concentration, and L/G ratio on the mass transfer performance of the built spray column.
5. Ascertain the efficiency of spray column in terms of the interfacial area for gas-liquid contact.

Chapter I in this dissertation provides the motivation for studying sprays for CO_2 capture applications, and outlines the objectives of the study. Background on mass transfer, solvents tested, spray technology, and work of previous researchers is provided in Chapters II, III, and IV, respectively. The experimental setup, procedure, testing methods, and calculations used in this work are described in detail in Chapter V. MEA and NaOH results are presented in Chapters VI,

and VII, respectively. Finally, the conclusions and recommendation from this work are summarized in Chapter VIII.

CHAPTER II

MASS TRANSFER & SOLVENT CHEMISTRY

The prime objective of this chapter is to introduce various aspects of mass transfer with chemical reaction relevant to the absorption of CO_2 in either MEA, or NaOH. Mass transfer coefficients, fundamental mass transfer models, effect of chemical reaction on mass transfer, contactor mass transfer coefficients, and chemistry of CO_2-MEA, and CO_2-NaOH will be discussed in this chapter.

II.1. Mass transfer across a gas-liquid interface

Mass transfer can be defined as the process of movement of a component from one location to another based on the differences in the concentration of that component at those two locations (Seader and Henley 2006). In gas absorption processes such as CO_2 capture from flue gas, this movement of one component takes place across a gas-liquid interface as shown in Figure 2.1.

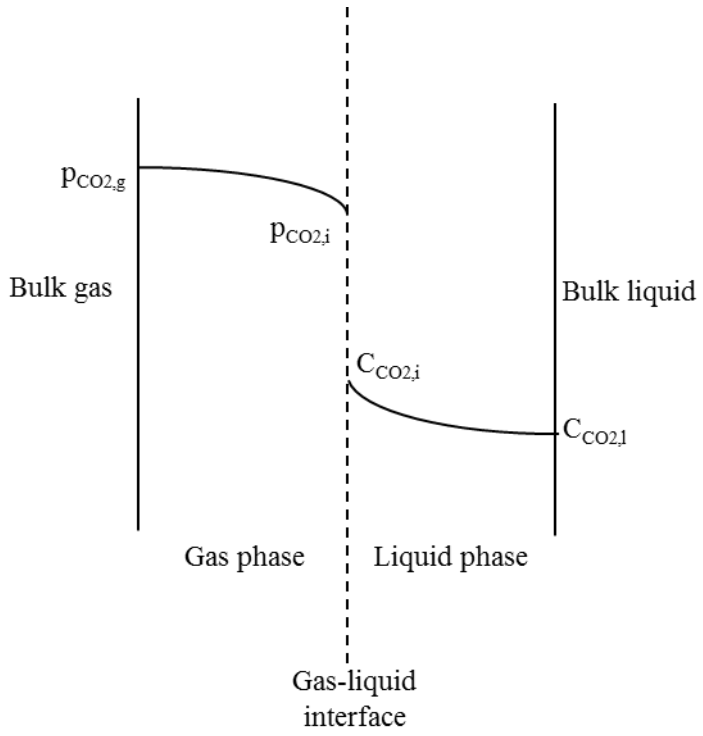

Figure 2.1. Mass transfer of CO_2 into a liquid across the gas-liquid interface [Adapted from Treybal, R.E. (1980)]

Consider absorption of CO_2 from bulk gas into a liquid across the gas liquid interface. CO_2 diffuses from the bulk gas to the interface, dissolves at the interface, and then diffuses into the liquid. It is assumed that the concentration of CO_2 on the gas and liquid side are in equilibrium with each other at the interface.

The molecular flux, as defined in Equation 2.1, is the ratio of the driving force for movement of a component such as CO_2 to the resistance for such a movement. Such a definition of flux is also applicable to other transport processes of heat, and momentum.

$$Flux = \frac{driving\ force}{resistance} \qquad (Eq\ 2.1)$$

Ignoring the bulk movement of CO_2, the steady-state, molar flux of CO_2 from the bulk gas to the interface can be expressed as Equation 2.2 below-

$$N_{CO2} = \frac{p_{CO2,g} - p_{CO2,i}}{R_{CO2,g}} \quad (Eq\ 2.2)$$

where,

N_{CO2} = molar flux of CO_2, kmol/m^2.s

$p_{CO2,g}$ = partial pressure of CO_2 in the bulk gas, atm

$p_{CO2,i}$ = partial pressure of CO_2 at the interface, atm

$R_{CO2,g}$ = resistance to transport of CO_2, atm.m^2.s/kmol.

Defining the local gas side mass transfer coefficient as the reciprocal of the resistance to transport of CO_2, yields Equation 2.3 below -

$$N_{CO2} = k_g \left(p_{CO2,g} - p_{CO2,i}\right) \quad (Eq\ 2.3)$$

where,

k_g = local gas side mass transfer coefficient, kmol/m^2.s.atm.

Under steady state conditions, the molar flux of CO_2 from the bulk gas to the interface must equal the molar flux of CO_2 from the interface to the bulk liquid. Analogous to Equation 2.3, the steady state molar flux of CO_2 from the interface to the bulk liquid can be quantified by Equation 2.4 below –

$$N_{CO2} = k_l^{\circ} \left(C_{CO2,i} - C_{CO2,l}\right) \quad (Eq\ 2.3)$$

where,

k_l^0 = local physical liquid side mass transfer coefficient, m/s

$C_{CO2,i}$ = concentration of CO_2 at the interface, kmol/m^3

As the interfacial concentrations are difficult to determine, the molar flux can be quantified in terms of the overall driving force as shown in Equations 2.4, and 2.5 below –

$$N_{CO2} = K_G \left(p_{CO2,g} - p_{CO2}^{*}\right) \quad (Eq\ 2.4)$$

$$N_{CO2} = K_L \left(C_{CO2}^{*} - C_{CO2,l}\right) \quad (Eq\ 2.5)$$

where,

K_G = overall gas side mass transfer coefficient, kmol/m^2.s.atm

p_{CO2}* = partial pressure of CO_2 in equilibrium with the bulk liquid phase CO_2 concentration
K_L = overall liquid side mass transfer coefficient, m/s
C_{CO2}* = concentration of CO_2 in equilibrium with the bulk gas phase concentration of CO_2, kmol/m^3.

The interfacial partial pressure of CO_2, and the interfacial concentration of CO_2, is related to each other by the Henry's constant as seen in Equation 2.6 below -

$$p_{CO2,i} = C_{CO2,i}\, H_{CO2} \qquad (Eq\ 2.6)$$

where,
H_{CO2} = Henry's constant, m^3.atm/kmol.

The relationship between the overall mass transfer coefficient on either the gas or the liquid side, and the local mass transfer coefficients are presented as Equation 2.8, and 2.9, respectively.

$$\frac{1}{K_G} = \frac{1}{k_g} + \frac{H_{CO2}}{k_l^{\circ}} \qquad (Eq\ 2.8)$$

$$\frac{1}{K_L} = \frac{1}{H_{CO2}\, k_g} + \frac{1}{k_l^{\circ}} \qquad (Eq\ 2.9)$$

In case where the resistance to mass transfer is dominated by the gas side, the overall mass transfer coefficients reduce to the form of Equations 2.10, and 2.11. For liquid resistance dominated systems, the overall mass transfer coefficients reduce to the form of Equations 2.12, and 2.13.

$$\frac{1}{K_G} = \frac{1}{k_g} \qquad (Eq\ 2.10)$$

$$\frac{1}{K_L} = \frac{1}{H_{CO2} k_g} \qquad (Eq\ 2.11)$$

$$\frac{1}{K_G} = \frac{H_{CO2}}{k_l^{\circ}} \qquad (Eq\ 2.12)$$

$$\frac{1}{K_L} = \frac{1}{k_l^{\circ}} \qquad (Eq\ 2.13)$$

II.2. Mass transfer theories

Multiple theories have evolved to explain the process of mass transfer of one component to another. A brief description of such theories is presented below.

II.2.1. Film theory

The two film theory proposed by Lewis and Whitman (1924), proposes the establishment of a stagnant film on either side of the gas-liquid interface as shown in Figure 2.2.

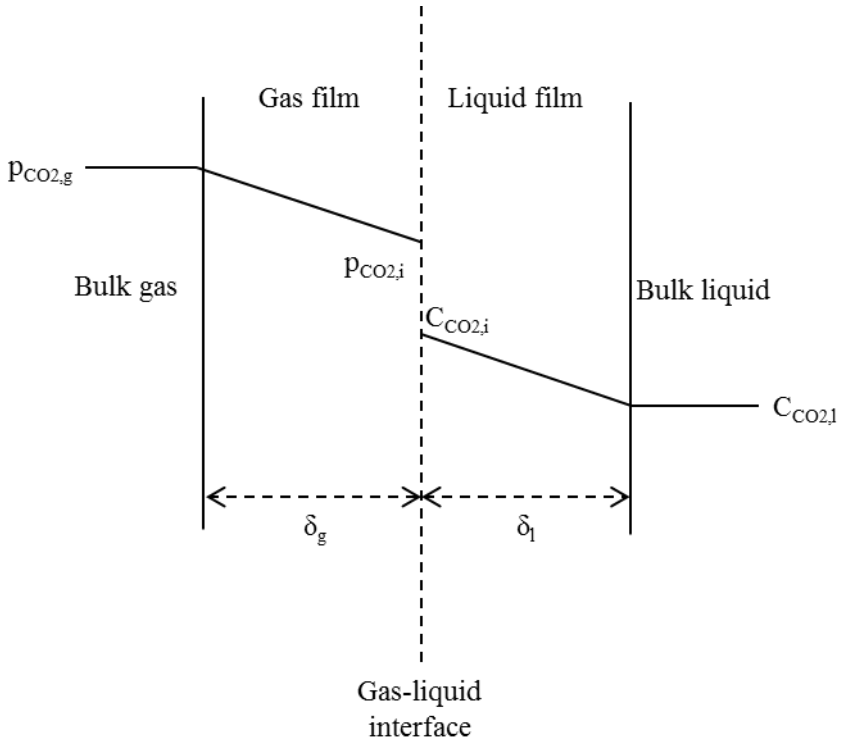

Figure 2.2. Film theory
[Adapted from Treybal, R.E. (1980)]

The films on both side of the interface are assumed to be infinitely thin such that at steady state, all of the mass transfer occurring across the interface is purely due to molecular diffusion. Since, the bulk phases are assumed to be well mixed, the concentration gradients, and hence the resistance to diffusion, are both limited to the stagnant film on either side of the interface. By applying proper boundary conditions, the molar flux of CO_2 results as follows:

$$N_{CO2} = \frac{D_{CO2,l}\left(C_{CO2,i} - C_{CO2,l}\right)}{\delta_l} \qquad (Eq\ 2.14)$$

where,

$D_{CO2,l}$ = liquid diffusion coefficient of CO_2, m^2/s

δ_l = liquid film thickness, m.

Comparing Equations 2.3, and 2.14 results in the following relationship between the local physical liquid side mass transfer coefficient and the diffusivity.

$$k_l^{\circ} = \frac{D_{CO2,l}}{\delta_l} \qquad (Eq\ 2.15)$$

The film theory thus predicts a first order dependence of the local physical liquid mass transfer coefficients with the diffusivity. Sherwood and Holloway (1940) performed extensive tests on multiple packings to quantify the liquid phase resistance to absorption inside packed columns. The results from their tests indicated that the local physical mass transfer coefficient varies with the 0.47 power of diffusivity. The film theory fails to predict the correct relationship between the local physical liquid side mass transfer coefficient and the diffusivity. Further, the film theory provides an unrealistic picture of liquid flow inside packed columns (Vivian and Peaceman 1956). The stagnant liquid film is found to be adjacent to the solid packing surface, rather than at the gas-liquid interface.

II.2.2. Penetration theory

The Penetration theory was proposed by Higbie (1935) to quantify the liquid phase mass transfer resistance. Liquid elements are assumed to flow with uniform velocity from the bulk liquid to the gas-liquid interface, and then return back to the bulk liquid. At the interface, the solute gas "penetrates" a short distance into the liquid element. Thus, the mass transfer occurs during a series of brief contacts between the solute gas, and the liquid element at the interface. Each liquid

element is assumed to spend a constant time (called exposure time) at the interface. Under such conditions, the molar flux of CO_2 is:

$$N_{CO2} = 2\left(C_{CO2,i} - C_{CO2,l}\right)\sqrt{\frac{D_{CO2,l}}{\pi\, t_e}} \qquad (Eq\ 2.16)$$

where,

t_e = exposure time or time the liquid element spends at the interface, s

The penetration theory thus predicts a better match with experimental observations in correlating the local physical liquid side mass transfer coefficient and the diffusivity.

II.2.3. Surface renewal theory

The surface renewal theory (Danckwerts 1951) is an improvement over the penetration theory. Unlike the penetration theory, the surface renewal theory assumes that liquid elements spend varying periods at the interface. The exposure time is not constant. The gas-liquid interface then becomes a collection of liquid elements with varying exposure time histories. As a result, the average mass flux needs to be determined. Further, the theory assumes that the probability of individual liquid elements being replaced at the interface is independent of the time spent by those liquid elements at the interface. The molar flux is given by:

$$N_{CO2,avg} = \left(C_{CO2,i} - C_{CO2,l}\right)\sqrt{D_{CO2,l}\, s} \qquad (Eq\ 2.17)$$

where,

s = fractional rate of replacement of individual elements at the interface.

The local physical liquid side mass transfer coefficient then becomes:

$$k_l^{\circ} = \sqrt{D_{CO2,l}\, s} \qquad (Eq\ 2.18)$$

The surface renewal theory, like the penetration theory, predicts the correct dependence of the local physical liquid side mass transfer coefficient on the diffusivity. However, like the penetration theory, the surface renewal theory is time dependent.

II.2.4. Eddy diffusivity theory

The eddy diffusivity theory, unlike surface renewal and penetration theories, is time-independent, but predicts the correct order of dependence of the local physical liquid mass transfer coefficient with the diffusivity. According to this theory, molecular diffusion dominates the mass transfer in the region around the gas-liquid interface. Away from the interface, the influence of fluid "eddies" becomes significant. The molar flux then becomes:

$$N_{CO2} = \left(C_{CO2,i} - C_{CO2,l}\right) \frac{2}{\pi} \sqrt{D_{CO2,l}\, e} \qquad (Eq\ 2.19)$$

where,

$D_{CO2,l}$. e = eddy diffusivity , m^2/s.

The local physical liquid side mass transfer coefficient is presented below as Equation 2.20.

$$k_l^{\circ} = \frac{2}{\pi} \sqrt{D_{CO2,l}\, e} \qquad (Eq\ 2.20)$$

All four fundamental mass transfer theories discussed previously are simple mathematical models used to account for mass transfer across a gas-liquid interface. These theories are used as starting points to develop correlations.

II.3. Mass transfer with chemical reaction

II.3.1. Reaction regimes

Mass transfer with chemical reaction is of particular relevance for absorption of CO_2 in either MEA, or NaOH. Both MEA and NaOH are reactive solvents and as such the CO_2 in the liquid gets bound to the solvent, either in the form of carbamate, carbonate, or bicarbonate, because of

chemical reactions. For low pressure applications, the solubility of CO_2 is insufficient to absorb and store CO_2 in the liquid phase. By use of a reacting solvent such as MEA, or NaOH, the absorption rates can be increased beyond the limits of physical absorption.

Absorption with a chemical reaction can be classified based on the rate of reaction. Instantaneous, fast, intermediate, and slow are the typical reaction cases discussed here. Levenspiel (1999) provides a detailed description of the various regimes of mass transfer with reaction. These four regimes are explained with a pictorial representation of the film theory as depicted in Figure 2.3.

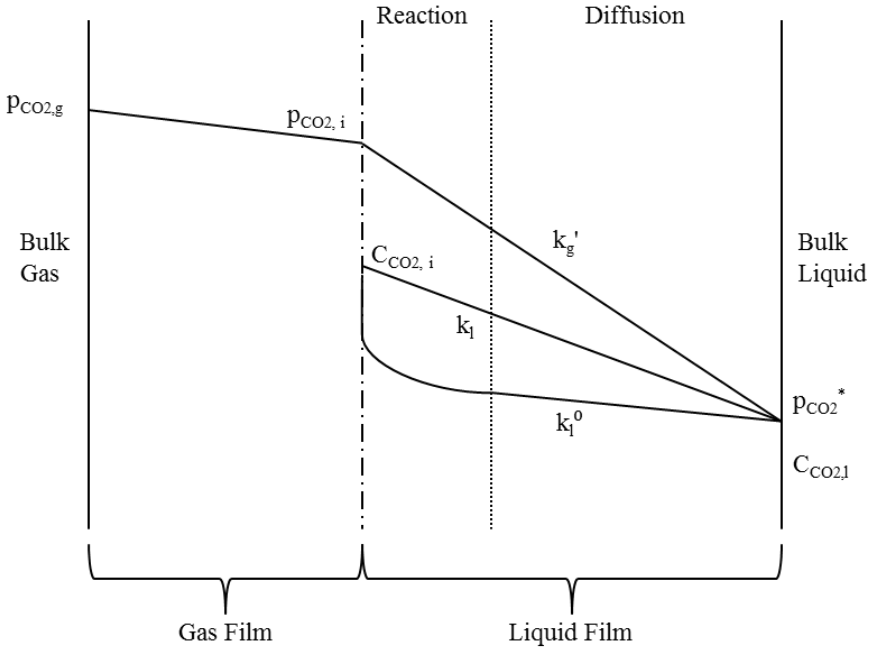

Figure 2.3. Mass transfer of CO_2 across the interface with reaction in the liquid [Adapted from Tsai, R.E. (2010)]

Consider Figure 2.3 above. CO_2 from the bulk gas diffuses to the gas-liquid phase based on the partial pressure driving force. At the interface, the CO_2 molecules dissolve into the liquid solvent based on the solubility (inverse of the Henrys constant). Further, the dissolved CO_2 starts diffusing towards the bulk liquid based on the concentration gradient on the liquid side. As this

CO_2 starts diffusing through the liquid, it starts reacting with it. Based on the rate of this reaction, the CO_2 could diffuse all the way through to the bulk liquid.

In case of an instantaneous reaction, the dissolved CO_2 reacts instantaneously with the liquid. As a result, the entire resistance to mass transfer is associated with the diffusion of CO_2 to the gas-liquid interface. The thickness of the reaction film as depicted in Figure 2.3 would disappear.

In a fast reaction case, the reaction of the CO_2 in the liquid is much slower (compared to the instantaneous case). The CO_2 molecules diffuse beyond the gas-liquid interface. However, all of the diffusing CO_2 molecules react with the liquid before reaching the bulk liquid. Since the CO_2 molecules diffuse beyond the interface, there is a finite resistance to mass transfer on the liquid side. The diffusion on the gas side no longer dominates the mass transfer.

In an intermediate reaction case, the diffusing CO_2 molecules do not get consumed in the reaction film. Some of the molecules do reach the bulk liquid. Most of the reaction takes place in the liquid diffusion film (Figure 3.3).

In a slow reaction case, the diffusing CO_2 molecules reach the bulk liquid. Most of the CO_2 molecules get consumed in the bulk liquid. The phase diffusion resistance dominates the mass transfer.

II.3.2. Enhancement factor

The enhancement factor (E) is a measure of the improvement in mass transfer rates due to chemical reaction. As seen in Equation 2.21, the enhancement factor is defined as the ratio of the actual rate of mass transfer with chemical reaction to the rate of mass transfer without chemical reaction, under the same driving force (Astarita, Savage *et. al.* 1983).

$$E = \frac{k_l}{k_l^{\circ}} \geq 1 \qquad (Eq\ 2.21)$$

To account for the enhancement factor, Equation 2.3 is re-stated as Equation 2.22 below.

$$N_{CO2} = E\, k_l^{\circ} \left(C_{CO2,i} - C_{CO2,l}\right) \qquad (Eq\ 2.22)$$

The improvement in mass transfer rates due to a chemical reaction can be attributed to two reasons. First, as the diffusing CO_2 molecules react with the liquid, the concentration of CO_2 in the bulk liquid remains largely unchanged. In the case of physical absorption, compared to absorption with chemical reaction, the driving force would reduce once CO_2 molecules started diffusing in to the bulk liquid. Second, the enhancement factors can provide significant improvement in the mass transfer rates. Wetted wall column measurements with MEA have shown enhancement factors in the order of 80-100 (Dugas 2009). Thus, in low pressure applications such as CO_2 capture from flue gas, chemical solvents are needed.

II.3.3. Concept of $k_g^{'}$

The CO_2 molar flux equations with the effect of chemical reactions are stated below.

$$N_{CO2} = K_G \left(p_{CO2,g} - p_{CO2}^{*}\right) \qquad (Eq\ 2.23)$$

$$N_{CO2} = k_g \left(p_{CO2,g} - p_{CO2,i}\right) \qquad (Eq\ 2.24)$$

$$N_{CO2} = K_L \left(C_{CO2}^{*} - C_{CO2,l}\right) \qquad (Eq\ 2.25)$$

$$N_{CO2} = k_l \left(C_{CO2,i} - C_{CO2,l}\right) \qquad (Eq\ 2.26)$$

Equation 2.26 can be re-stated with the incorporation of the enhancement factor, and change in the driving force from a concentration basis to a partial pressure basis as shown in Equation 2.27.

$$N_{CO2} = \frac{E\, k_l^{\circ}}{H_{CO2}} \left(p_{CO2,i} - p_{CO2}^{*}\right) \qquad (Eq\ 2.27)$$

The first term on the right hand side of Equation 2.27 provides the definition of k_g'. k_g' is the local chemical liquid side mass transfer coefficient expressed in gas driving force (pressure) units as seen in Equation 2.28 below.

$$k_g' = \frac{E\, k_l^{\circ}}{H_{CO2}} \qquad (Eq\ 2.28)$$

There are two distinct advantages to using the concept of k_g' to quantify mass transfer rates. First, it is convenient to measure partial pressure changes in the feed gas to account for molar flux of CO_2 rather than the liquid phase concentration changes while running experiments (Dugas 2009). Second, k_g' has contributions of reaction (E), and solubility ($1/H_{CO2}$) built in. Measurement of k_g' rates do not require evaluation of Henry's constant. Equation 2.8 is re-stated below for the case of absorption with chemical reaction using the concept of k_g' as Equation 2.29.

$$\frac{1}{K_G} = \frac{1}{k_g} + \frac{1}{k_g'} \qquad (Eq\ 2.29)$$

II.3.4. Pseudo 1st order reaction

As pointed out earlier, the reactions of CO_2-MEA, and CO_2-NaOH, both are considered fast (Dugas 2009, Tsai 2010). The pseudo 1st order reaction is an approximation applicable to systems exhibiting fast reactions where the resistance to gas side diffusion is negligible. Under this approximation, the liquid phase concentrations of both the reactants and the products are assumed to be constant. Such an approximation is acceptable when,

1. the free amine or hydroxide concentration is high
2. the CO_2 molar flux is low or
3. the local physical liquid side mass transfer coefficient is high.

Haubrock et al (2005) have quantified the above three requirements in terms of the Hatta number, and the infinite enhancement factor (E_∞). Under the approximation of pseudo 1st order reaction, the chemical local liquid side mass transfer coefficient expressed in terms of gas units (k_g') reduces to the form of Equation 2.30 below:

$$k_g' = \frac{\sqrt{D_{CO2,l}\, k_2\, [C_{solv}]}}{H_{CO2}} \qquad (Eq\ 2.30)$$

where,

$[C_{solv}]$ = active concentration of the solvent, kmol/m^3

k_2 =reaction constant, m^3/kmol.s

A careful observation of Equation 2.30 reveals three important points. First, k_g' purely depends on the system properties. Second, k_g' accounts for all the three factors contributing to the CO_2 flux on the liquid side: the solubility ($1/H_{CO2}$), the diffusion coefficient ($D_{CO2,l}$), and the reaction (k_2). To compare the absorption rates of two solvents robustly, the k_g' rates need to be utilized. Third, k_g' can be calculated analytically using Equation 2.30 which allows for the measurement of interfacial areas as discussed in Chapter V.

II.4. Mass transfer coefficients in contactors

Mass transfer coefficients in continuous contactors (packed or spray) can be derived in a fashion similar to the one presented in Section II.1. A detailed derivation of such mass transfer coefficients based on the film theory can be found in Treybal (1980). Only the eventual formulae are presented in this section.

The overall volumetric mass transfer coefficient in continuous contactors can be calculated using Equation 2.31 below:

$$K_G a_e = \frac{N_{CO2}}{A_C\, Z\, P_T\, \Delta y_{lm}} \qquad (Eq\ 2.31)$$

where,

$K_G a_e$ = overall volumetric mass transfer coefficient, kmol/m^2.min.atm

N_{CO2} = molar CO_2 flux, kmol/min

A_C = cross sectional area of the column

P_T = total pressure, atm

Δy_{lm} = logarithmic driving force.

The CO_2 flux can be calculated based on either the change in CO_2 composition either in the gas phase or the liquid phase. The CO_2 flux quantification based on the changes in gas phase are presented as Equation 2.32:

$$N_{CO2} = G\left(y_{CO2,in} - y_{CO2,out}\right) \qquad (Eq\ 2.32)$$

where,

G = total gas rate, kmol/min

y = CO_2 mole fraction.

Rearranging and combining equations 2.31, and 2.32 results in:

$$Z = \left[\frac{G}{K_G a_e A_C P_T}\right]\left[\frac{y_{CO2,in} - y_{CO2,out}}{\Delta y_{lm}}\right] \qquad (Eq\ 2.33)$$

The first term on the right hand side of Equation 2.33 is referred to as the Height of a Transfer Unit (HTU), while the second term is referred to as the Number of Transfer Units (NTU).

II.5. Solvent chemistry

This work focusses on two solvents; MEA, and NaOH. The following section provides a brief description of the reaction chemistry.

II.5.1. MEA

Monoethanolamine is a primary amine wherein the nitrogen atoms are attached to one carbon atom. The structure of an MEA molecule is showcased in Figure 2.4 below. Detailed amine chemistry can be found in the text of Kohl and Nielson (1997).

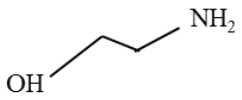

Figure 2.4. Structure of MEA

The reaction of CO_2 with MEA results in two primary products, carbamate and bicarbonate. Equations 2.34, and 2.35 showcase the reactions for carbamate formation and bicarbonate formation, respectively. Detailed reaction chemistry can be found in Blauwhoff, Versteeg et.al. (1983).

$$CO_2 + 2\,MEA \leftrightarrow MEACOO^- + MEANH_2{}^+ \qquad (Eq\ 2.34)$$

$$CO_2 + OH^- \leftrightarrow HCO_3{}^- \qquad (Eq\ 2.35)$$

It is essential to note, for a CO_2-MEA system, the bicarbonate formation becomes significant at high loadings (Dugas 2009). The bicarbonate formed is much more stable than the carbamate.

II.5.2. NaOH

The reaction of CO_2 with NaOH proceeds in two steps as outlined in Equations 2.36, and 2.37 below.

$$CO_2 + OH^- \leftrightarrow HCO_3{}^- \qquad (Eq\ 2.36)$$

$$HCO_3{}^- + OH^- \leftrightarrow CO_3{}^{2-} + H_2O \qquad (Eq\ 2.37)$$

The rate of reaction for the carbonate formation (Equation 2.37) is much greater than the reaction rate for formation of bicarbonate (Equation 2.36). With sufficient availability of free hydroxide (OH^-), the concentration of bicarbonate becomes insignificant. Under these conditions, the overall reaction reduces to the form presented in Equation 2.38 below.

$$CO_2 + 2\,OH^- \rightarrow CO_3{}^{2-} + H_2O \qquad (Eq\ 2.38)$$

It must be pointed out, that although the reactions for the CO_2-NaOH system and CO_2-MEA systems proceed in similar fashion, the reaction products of the CO_2-NaOH system are much more stable. The overall reaction between CO_2-NaOH presented as Equation 2.38, is considered irreversible (Tsai 2010). It is this irreversibility that makes regeneration of NaOH solvent practically impossible.

CHAPTER III

SPRAY FUNDAMENTALS

The objective of this chapter is to introduce terminologies commonly used in spray literature. In this chapter, an introduction to sprays, process of atomization, dropsize quantification, and Phase Doppler Interferometry (PDI), will be made.

III. 1. Introduction to sprays

Sprays are widely used in the chemical industry. Humidification, flue gas desulfurization, particulate removal and gas conditioning are some of the most common operations in chemical engineering utilizing sprays (Rousseau 1987; Mycock, Mckenna *et.al.* 1995). Sprays can be defined as dynamic systems of gas-liquid interactions in which the liquid is dispersed in the form of droplets, while the gas is continuously entrained (Lipp 2013a). The dynamic nature of sprays can be attributed to the momentum exchange between the dispersed liquid droplets, and the continuous gas.

Atomization is the process of break-up of liquid sheets or jets into droplets (Lefebvre 1988). Drops are formed by forcing liquid through a small opening in the nozzle under pressure. The emerging liquid in the form of ligaments or jets is inherently unstable and starts breaking up. These separated ligaments and jets eventually fold into, and contract into liquid droplets downstream of the nozzle tip.

III.2. Spray characteristics

Spray characteristics provide a qualitative and quantitative description of the spray. Spray characteristics can help in nozzle selection (Lipp 2014). Figure 3.1 shows most of the spray characteristics.

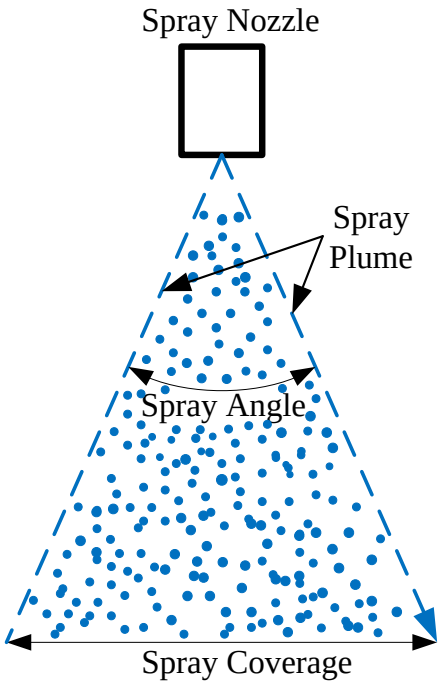

Figure 3.1. Spray characteristics
[Adapted from Lipp (2013a)]

III.2.1. Spray pattern

A spray pattern is a qualitative description of the distribution of the liquid in the area wetted by the spray. This liquid distribution is visualized / looked at from the top of the spray as seen in the Figure 3.2 below. Commercial nozzles produce one of four commonly seen patterns: full cone, hollow cone, flat fan, or solid stream (Lipp 2014; Schick 2014). For applications involving sprays inside columns, a full cone nozzle, which distributes the liquid uniformly inside the plume is recommended (Lipp 2013a). Pagcatipunan, and Schick (2005) provide a summary of the typical spray patterns and their applications.

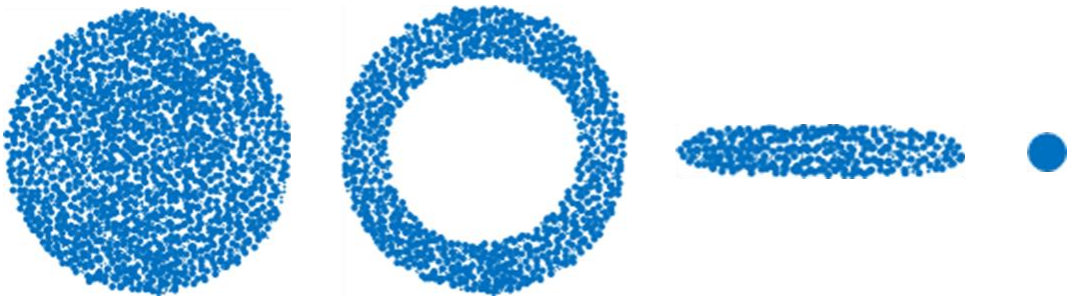

(a) (b) (c) (d)

Figure 3.2. Spray patterns; (a) – full cone; (b) – hollow cone; (c) – flat fan; (d) – solid stream [Adapted from Lipp (2013a); Pagcatipunan, and Schick (2005)]

III.2.2. Spray angle

The spray angle is the initial angle formed by exiting fluid streams at the boundary of the spray plume. Typically, commercial nozzle vendors provide a singular spray angle number at a fixed supply pressure or liquid flowrate. Knowledge of the spray angle can help in deducing the spray coverage downstream of the nozzle. Inside a column, a spray with a larger angle will provide greater coverage at shorter distances downstream of the nozzle than spray with a smaller angle. However, a large spray angle can also lead to the spray plume hitting the column wall at a short distance downstream of the nozzle.

III.2.3. Spray coverage

The spray coverage is the radial distance between the extremities of the spray plume at a given distance downstream of the nozzle. Under the assumption of a uniform spray angle, the spray coverage can be calculated using Equation 3.1 as follows:

$$C_r = 2\, Z_S \tan\left(\frac{\theta}{2}\right) \qquad (Eq\ 3.1)$$

where,

Cr = coverage, m

Zs = axial distance downstream of the nozzle, m

θ = spray angle

III.3. Dropsize

III.3.1. Typical average diameters

A commercial spray nozzle produces a range of drop sizes. A summary of the typical diameters used to quantify dropsize distributions are tabulated below.

Table 3.1. Typical average drop diameter definitions (Mugele 1960; Winter 1974)

Diameter / Parameter	Symbol	Formula	Applications / Description
Arithmetic mean	D_{10}	$\frac{\sum_i n_i \, {d_i}^3}{\sum_i n_i}$	Evaporation applications
Surface area mean	D_{20}	$\sqrt{\frac{\sum_i n_i \, {d_i}^3}{\sum_i n_i}}$	Surface area controlling applications; absorption
Volume mean	D_{30}	$\sqrt[3]{\frac{\sum_i n_i \, {d_i}^3}{\sum_i n_i}}$	Volume controlling applications; hydrology
Sauter mean	D_{32}	$\frac{\sum_i n_i \, {d_i}^3}{\sum_i n_i \, {d_i}^2}$	Efficiency calculations, mass transfer rates, reactions
10% Volume	$D_{V0.1}$	-	10% of the drops are that size or lower by volume
90% Volume	$D_{V0.9}$	-	90% of the drops are that size or lower by volume
Volume median	$D_{V0.5}$	-	50% of the drops are that size or lower by volume
Relative span factor	RSF	$\frac{D_{V0.9} - D_{V0.1}}{D_{V0.5}}$	Compare dropsize from various nozzles
Maximum stable	D_m	-	Drops that size or greater break-up during their lifetime

III.3.2. Effect of liquid and gas rates

Increasing the liquid rate through a nozzle results in smaller dropsizes. Increasing the liquid rate through a nozzle invariably involves increasing the supply pressure which provides greater energy for atomization. Increasing gas rate results in premature breakup of liquid sheets or jets (Liu 1999). Increasing the relative velocity of gas has been found to lower the minimum break up

wavelength of oscillating jets emerging from the nozzle tip (Liu 1999; Webber 1931). The diameter of drops emerging from these disintegrating jets is proportional to the wavelength of oscillation (Liu 1999; Webber 1931). Hence, increasing gas rate results in smaller dropsize.

III.3.3. Effect of liquid physical properties

Physical properties of viscosity, surface tension, and density are known to affect the dropsize emerging from commercial nozzles. An increase in viscosity and surface tension results in an increase in the dropsize. Increased viscosity and or surface tension results in an increase in the energy requirement for atomization (Schick 2014). An increase in density of the liquid is found to lower the dropsize.

III.3.4. Uncertainties in dropsize measurements

Dropsize measurements can be deduced from a multitude of techniques. No two techniques are alike with regards to set up, limits of measurements, and post processing. Dodge (1987) provides a summary of performance comparison of multiple dropsize techniques. Two challenges are frequently encountered in spray measurements. The first, is to assess the accuracy of dropsize measurements. The second is to determine the reproducibility of measurements.

Dropsize measurement techniques can differ significantly from each other, and hence it is hard to ascertain the accuracy of dropsize measurements. Even within each technique, the accuracy of dropsize measurements depend greatly on the optical and, post processing settings, and the location of measurement within the spray plume (dense or diffused regions). A need for the development of a primary standard for spray measurements is felt (Lipp 2013a). To get better confidence in the accuracy of dropsize measurements, one or more techniques can be employed. Thus, ascertainment of the accuracy of dropsize measurements is non-trivial.

Repeatability of dropsize measurements can be checked by making multiple measurements at the same location, and conditions. Repeatability of dropsize measurements is greatly affected by the

number of drops sampled (number count) during measurement. According to Lipp (2013a), most sprays require 50, 000 sampling points to ascertain the uncertainty. However, collection of such large sampling numbers may not be feasible due to limitations on the solvent inventory (for non-water systems), reaction time, and number of measurement points within the spray plume (for a fixed experimental run period). A second method to ensure repeatability of measurements is to check the variability in the average diameter values over multiple runs. In case of reactive systems, the variation in Sauter mean diameter can be checked over multiple runs. According to Schick (2014), dropsize measurements within ± 6% of each other are considered the same. Thus, by collecting a large enough sample, and checking the repeatability of Sauter mean (or another statistical average) over multiple measurements, the reproducibility can be ascertained.

III.4. PDI

Phase Doppler Interferometer (PDI) is the state of the art system for characterizing liquid sprays. PDI systems can simultaneously measure velocity, size and concentration of liquid drops in a spray. Since, the instrument measures phase shift and frequency shift of light, as opposed to light intensity, the instrument is less susceptible to signal degradation. Moreover, the instrument provides a direct measurement of the drop size and velocity, and as such requires no calibration (Lipp 2013a,). The PDI is considered as the most versatile spray diagnostic instrument today (Lipp 2013b, Bade 2014). However, due to its point nature, multiple locations within the spray plume need to be sampled with the PDI to get a representative description of the spray characteristics.

The origin of the present day PDI system can be traced to the work of Bachalo (1980) and then Bachalo and Houser (1984). Early measurement techniques for characterizing dropsize and velocity, were limited by high spray density, small size (< 200 μm), and inability to measure velocity and size simultaneously (Bachalo 1980, Albrecht, Borys *et.al.* 2003). Bachalo (1980)

described how scattered light from spherical particles resulted in a phase shift of light, which in turn could be used to measure diameter of that particle.

III.4.1. PDI Technique

The PDI/PDPA (Phase Doppler Particle Analyzer) system consists of a laser transmitter, receiver, signal processor and software for processing the data as shown in Figure 3.3. The laser transmitter emits two laser beams which intersect at a point creating the measurement or probe volume. As the liquid drop moves across the measurement volume, it creates a sweeping interference pattern (bright and dark bands) across the aperture of the receiver. Measurement of the 'Doppler shift' and the phase shift at the off-axis receiver permits calculation of drop velocity and diameter, respectively (Bachalo 1980; Bachalo and Houser 1984).

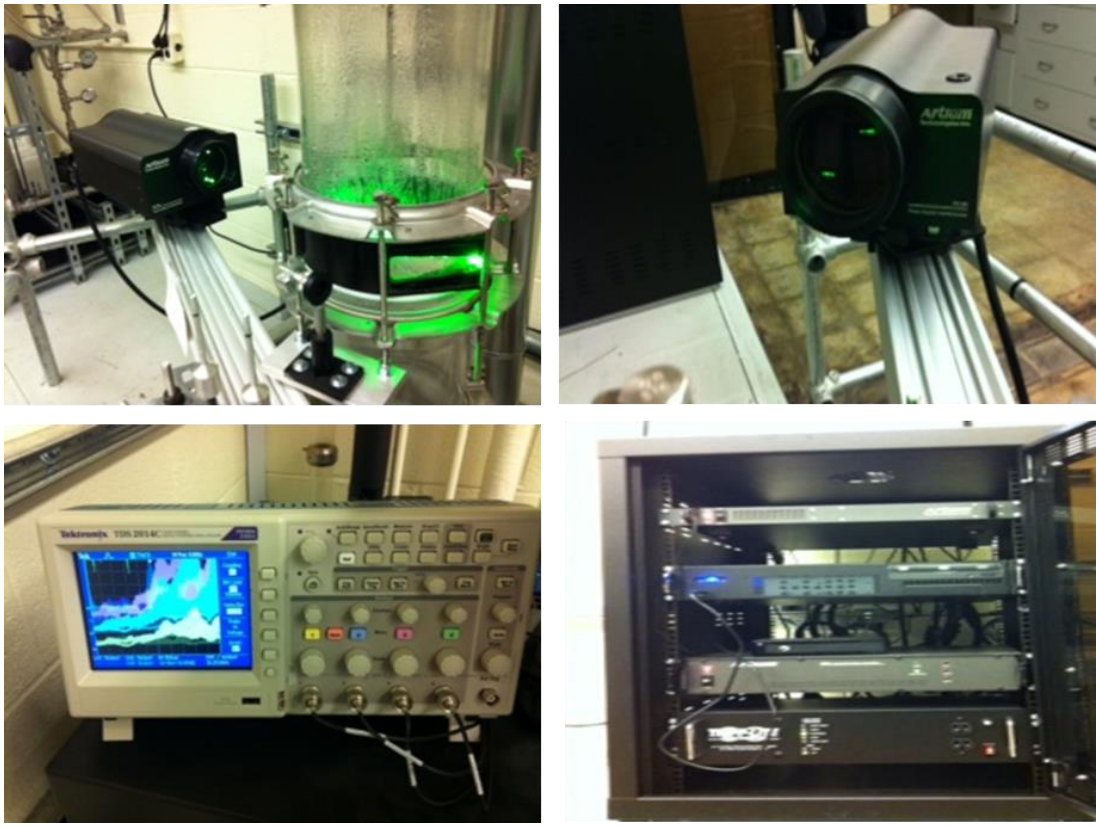

Figure 3.3. PDI components

Top row (left to right) – Transmitter, Receiver

Bottom row (left to right) – Oscilloscope, Signal processors

III.4.2. Effect of variables

The following section provides a brief qualitative summary of the effects of some of the manipulated variables on the PDI performance. Knowledge of these variables greatly helps in practical operation of the PDI.

III.4.2.i. Acquisition time/number of data points

The PDI data acquisition can be set up in two modes; acquisition period (or time), and the number of points recorded. By keeping the acquisition period constant during a radial traverse, the total volume captured by the PDI as a fraction of the total liquid sprayed can be easily computed. The acquisition period or the number of data points recorded can be increased to improve the reproducibility of results.

III.4.2.ii. Focal length

The PDI transmitter and receiver have lenses attached to them. Each lens has a characteristic focal length. Short focal lengths improve sensitivity of the PDI to small drops. Larger focal length lenses are required to measure large drops. Reducing the focal length results in a smaller probe area and better resolution.

III.4.2.iii. PMT gain

The three detectors in the PDI receiver are made up of Photo Multiplier Tubes (PMT). These tubes convert images of scattered light in to electrical signals. Each of these tubes has a 1000 mV detection limit. If a majority of the drops passing through the probe area result in electric signals around the 1000 mV range, then saturation errors become significant. Proper adjustment of the PMT gain is key in ensuring saturation errors do not become significant.

By changing the gain setting of PMT tubes, the PDI can be made sensitive to either large drops or small drops. Increasing the PMT gain makes the PDI more sensitive to small drops, and vice-versa. The increasing PMT gain results in reduction of the probe area.

III.4.2.iv. Aperture width

A prime limitation of the PDI technique is that only one drop at a time can be present in the probe area. Presence of more than a single drop results in coincidence errors (Bade 2014). The slit aperture width can be manipulated to limit the size of the sample volume in the receiver slit. For dense sprays, a small aperture width is required. Selection of too small an aperture width can result in recording of a small number count by the PDI. The acquisition period or number of drops recorded may need to be increased to compensate for the lower number count.

CHAPTER IV

LITERATURE REVIEW

The prime objective of this chapter is to provide a review of the work of previous researchers. The review is limited only to mass transfer / absorption studies inside spray columns. It should be noted that the equations presented in this chapter are associated with the units used by the corresponding investigators in their work.

Earliest investigators of spray columns focused on developing mass transfer correlations to aid design of spray columns. These equations sought to establish an observed relationship between the mass transfer coefficients and the gas rate, liquid rate, and the column height, respectively. Typically, absorption experiments were run in lab scale columns to develop these correlations.

Hixson and Scott (1935) performed absorption experiments in a lab scale spray column (7.3 cm diameter and variable height of 48-137 cm). Ammonia-water, sulfur dioxide-water, and benzene-oil were the systems tested. The objective of their work was to evaluate the effects of the gas rate, liquid rate, and column height on the overall mass transfer coefficient. The observed experimental data was used to develop their correlation presented below as Equation 4.1. Bonilla, Motles and Wolf (1950) also came up with a similar expression.

$$K_G a_e = \frac{2.97 \times 10^{-5} G'^{0.8} L'^{0.9}}{Z^{0.5}} \qquad (Eq\ 4.1)$$

Where,

$K_G a_e$ = mass transfer coefficient, lb/min.ft^3.mm Hg

G = specific gas rate, lb/ft^2.min

L = specific liquid rate, lb/ft^2.min

Z = column height, ft.

Pigford and Pyle (1951) tried to check the performance of spray absorption columns. Rates of absorption of oxygen and ammonia, evaporation rates of water, and desorption rates of oxygen into air were measured in 12 inch diameter and 31.5 inch diameter spray columns of varying heights. Because of fresh liquid surface generation, high rates of mass and heat transfer were observed in regions close to the spray nozzle. The number of transfer units per column height was found to be lower for tall columns. The number of transfer units was found proportional to the liquid rate.

Ranz and Marshall (1955) investigated the evaporation of water drops. For transfer to and from drops in motion relative to the gas stream, the mass transfer coefficient was calculated using Equation 8. Such an equation was previously presented by Frossling (1938) and later confirmed by Bose and Pei (1964).

$$S_h = 2 + 0.6\, {R_e}^{0.5}\, {S_c}^{0.3} \qquad (Eq\ 4.2)$$

$$S_h = \frac{R\ T\ k_g\ d}{D_{CO2,g}} \qquad (\text{Eq } 4.3)$$

$$R_e = \frac{Q_g\ \rho_g\ d}{A_c\ D_{CO2,g}} \qquad (Eq\ 4.4)$$

$$S_c = \frac{\mu_g}{\rho_g\ D_{CO2,g}} \qquad (Eq\ 4.5)$$

Where,

k_g = local gas side mass transfer coefficients, kmol/m^2.s.Pa

D = diffusivity, m/s^2

Q_G = gas rate, m^3/s

ρ_G = density of gas, kg/m^3

μ_G = viscosity of gas, kg/m.s

d = hydraulic diameter, m

A_c = cross sectional area of column, m^2

R = gas constant = 8.314, J/mol k

T = temperature, K

Mehta and Sharma (1970) evaluated the effects of gas rates, liquid rates and drop size on the volumetric liquid and gas side mass transfer coefficients ($k_l a_e$ and $k_g a_e$) and the interfacial area (a_e), respectively. Four spray nozzles (1plate type and 3 full cone) were tested in two spray columns of varying heights. Absorption of CO_2 in water, SO_2 in NaOH, and CO_2 in NaOH were used to measure the liquid side mass transfer coefficient ($k_l a_e$), gas side mass transfer coefficient ($k_g a_e$) and, the interfacial area (a_e), respectively. The amount of gas absorbed was found to be a function of the surface area of the drops, relative velocity of the drops and residence time of the drops in the column. It was found that the physical properties of viscosity and density had no effect on the drop size. Increasing gas rate was found to increase both the liquid and gas side mass transfer coefficients. At high gas velocities, $k_l a_e$ and k_l were found to be proportional to 1.03 and 0.66 power of liquid rate, respectively. On the other hand, at low gas velocities, $k_l a_e$ and k_l were proportional to the 0.78 and 0.36 power of liquid rate, respectively. Increasing oscillation of liquid drops and increased internal circulation were the reasons attributed to explain this trend. The gas side mass transfer coefficient ($k_g a_e$) was found to be proportional to the 0.78-0.82 power of gas velocity. The interfacial area (a_e) was found to increase with both the liquid and the gas velocity, respectively. The interfacial area (a_e) was found to vary from 30 – 75 m^2/m^3.

Pinnilla, Diaz and Coca (1984) evaluated the mass transfer coefficients in the gas phase, liquid phase, interfacial area, and axial dispersion using a solid cone nozzle. The spray column used consisted of two sections: a 0.95 m high, 0.45 m diameter top section; and a 0.5 m high, 0.3 m diameter bottom section. The smaller bottom section minimized the gas backflow. The gas phase mass transfer coefficients were evaluated for a SO_2-NaOH system, while the liquid phase mass

transfer and interfacial areas were determined by absorbing CO_2 into a carbonate-bicarbonate solution, respectively. Gas and liquid phase dispersion measurements were carried out by observing the response of the streams to tracer injections, SO_2 and KCl, respectively. The volumetric gas side mass transfer coefficient ($k_g a_e$) was found to vary as the 0.82 power of the gas flow rate and 0.95 power of the liquid flow rate. Unlike the findings of Mehta and Sharma (1980), the liquid mass transfer coefficient was found to decrease with increasing liquid rate. Reduction in drop size and hence the internal circulation with increasing liquid rate were reasons provided to explain this trend. Liquid flow rate was found to have marginal effect on the gas phase axial dispersion. At a fixed liquid rate, the gas phase axial dispersion remained constant till a gas velocity of 1.2 m/s was reached. Beyond this gas velocity, the gas phase axial dispersion was found to increase with increasing gas rate. The liquid and gas flow rates employed in their work were found to have no effect on the liquid phase axial dispersion.

Taniguchi (1997) measured the absorption rates of CO_2 into water (physical absorption) and NaOH (chemical absorption) over a wide range of liquid and gas rates in an acrylic resin spray column (0.18 m diameter, 0.5 m height). A 0.78 mm orifice diameter nozzle was used (Spray Systems Co. Type ¼ TDD1-35). Taniguchi concluded that drop coalescence, collisions and secondary break-up were insignificant. Internal circulation of drops and oscillation had negligible impact on the physical absorption rates. Absorption rates of CO_2 into NaOH were well predicted by the solid sphere model (Carslaw and Jaeger 1959). Taniguchi (1999) later extended the study to the NH_3-Water system. The absorption rates were found to be affected by both the gas phase and liquid phase resistances in the vicinity of the exit nozzle. The gas phase mass transfer flux showed good agreement with the model of Ranz and Marshall (1955).

Dimiccoli, Serio and Santacesaria (2000) investigated mass transfer rates in physical ($CO_2 – H_2O$) and chemical absorption (ethoxylation of nonpolyphenol and fatty acids, and CO_2- NaOH) in a concurrent spray contactor. Droplets produced by their spray nozzle were quantified in terms of the

mean diameter and distribution, mean flight path of the drops and the average flight time of drops. The drop size distribution, measured using a laser scattering technique, was found to remain unchanged at different locations in the spray cone and with time, indicating drop coalescence to be insignificant. The absorption data indicated that the mass transfer flux occurring at the inner wall was insignificant compared to the flux during the drop flight. Further, the drop flight absorption data was analyzed using the approaches of both Crank (1957) (considering the droplets to be internally stagnant), and Srinivasan and Aiken (1988) (with the droplets to be internally well mixed). The approach of Srinivasan and Aiken (1988) closely matched the experimental data. However, for the CO_2-NaOH system, an enhancement factor correction was required to account for the increase in absorption rates due to the fast reaction between CO_2 and NaOH.

Yeh and Rochelle (2003) investigated liquid phase mass transfer in a laboratory scale and pilot scale spray column by desorbing CO_2 from an Air-Water system. A quench sampling technique was employed to reduce mass transfer during sample collection. The mass transfer occurring in the spray zone was modeled as the sum of the contributions of the sheet break-up and drops separately. It was found that sheet break-up accounted for almost 60% of the liquid transfer units in the spray zone. Contributions of spray impact on column wall and liquid pool were significant and accounted for almost half of the total liquid transfer units.

Kuntz (2006) was the first to study absorption of CO_2 into dispersed MEA inside a small lab scale spray column. Effect of liquid rate, gas rate, CO_2 gas composition, loading, MEA concentration, and nozzle size on the mass transfer rate was ascertained. The mass transfer rate was quantified in terms of the overall mass transfer coefficient ($K_G a_e$). Further, an attempt was made to split $K_G a_e$ into the local liquid side mass transfer coefficient (k_g'), and the interfacial area (a_e). The interfacial area was calculated based on the Mugele (1960) correlation to compute the maximum stable dropsize diameter (D_m). k_g' was calculated analytically based on the assumption of pseudo 1st-order reaction similar to the calculation of a_e with low normality Sodium Hydroxide (NaOH) as the solvent.

Turpin, Couvert *et. al.* (2008) measured interfacial areas in a glass spray column (0.15 m diameter and 1 m height) using the CO_2-NaOH system. The interfacial area was deduced from Equations 4.6 and 4.7 below.

$$a_e = \frac{N_{CO2}}{V\ \Delta {C_{CO2}}^* \sqrt{D_{CO2} k_2 C_{NaOH}}} \qquad (Eq\ 4.6)$$

$$\Delta {C_{CO2}}^* = \frac{\left({C_{CO2,in}}^* - {C_{CO2.out}}^*\right)}{ln\left(\frac{{C_{CO2,in}}^*}{{C_{CO2,out}}^*}\right)} \qquad (Eq\ 4.7)$$

Where,

a_e = interfacial area, m^2/m^3

N_{CO2} = flux of CO_2, kmol/s

k_2 = reaction constant, m^3/kmol.s

C = concentration, kmol/m^3

D = diffusivity, m^2/s

Further, the interfacial area inside the spray column was found to be strongly dependent on the gas velocity, and practically independent of the liquid velocity. Their data was used to develop the following correlation for the interfacial area.

$$a_e = 294\ {U_l}^{0.01}\ {U_g}^{0.87} \qquad (Eq\ 4.8)$$

Where,

U_l = superficial liquid velocity, m/s

U_g = superficial gas velocity, m/s

Javed, Mahmud *et.al.* (2010) studied the performance of swirl gas flow to spray CO_2 capture by absorbing CO_2 in NaOH. Effect of gas and liquid rates, counter flow and co-flow arrangements, scrubber height, and nozzle type on the mass transfer coefficients was evaluated. Effect of swirl gas flow was found to enhance mass transfer rates significantly. Further, the counter current gas liquid flow arrangement was found to provide greater mass transfer rates.

Koller, Wappel *et.al.* (2011) measured cyclic absorption rates of CO_2 inside a pilot plant size spray column. 30 wt% MEA was used as the test fluid. The study attempted to mimic real-world, CO_2 absorption from flue gas exhaust of power plants. The mass transfer performance of the pilot spray column was quantified in terms of the %CO_2 removal efficiency. Effect of L/G ratio, and nozzle size on the % CO_2 removal efficiency was ascertained.

Bandyopadhyay and Biswas (2012) investigated CO_2 capture in a Perspex Spray column (0.19 m diameter and 2 m height) using NaOH as the solvent. The spray nozzle employed in their study was a two-phase critical flow atomizer capable of producing very fine and uniform spray. The mean droplet size and the size distribution were measured using a Phase Doppler Particle Analyzer (PDPA). The interfacial area provided by the spray column (with the two phase atomizer) was measured experimentally using the standard chemical technique. Further, an equation for the interfacial area was proposed to correlate their data as shown below.

$$a_e = 200\ {Q_{CO2}}^{-0.6465}\ {U_g}^{0.7481}\ {Q_l}^{0.4362} \qquad (Eq\ 4.9)$$

Where,
a_e = interfacial area, m^2/m^3
U_g = superficial gas velocity, m/s
Q_{CO2} = CO_2 flowrate, l/h
Q_l = liquid flowrate, m^3/s

In spite of the moderate availability of spray absorption literature, the following gaps listed below are observed.

1. There is a need to measure mass transfer rates in terms of K_Ga_e for CO_2-MEA system robustly. In the work of Kuntz (2006), K_Ga_e measurements were confined to only the spray zone inside the column prior to the spray plume reaching the wall. The height of this spray zone was never quantified or measured experimentally. Since, absorption

measurements were conducted in only the spray zone, contribution of wall flow to absorption could not be ascertained. Contribution of wall flow in small sized spray columns can be significant and result in loss of surface area (Lipp 2013b). Koller, Wappel *et. al.* (2011) never quantified performance of the spray contactor in terms of $K_G a_e$. Further, variations in the inlet loading, and concentration of MEA were not reported.

2. Effect of amine concentration on spray absorption rates must be analyzed further. Unlike packed columns, increasing MEA concentration has been found to increase the absorption rates inside spray columns (Strigle 1994; Kuntz 2006). Kuntz (2006) attributed this rate increase to the increasing free MEA content. However, the effect of increasing concentration on the area of gas-liquid contact was never robustly calculated. Hence, the contribution of free MEA content on the absorption rates might have been under-predicted.
3. For the CO_2-MEA system, no attempts have been made to measure dropsizes across the spray plume experimentally. Utilization of dropsize measurements in computing surface areas has been rarely attempted (Tamhankar, King *et. al.* 2014b). Estimates of average dropsize in sprays based on correlations can differ significantly from experimental measurements. Quantification of the surface area or interfacial area based on singular, average dropsize estimates such as D_m or D_{32}, can lead to erroneous results. Typically, a range of dropsizes is encountered inside the spray plume. Further, dropsize distributions vary with location inside the spray plume. Computation of available area for gas-liquid contact based on singular estimates can thus be unrealistic.
4. Interfacial area measurements inside spray columns can provide insight into surface area availability. Correlations developed by Turpin, Couvert *et. al.* (2011), and Bandyopadhyay and Biswas (2012) are not scalable. The interfacial area computed in both correlations is independent of the nozzle characteristics which is unrealistic. Effect of nozzle geometry,

and hence dropsize on the interfacial area needs to be ascertained and accounted for in such correlations for robustness.

CHAPTER V

EXPERIMENTAL METHODS & CALCULATIONS

The main purpose of this chapter is to describe the methods and calculations adopted in order to complete the objectives laid out in the introduction section. In this chapter, the equipment description and setup, procedure for experiments, details of supporting methods, and calculations used are detailed. A detailed vendor list provided in Appendix H, should aid in any re-building or modification efforts in the future.

V.1. Experimental setup

The overall experimental setup can be divided into the following sections; the spray column, gas injection, solvent feed and sump, spray nozzle, and the PDI. Details of each section are outlined below. The overall setup is outlined in Figure 5.1.

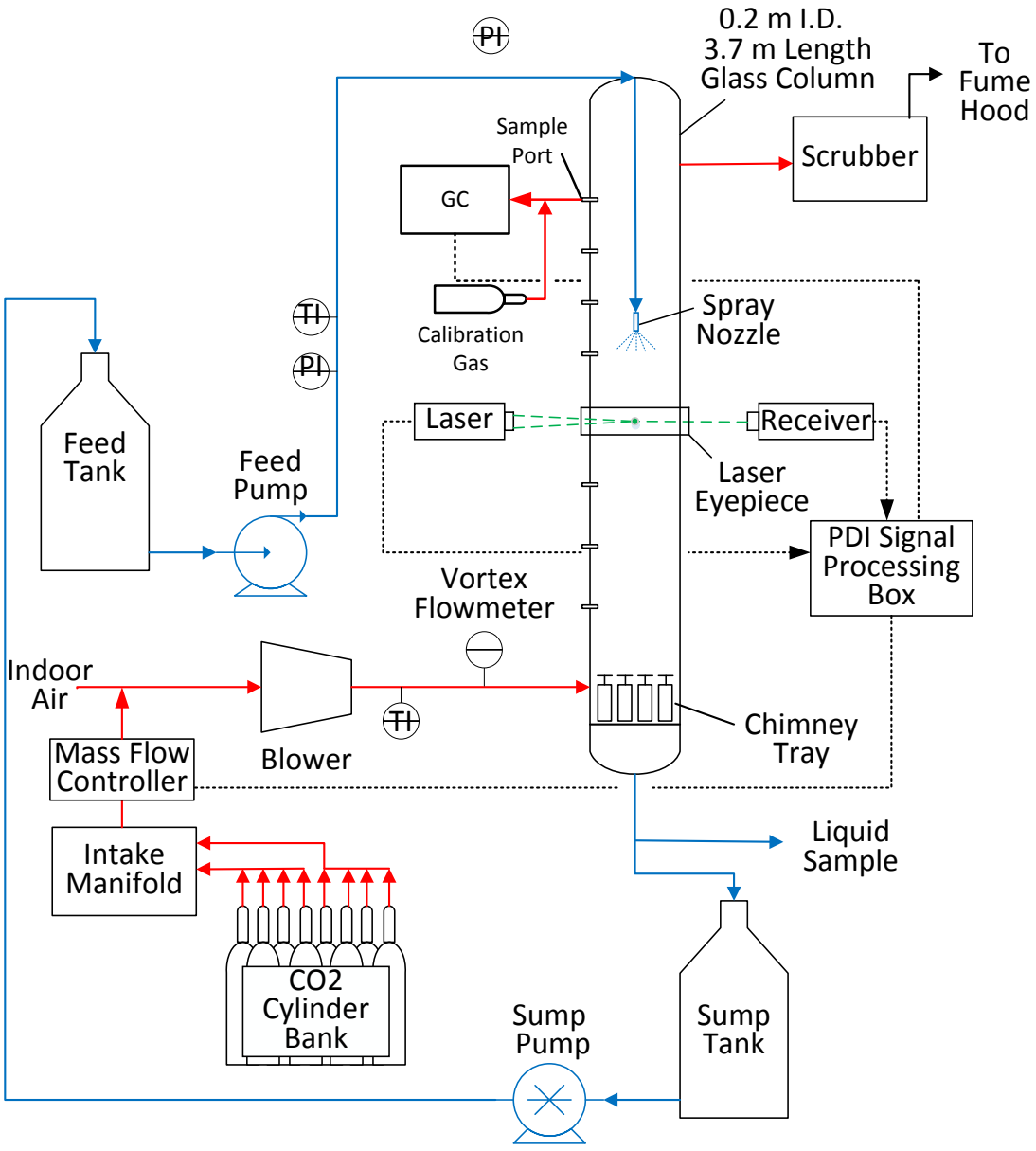

Figure 5.1. Experimental setup

V.1.1. Spray column

The spray column is made up of nine, 0.3048 m (12 inch), 0.2027 m (7.98 inch) ID borosilicate glass (QVF® SUPRA) sections. Cylindrical column head and sump sections provide outlets for nozzle entry, and solvent exit, respectively. The total height of the column is approximately 3.7 m

(12 feet). The column was located between two floors and supported on unit-struts attached to the building wall. Figure 5.2 shows the top and bottom sections of the column.

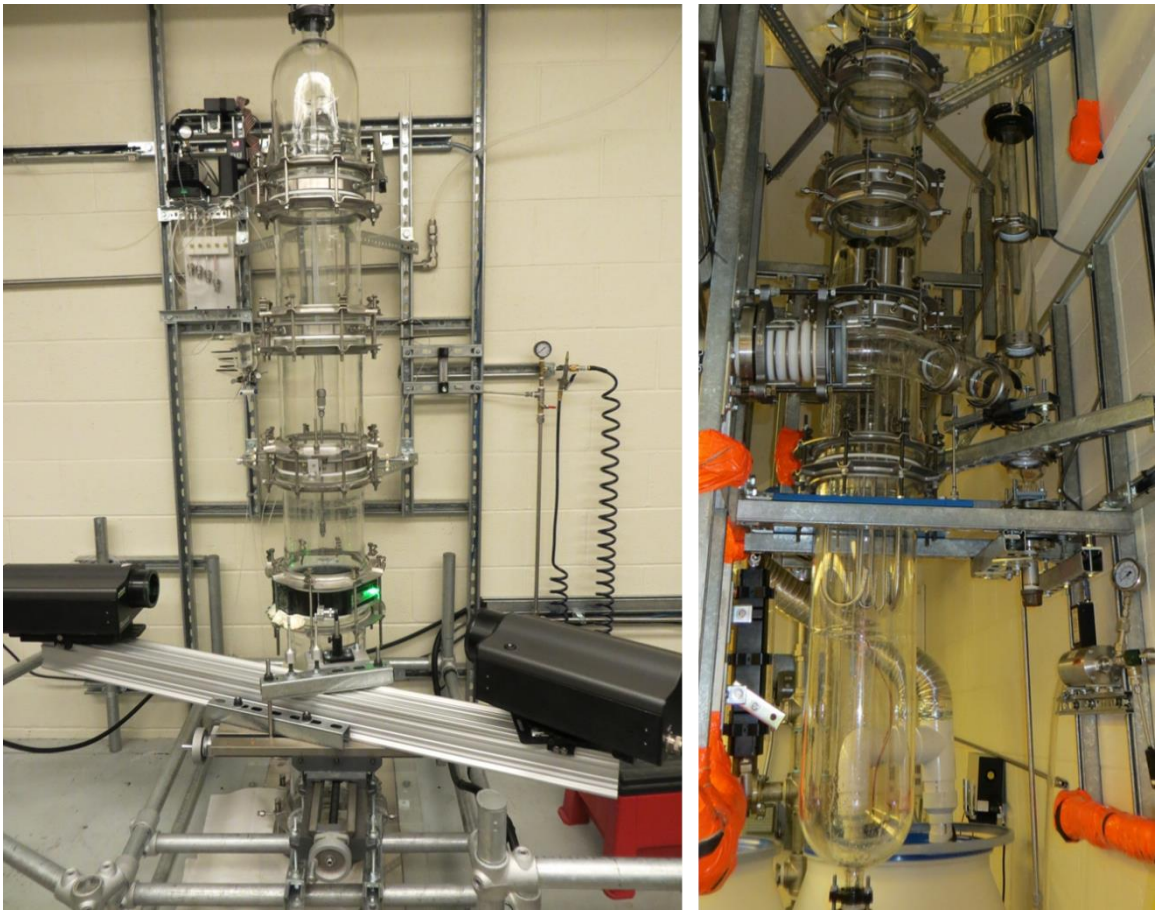

Figure 5.2. Top and bottom sections of the spray column

Before connecting two glass sections, 0.0254 m (1 inch) stainless steel custom plates where inserted between the two glass sections. Each custom plate had four, 0.0064 m (¼-inch) NPT bored holes which permitted insertion of stainless steel tubes to remove gas samples for composition analysis. Teflon gaskets where placed on top and bottom of these custom plates. Glass sections above and beneath each custom plate were placed on the custom plates and aligned so that the inner wall of the two glass sections and the custom plate formed a smooth continuous surface and then flanged together. Figure 5.3 shows the two adjoining glass sections with the custom plate between, and the custom plate with NPT bores.

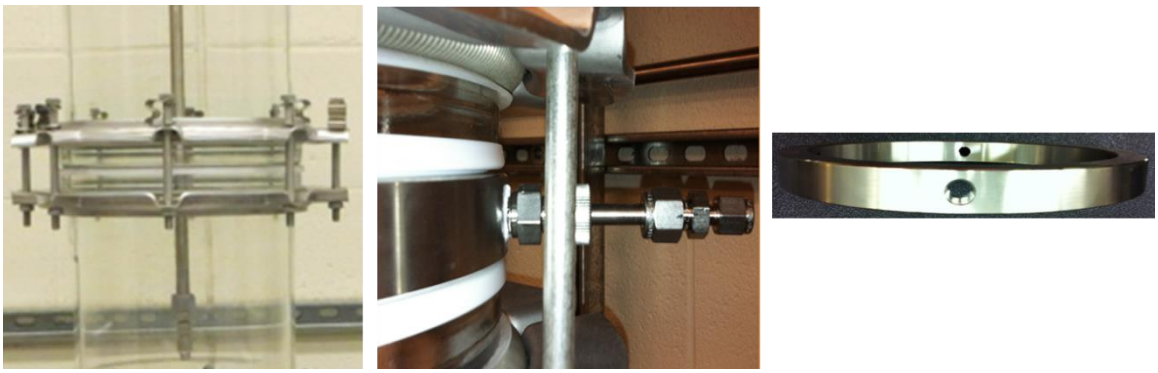

Figure 5.3. Connection of two glass sections and custom insert plate

The bottom section of the column consists of a cylindrical sump section, glass tee section, and a chimney tray section. The liquid exit opening on the cylindrical sump section had an ID of 0.025 m and ensured a liquid seal at the bottom for all experimental conditions. Counter current gas for all of the experiments is injected into the spray through the glass tee. The chimney tray is located above the glass tee section. The chimney tray consists of seven chimneys with circular windows and a roof. The main purpose of the chimney tray is to minimize the gas liquid contact at the bottom of the column. Pictures of the gas injection tee and the chimney tray are presented below as Figure 5.4.

Figure 5.4. Gas injection tee and chimney tray

The spray nozzle is introduced into the spray column through the central opening on the cylindrical column head. The spray nozzle is attached to a 0.2032 m (8-inch) long, 0.0064 m (1/4-inch) diameter stainless steel tubing, which is then attached to a 0.0127 m (1/2-inch) diameter

flexible, PFA tubing by means of proper connectors. The nozzle is held inside the column with the help of a custom nozzle holding disc as shown in Figure 5.5 below. By ensuring that the four, 0.3048 m (12-inch) long, stainless steel rods attached to the nozzle holding disc protrude equally inwards, the nozzle and the holding disc can be centered at the geometric center of the column.

Figure 5.5. Nozzle holding disc

[Reprinted from Atomization and Sprays, Volume 24, Y. S. Tamhankar, J. R. Whiteley, M. R. Resetarits, and C. P. Aichele, Spray Droplet Characterization Inside A Glass Column Through Dense Wall Flow, Pgs. 115-128, 2014, with permission from Begell House, Inc]

In order to permit PDI measurements through dense wall flow along the column wall, a custom designed eye-piece was utilized (Tamhankar, Whiteley *et.al.* 2014a). This eyepiece had multiple salient features including: windows located away from the inner periphery of the column wall, provision for forward and backward scatter modes of operation of the PDI, and an air purge on the central slit to prevent liquid build up affecting beam entry into the column (as shown in Figures 5.6 and 5.7 below). Black anodized aluminum was used to construct the main body of the eye-piece, while the glass windows were composed of fused silica (Refractive Index at 500 nm = 1.4623). Black anodized aluminum is non-reactive (after oxidation) and rigid. The black color on the eye-piece prevented secondary reflections.

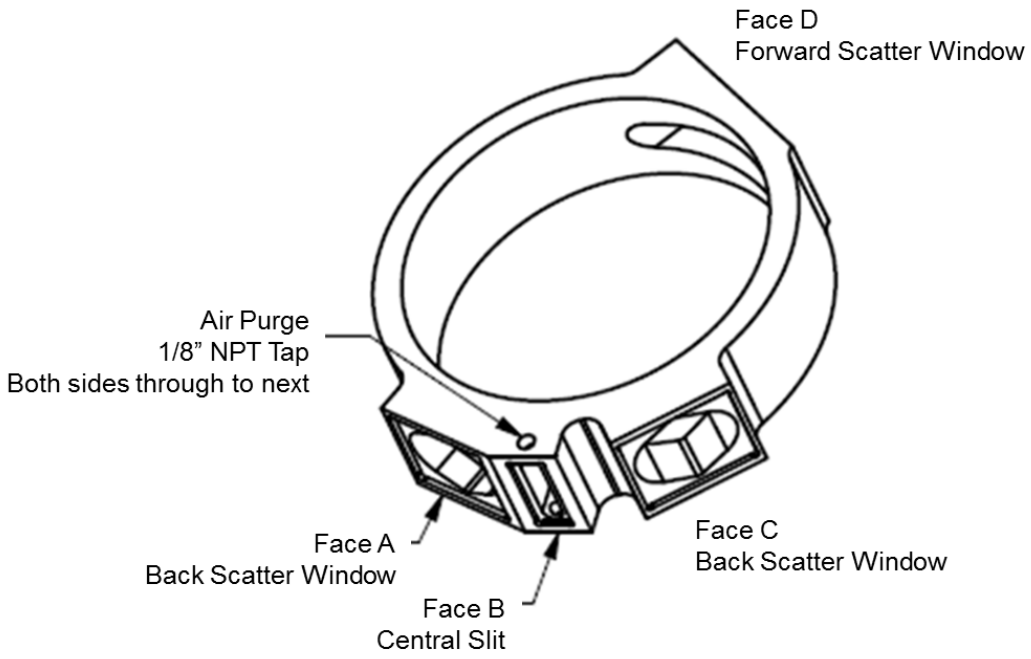

Figure 5.6. Schematic of the eye-piece with all four faces

[Reprinted from Atomization and Sprays, Volume 24, Y. S. Tamhankar, J. R. Whiteley, M. R. Resetarits, and C. P. Aichele, Spray Droplet Characterization Inside A Glass Column Through Dense Wall Flow, Pgs. 115-128, 2014, with permission from Begell House, Inc]

Figure 5.7. Eye-piece with central slit and windows

[Reprinted from Atomization and Sprays, Volume 24, Y. S. Tamhankar, J. R. Whiteley, M. R. Resetarits, and C. P. Aichele, Spray Droplet Characterization Inside A Glass Column Through Dense Wall Flow, Pgs 115-128, 2014, with permission from Begell House, Inc]

The windows on the eye-piece where positioned so as to permit the use of either forward scatter or backward scatter modes of the PDI. The angle between the beam entry and the far side receiver window (forward scatter) centerline was about 140°. A 25° angle existed between the beam entry – left receiver window, while a 35° angle existed between the beam entry and right receiver window. The angles and dimensions of the eye-piece are highlighted in Figure 5.8 below.

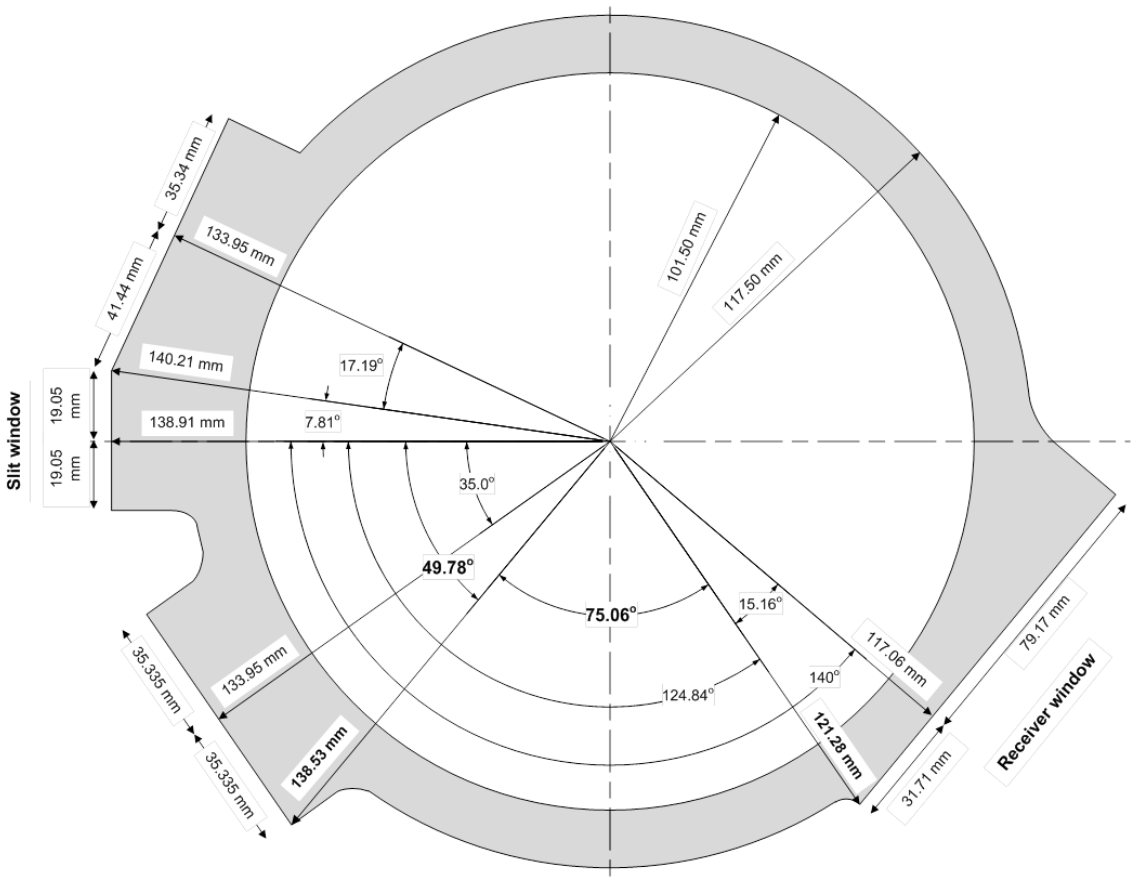

Figure 5.8. Eye-piece dimensions

[Reprinted from Atomization and Sprays, Volume 24, Y. S. Tamhankar, J. R. Whiteley, M. R. Resetarits, and C. P. Aichele, Spray Droplet Characterization Inside A Glass Column Through Dense Wall Flow, Pgs. 115-128, 2014, with permission from Begell House, Inc]

Since the central slit and windows are located away from the inner wall of the spray column, flat glass pieces could be attached to the slit and window openings. Flat glasses prevented any curvature issues that might have resulted from use of rounded glass. A marginal air flowrate of

11 Lit/min was sufficient to prevent build-up of liquid in the central slit window. This low air purge rate ensured that the accumulated liquid did not get blasted into the spray plume thereby affecting the spray plume dynamics.

V.1.2. Gas injection section

The gas injection system consisted of a 3-phase centrifugal blower, CO_2 heater manifold, bank of CO_2 cylinders, mass flow controller for CO_2 injection, and vortex flow meter for measurement of total gas rate into the spray column. Figure 5.9 showcases most components of the gas injection section.

Figure 5.9. Gas injection section

The 3-phase centrifugal blower (Atlantic Blowers, Model AB -800) is capable of delivering up to 11.3 m^3/min (400 ft^3/min) of air at 60 Hz supply frequency. Using a variable frequency drive, the flow rate delivered to the spray column was reduced.

CO_2 from an 8-cylinder bank was injected into the suction piping of the air blower. The CO_2 from the cylinder bank was heated using a two-bank heating manifold (Harris Products Group, Model 220 HL). The manifold ensured uninterrupted CO_2 supply for all experimental runs. When the

CO_2 cylinder bank supply pressure drops to 50 psig, the manifold automatically switches to the second bank.

A Brooks mass flowmeter (Model # 0254/SLA583S) and controller was used to inject the appropriate amount of CO_2 into the suction piping of the blower. In order to ensure sustained delivery of CO_2 to the mass flowmeter at the rated supply pressure, the intermediate piping between the manifold and the mass flowmeter was covered with heat tape coupled to a variable voltage meter. The accuracy of the mass flowmeter was dependent on a supply pressure of 3.4 atm g (50 psig). The manifold heater could only ensure supply of CO_2 gas to the outlet of the manifold. In trial runs, freezing of CO_2 inside the piping downstream of the manifold was observed.

The total gas flow rate supplied to the spray column was measured using a vortex meter (Rosemount, Model # 8800DF010SA1N1D1M5). The vortex meter has a maximum capacity of 3.05 m^3/min (108 ft^3/min). Prior to experimentation, the accuracy of the vortex meter was ascertained with the use of a manometer. The precision of the vortex meter was found to be within ±5%.

V.1.3. Solvent feed & sump section

The solvent feed and sump section consisted of two, 0.0606 m^3 (16 gallon) stainless steel tanks, a centrifugal pump, spray nozzle, and liquid sampling unit. The solvent to be sprayed is charged to the feed tank. In order to pump a small volume of solvent through the nozzle opening, a high head, 316 stainless steel centrifugal pump (Grundfos, Model # A-97568345-P10-1248) was utilized. To control the flowrate of the solvent precisely, a combination of varying pump frequency, throttling of the valves on the pump discharge, and recirculation lines were used. A rotameter on the pump discharge line (Swagelok, VAF-M3-1-2-A9R, Range: 0 – 0.5 GPM) was

used to measure the liquid flowrate. The overall % absolute average deviation (%AAD) for the rotameter over its entire range for the entire range was found to be 0.2%.

The liquid from the bottom of the column is collected in the sump tank. After the feed tank is exhausted, the liquid from the sump tank is pumped back into the feed tank using a positive displacement pump. Thus, the solvent from the first charge to the feed tank is eventually re-used.

Liquid samples are collected from the outlet of the column, by means of a 3-drain valve, liquid sampling unit shown below.

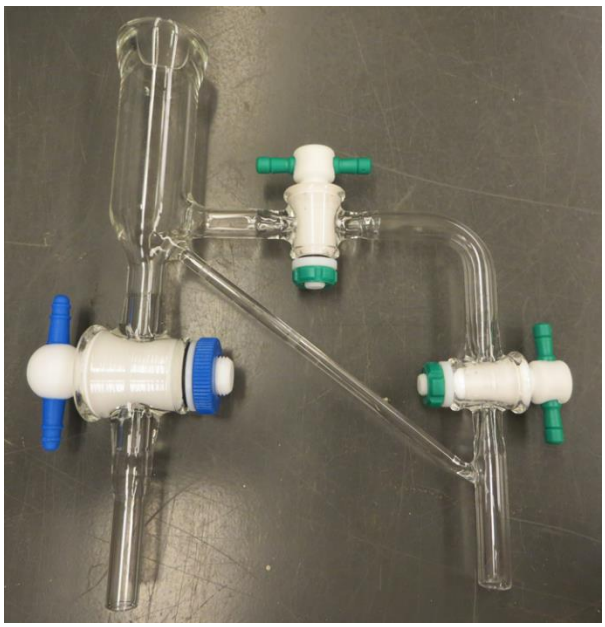

Figure 5.10. 3-drain valve sampling unit

V.1.4. Nozzle

A BETE MaxiPass® L (MPL) nozzle was tested in this work. Details of the nozzle are presented in Table 5.1 below.

Table 5.1. Nozzle details (Bob Bys 2012)

Nozzle: BETE MPL 0.30 N	Type: Full cone, 53^0 at 3 atm
Free passage diameter: 1.1 x 10^{-3} m	Material of Construction: 316 SS
Vendor water data:	
Flow rate: 6.3 – 15.9 x 10^{-4} m^3/min	Supply pressure: 0.7 – 6 atm
Sauter mean diameter: 200 – 120 µm	

V.1.5. PDI system

The PDI system measures droplet size and velocity simultaneously. A 1-dimensional PDI (Artium Technologies, Model # MD-100) was used for this work. The PDI is cable of measuring drops from 2 μm – 200 mm. The PDI system used in this work was set up to measure velocity in the vertical or spray axial direction. Drops moving downward are recorded as having positive velocities, while drops moving upward are recorded as having negative velocities. The optical settings used in the PDI for this work are highlighted in Table 5.2 below.

Table 5.2. PDI settings

Transmitter	Receiver
Wavelength: 532 nm	Front focal length: 500 mm
Focal length: 500 mm	Back focal length: 505 mm
Beam separation: 59.5 mm	Slit aperture: 250 μm
Beam diameter: 2.33 mm	PMT gain: 200 – 375 mV
Acquisition period: 2 minutes	

The PDI was mounted on a two directional rail system as shown in Figure 5.11 below. Movement of the rail system allowed the beam intersection or the probe volume to be moved to multiple locations within the spray plume. Each rail had a (min) division of 2.54×10^{-4} m (0.01 inches).

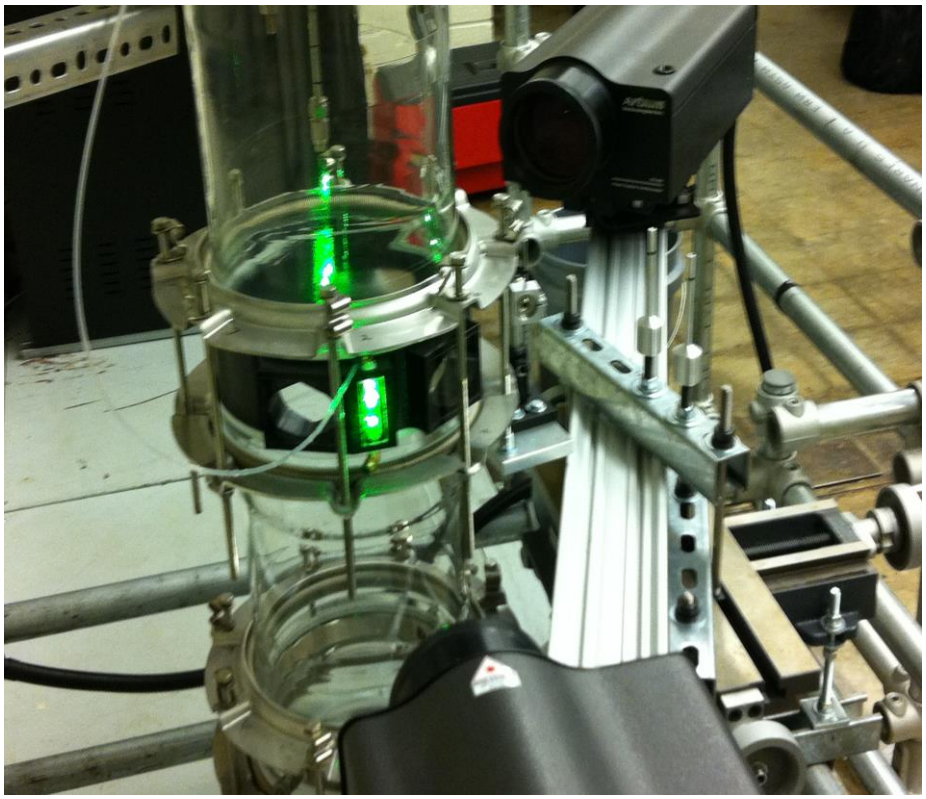

Figure 5.11. PDI system mounted on rail

Since the central slit on the eye-piece is narrow, the probe volume could realistically be moved along the diameter of the column (in a thin line). Further, since the transmitter and the receiver of the PDI are mounted on the same supporting beam, the radial traverse of the beam intersection or probe volume was practically limited to a region along the radius of the column, in line with the slit on the eye-piece, but away from the slit as shown in Figure 5.12.

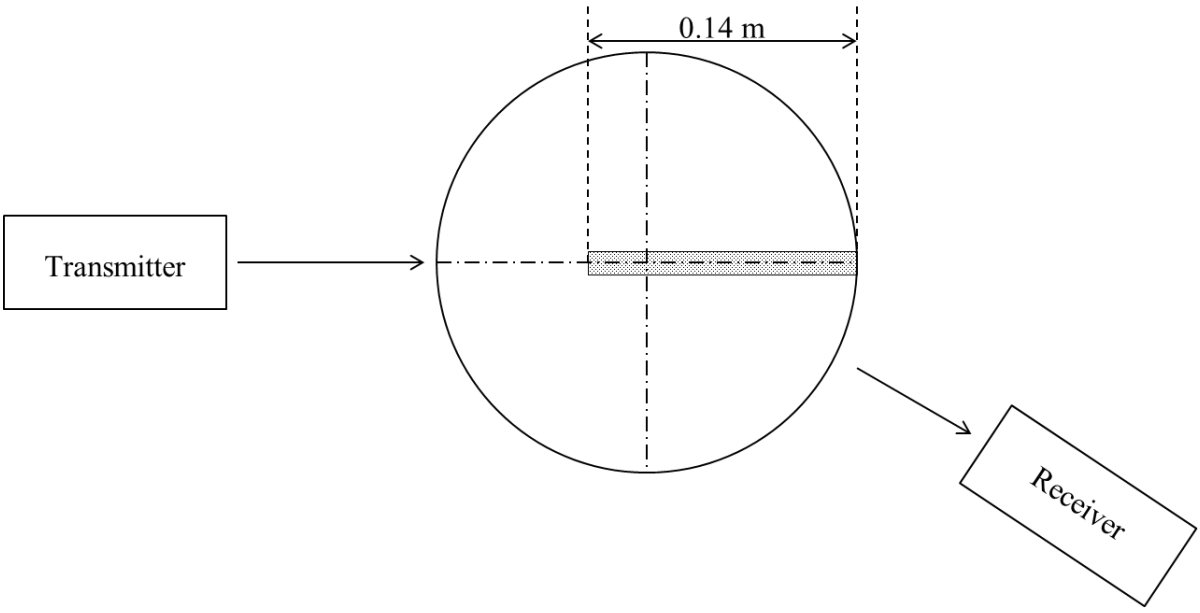

Figure 5.12. Practical range of PDI probe volume movement

V.2. Experimental procedure

Two separate set of experiments were conducted with a CO_2-MEA system; mass transfer rate measurements, and dropsize measurements. A separate campaign for a CO_2-NaOH system for interfacial area measurements was also conducted. The procedure for mass transfer runs described below, is applicable to both the mass transfer rate measurements for CO_2-MEA, and the interfacial area measurements with CO_2-NaOH. Separate operating procedures for individual equipment or components are described in Appendix G.

V.2.1. Mass transfer measurements

The solvent to be used for the experimental runs was prepared and charged to the feed tank. As the 0.015 m^3 charge of solvent was prepared in four batches, the total charge of the solvent was recirculated within the feed tank for about 5 minutes. A liquid sample was then drawn from the feed pump drain line. This sample was later analyzed to check the concentration and inlet loading of the charged solvent. The solvents where mixed initially to the right concentrations gravimetrically. A single batch of unloaded, 30 wt% MEA solution was prepared by mixing 9.28

kg of MEA (98 wt%, Acros Organics) with 20.71 kg of de-ionized water. 12.24 kg of MEA (98 wt%, Acros Organics) was mixed with 18.42 kg of de-ionized water to prepare a batch of unloaded, 40 wt% MEA solution.

The air blower was started at a fixed delivery rate. Once the temperature gauge on the blower discharge line became stable, CO_2 injection into the suction piping of the blower was started. The CO_2 injection rate was controlled using the mass flow meter. After about five minutes of CO_2 injection, the inlet gas was pulled into the online gas chromatograph located at the top of the spray column for ascertaining the CO_2 content of the countercurrent gas. The set point of the mass flow controller was manipulated to ensure that the CO_2 reading from the gas chromatograph was approximately 12%.

Before the gas sample was analyzed by the gas chromatograph, the gas sampling system was prepared. The gas chromatograph sampling system consisted of a knockout condenser, a bank of tubes with Drierite® desiccant and molecular sieves, a vacuum pump, and a particle filter. The knockout condenser was filled with ice before sampling by the gas chromatograph and was re-filled as needed. The vacuum pump ensured that the gas from the column reached the inlet of the gas chromatograph. A combination of the knockout condenser and bank of desiccant tubes was sufficient to ensure moisture free gas delivery to the gas chromatograph inlet.

The solvent was sprayed into the column through the spray nozzle after two successive readings from the gas chromatograph registered the same concentration of CO_2 in the gas. The solvent feed pump was started at a frequency of 30 Hz. By manipulating the valves on the feed tank recirculation line and the discharge line from the pump, and by varying the frequency of the pump, the exact solvent flowrate through the nozzle was maintained.

The gas exiting from the top of the column was continuously analyzed by the gas chromatograph for changes in the gas CO_2 composition. When two successive gas chromatograph readings

registered the same value of CO_2 gas composition, attainment of steady state was ascertained. A liquid sample was then collected from the bottom of the column by means of the 3-valve sampling unit. Before collecting the liquid sample into glass vials, the lines in the 3-valve sampling unit were cleared. Typically, 3 consecutive gas chromatograph readings were sufficient to ascertain attainment of steady state. Each gas chromatograph reading took about 6 minutes to record the CO_2 composition of the gas. For most runs, the time for attainment of steady state ranged from 9 – 18 minutes. The liquid samples were then analyzed to determine the rich loading of the solvent, which in turn was used to compute the CO_2 flux.

It must be noted, in case of interfacial measurements with the CO_2-NaOH system, only indoor air was used for all runs. No CO_2 injection from the CO_2 cylinder bank was required. 0.0568 m^3 of 0.1 N NaOH solution was prepared by mixing 234 g of NaOH flakes (98 wt%, Alfa-Aesar) in de-ionized water.

V.2.2. PDI measurements

The PDI measurements were conducted in a separate campaign. The solvent was again prepared and charged to the feed tank as in the mass transfer runs. The nozzle was located at the desired axial location above the beam intersection. The nozzle was centered inside the column visually.

Before measurement of dropsize by the PDI, the beam alignment was checked. The beam alignment was checked by focusing the PDI beams on an external objective piece at its focal length as shown in Figure 5.13 below.

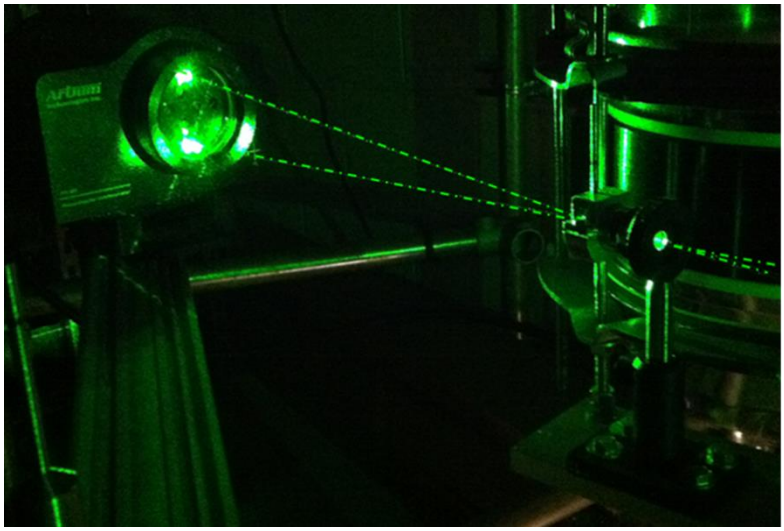

Figure 5.13. Laser beams focused on the external objective for beam alignment

The image of the two beams on a plane behind the objective piece was then viewed. By adjusting two set screws located underneath the PDI transmitter cover, the images of the two laser beams (in the form of filled circular dots) were made to move relative to each other. When the two beams were perfectly aligned, only a single circular dot on the plane behind the objective is seen. Once the beams were perfectly aligned, the cover on the transmitter was put back on. By using only the forward-backward rail, the beam intersection was then made to move from the external objective piece back into the spray column through the central slit of the eye-piece. Based on experience with previous trial runs with beam alignment, the beam intersection inside the column was moved 0.0127 m (0.5 inch) to the right by using only the left-right movement rail located close to the transmitter. A triangulation method was then used to calculate the exact location of the beam intersection inside the glass column (Whiteley 2012) based on four external measurements.

Once the nozzle and the beam intersection were centered at the geometric center of the column, a small amount of solvent was sprayed to check if the spray center coincided with the beam intersection. At times, the spray nozzle may be tilted slightly. The orientation of the nozzle can be

corrected with the help of a set of screws located on the outside of the column. These screws hold the stainless steel rods attached to the nozzle, holding the disc in the place.

Prior to starting the spray and PDI measurements, counter current gas flow is started and the composition of CO_2 in the gas is measured with the gas chromatograph. The AIIMS software (Artium Technologies) is opened. The acquisition period, PMT gain, refractive index of the solvent, and the file or run name are correctly entered. The oscilloscope which helps in gauging the strength of raw signals by the PDI is switched on.

The spray is then started at the desired flowrate. The beam intersection is observed through the slit aperture on the PDI receiver. The slit aperture is adjusted using three set screws located at the bottom of the PDI receiver such that the beam intersection appears at the center of the slit. When the beam intersection coincides with the slit aperture perfectly, it ensures that the drops pass through the center of the probe area formed by the two intersecting beams. The PDI is inherently more sensitive in measuring large drops (Sipperley 2013). Small drops need to pass through the center of the probe area or probe volume for the PDI receiver to sense them.

To record data, the start button on the AIIMS software window is clicked. After the conclusion of the set acquisition period, the AIIMS software showcases the results. With regards to dropsize distribution, the probe volume corrected (PVC) data should be utilized. After dropsize measurement at one location is completed, the beam intersection can be moved to the right or left by using the rail. The PMT gain may need to be adjusted based on the quality of signals. However, based on the nozzle characteristics, a PMT gain of around 300 mV was recommended as a starting point for all runs (Sipperley 2013).

V.3. Liquid composition analysis

In this section the methods and tests adopted to determine the loading of the solvent, and composition checks are described. For MEA mass transfer measurements, the change in the

solvent loading was used to determine the CO_2 flux. For the interfacial area measurements, the concentration of the solvent and the hydroxide depletion need to be checked. Total Alkalinity (TA) and Total Inorganic Carbon (TIC) are the two tests needed to complete all the liquid composition analysis.

V.3.1. Total alkalinity

The objective of the total alkalinity test was to determine or check the concentration of the solvent. The total alkalinity test in this work was performed in accordance with the procedure highlighted by Hilliard (2008). The test involved diluting the liquid sample 300 times by mass, and subsequent titration with 0.1 M H_2SO_4. With the addition of 0.5 ml H_2SO_4, the change in the pH of the diluted sample was checked. The H_2SO_4 addition is stopped when the change in pH becomes insignificant. Since the TA analysis was performed manually, each sample was analyzed twice and the average of the two readings was used. A detailed step-by-step procedure for TA analysis is described in Appendix E.

To ascertain the normality of the prepared NaOH solution, simple titration was used. No dilution was required. The prepared sample of NaOH was titrated against 0.1 M H_2SO_4. With the addition of 0.5 ml of H_2SO_4, the change in the pH of the sample was noted. The volume of H_2SO_4 at which the pH dropped significantly was then used to calculate the normality of the NaOH sample. As with MEA, all NaOH samples were analyzed twice, and the average value was used to compute the concentration of NaOH.

V.3.2. Total inorganic carbon analysis

The Total Inorganic Carbon (TIC) analysis permits the quantification of moles of CO_2 attached to the MEA in the liquid sample. The method was developed at the University of Texas (UT) at Austin (Critchfield 1998; Hilliard 2008; Dugas 2009; Closmann 2011; Freeeman 2011).

The TIC setup is highlighted in Figure 5.14 below. The setup includes a glass tee with a frit and septum, an empty tube with a frit, and a glass tube packed with desiccant, a sampling unit (Horiba, ES-510), and an Infrared analyzer (Horiba VIA-510).

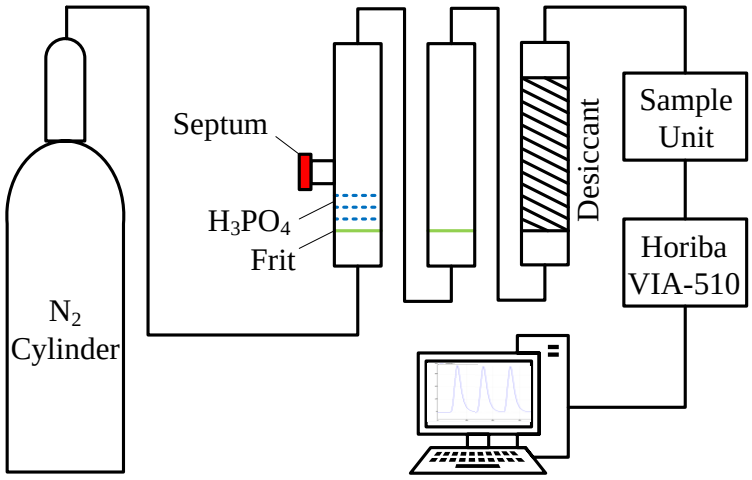

Figure 5.14. TIC setup

The bank of glass tubes consisted of one – 0.0127 m (1/2 inch) OD tee with septum, one – 0.0127 m (1/2 inch) OD glass tube with a frit 0.0508 m (2 inch) from the bottom, and a 0.0095 m OD (3/8 inch) empty glass tube. The useful lengths of all tubes are 0.1527 m (6 inch). To increase the speed of analysis, the following modifications to the setup at UT (Critchfield 1998; Hilliard 2008; Dugas 2009; Closmann 2011; Freeman 2011) were made:

1. First the diameter of the two front end tubes was increased from 0.0095 m to 0.0127 m. The tube diameter was increased to reduce the velocity of the N_2 carrier gas. During initial trials, most of the injected Phosphoric acid was found to be entrained.
2. The second tube with a frit at the bottom helped prevent carry-over of entrained Phosphoric acid.

3. Instead of using two banks of desiccant filled tubes, only one tube was used. The presence of the second tube with a frit did not warrant a need for two desiccant tubes. This greatly reduced the supply pressure of the N_2 gas to the glass tube bank. A supply pressure of 0.8166 atm (12 psi) was sufficient to drive the N_2 carrier gas into the sampling unit ES-510.

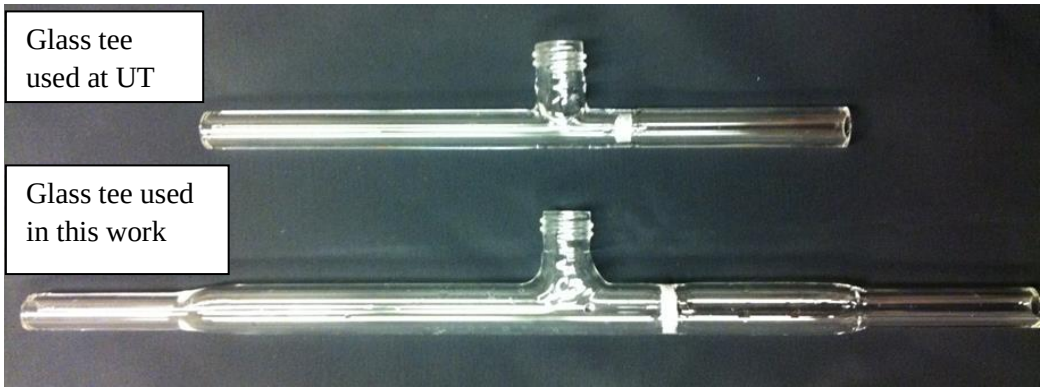

Figure 5.15. Glass tee modifications

To prepare the setup for testing, the 0.0095 m OD tube is filled with Magnesium Perchlorate ($MgClO_4$) desiccant held between two balls of glass wool. The three tubes are connected to each other by means of flexible tubing and Swagelok connectors. N_2 gas is then turned on to check for any leaks in the tubing, and to see if the flow of N_2 gas is registered on the rotameter on the sampling unit and the infrared analyzer. The N_2 flow is then stopped. 1 ml of 30 wt% Phosphoric acid is then injected into the tee through the septum. The N_2 flow is started again and adjusted to a steady value greater than 0.5 ml/min.

The liquid sample to be analyzed is diluted around 200 times, and the dilution factor is calculated. This diluted sample is then injected into the glass tee through the septum. Acidification of the diluted sample results in evolution of the CO_2 which is then swept into the Infrared analyzer by the N_2 carrier gas. The voltage output from the infrared analyzer is recorded by Pico Log software (Pico Technologies, UK). The area under the voltage peak is calculated. This peak area is then

used to calculate a concentration of CO_2 in the initial sample based on a previously generated calibration curve. The calibration curve correlates the area under the curve of the Pico Log voltage change to a known concentration of CO_2. A detailed step by step procedure for the TIC is described in Appendix F.

V.4. Experimental conditions

The experimental conditions used in this work are highlighted in Table 5.3 below. The MEA mass transfer runs, and PDI measurement runs were conducted separately from each other.

Table 5.3. Experimental conditions

MEA mass transfer measurements:			
MEA concentration (wt%)	30, 40	Gas rate (kmol/min)	0.0144
Temperature (^{0} C)	30	% CO_2 gas concentration (% mol)	0.12
Liquid rate x 10^4 (m^3/min)	7.6, 11.4	Gas velocity (m/s)	0.17
PDI measurements:			
Axial (m)	0.1524	Radial (m)	0, 0.0305, 0.061
	0.3937		0, 0.0381, 0.0762
Interfacial area measurements:			
Temperature (^{0} C)	30	Gas rate (kmol/min)	0.0144
Liquid rate x 10^4 (m^3/min)	7.6, 11.4	% CO_2 gas concentration (% mol)	0.04 – 0.06
		Gas velocity (m/s)	0.17

V.5. Calculations

In this section the equations and methodology used to calculate mass transfer coefficients, Sauter mean diameter, Planar surface area (P_{SA}), and interfacial area (a_e) are presented.

V.5.1. Mass transfer coefficients

The mass transfer coefficients were calculated based on the liquid CO_2 flux. The liquid CO_2 flux was quantified based on the liquid composition analysis. The liquid CO_2 flux was quantified using Equation 5.1 below.

$$N_{CO2} = L_{MEA}(\alpha_{rich} - \alpha_{lean}) \qquad (Eq\ 5.1)$$

Based on the measured loading, the logarithmic driving force across the height of the spray column is computed. The equilibrium partial pressure is calculated using the model of Xu (Rochelle 2009 b). Equations 5.2, and 5.3 show the calculation for the logarithmic driving force, and the equilibrium partial pressure, respectively.

$$\Delta p_{lm} = \frac{\left(p_{CO2,in} - {p_{CO2,in}}^*\right) - \left(p_{CO2,out} - {p_{CO2,out}}^*\right)}{ln\left\{\frac{\left(p_{CO2,in} - {p_{CO2,in}}^*\right)}{\left(p_{CO2,out} - {p_{CO2,out}}^*\right)}\right\}} \qquad (Eq\ 5.2)$$

$$\ln {p_{CO2}}^* = 44.2 - \frac{116000}{RT} - 29.7\alpha + \frac{11600}{T}\alpha + 17.3\alpha^2 \qquad (Eq\ 5.3)$$

The overall volumetric mass transfer coefficients can be calculated using Equation 5.4 below with the knowledge of the CO_2 liquid flux, logarithmic driving force, height of gas-liquid contact, and the cross sectional area of the column.

$$K_G a_e = \frac{N_{CO2}}{A_c\ Z\ \Delta p_{lm}} \qquad (Eq\ 5.4)$$

V.5.2. % CO_2 removal

The % CO_2 removal is a measure of the fraction of the incoming CO_2 absorbed in the Spray column. The % CO_2 removal can be quantified by using Equation 5.5 below.

$$\%\ CO_2\ removal\ efficiency\ = \left[\frac{N_{CO2}}{G_I\ Y_{CO2,in}}\right]100 \qquad (Eq\ 5.5)$$

V.5.3. Sauter mean diameter

The Sauter mean diameter is used extensively in quantifying droplet size for reactive systems. The Sauter mean diameter is a measure of the finess of the spray. The Sauter mean diameter represents the volume to area ratio of the ensemble of drops. The Sauter mean diameter can be calculated using Equation 5.6.

$$D_{32}\ = \frac{\sum_i n_i\ {d_i}^3}{\sum_i n_i\ {d_i}^2} \qquad (Eq\ 5.6)$$

V.5.4. Planar surface area

The PDI dropsize measurements at multiple locations within one axial plane were utilized to calculate the Planar Surface Area (P_{SA}) in that plane (Tamhankar, King *et. al.* 2014). The following assumptions regarding drop behavior are made in calculating the P_{SA}:

1. The entire volume of solvent sprayed gets distributed in the form of perfectly spherical drops. As a result, the volume of solvent sprayed equals the cumulative volume of all drops.
2. The number of drops moving axially upwards (entrained or secondary re-circulation) are negligible in comparison to drops moving axially downwards.

First, at the axial heights of PDI measurements used in this work, sufficient time and path length for drops to fold, and compress into perfect spherical drops was permitted (Bade 2014). By keeping the acquisition period constant in all radial traverse measurements of the PDI, the total volume of solvent sprayed in that acquisition period is calculated. Second, at low counter-current gas velocity used in this work, very little entrainment was observed. Hence, both assumptions regarding drop behavior were found to hold.

In the method, an axial plane inside the plume is divided into discrete, concentric circular zones such that the PDI radial measurement points fall within each of the concentric circular zones. Such a discretization has been used and propagated by Bade and Schick (2008). Figure 5.16 showcases the details of the measurement points, and division of the axial planes of the spray plume into concentric circular zones.

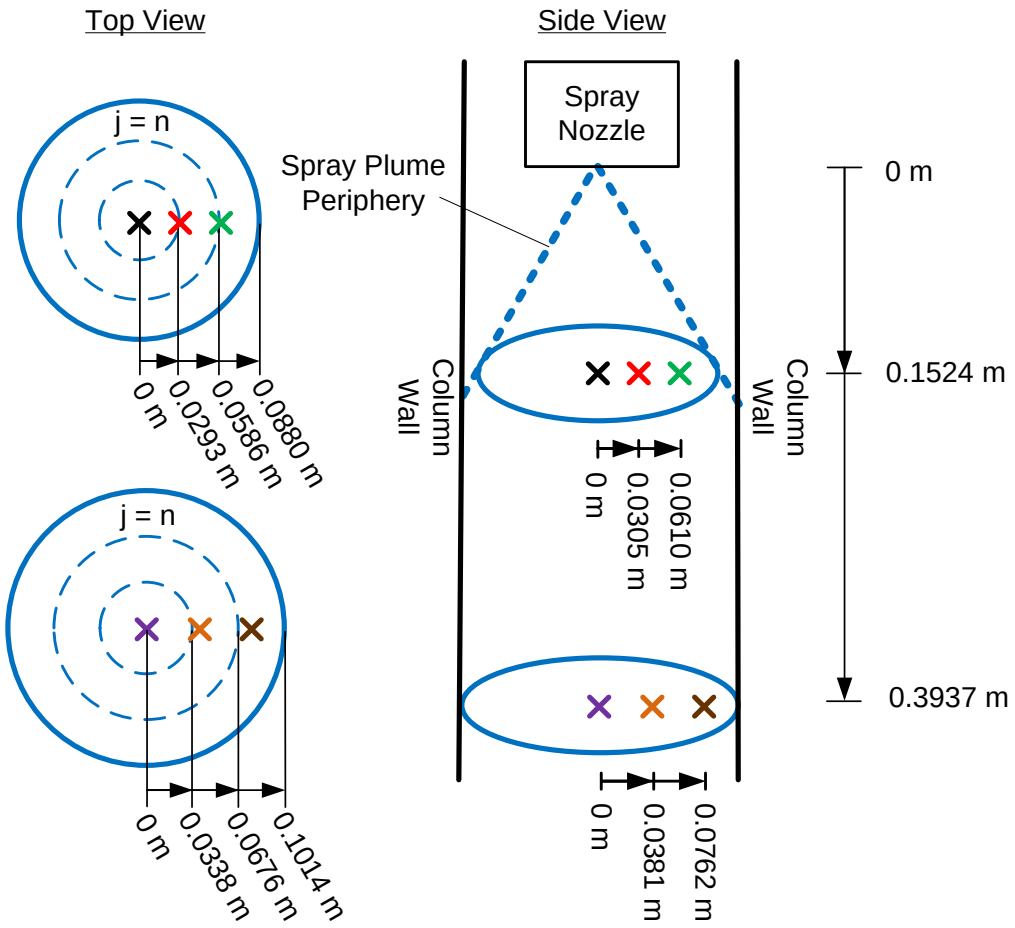

Figure 5.16. Discretization of spray axial planes

Since the axial planes are divided into multiple concentric zones, the volume of solvent sprayed within the acquisition period equals the sum of the volumes of solvent passing through each zone.

$$V_{spray} = \sum V_{j=n} \qquad (Eq\ 5.7)$$

Assuming, that the full cone nozzle distributes the solvent uniformly across the entire spray plume, the volume flux (m^3 of solvent/ m^2 of area) of solvent passing through the spray plume is constant at every point within the spray plume. In that case, the volume of sprayed solvent passing through each concentric circular zone can be computed using Equation 5.8 below.

$$\frac{V_1}{A_1} = \frac{V_2}{A_2} = \frac{V_3}{A_3} = \frac{V_n}{A_n} = \cdots\cdots\cdots\cdots = \frac{V_{spray}}{A_{plume}} \qquad (Eq\ 5.8)$$

Under the assumption that the location of PDI dropsize measurement is representative of all other locations within that zone, the drop count recorded by the PDI at that location for the pre-defined acquisition period is corrected (using correction factor C) in order to match the volume of all drops passing with the volume of solvent passing through that circular zone. The corrected count in each bin is then utilized to calculate the planar surface area in that zone.

$$S_{j=n} = \pi \sum (C\ n_i)\ {d_i}^2 \qquad (Eq\ 5.9)$$

The P_{SA} is calculated by adding the surface area of each concentric circular zone.

$$P_{SA} = \sum S_{j=n} \qquad (Eq\ 5.10)$$

Since the objective of computing PSA was to compare the two MEA concentrations, the PSA with each concentration of MEA was normalized by the PSA of water at the same test conditions. The Fractional Area (F_A), defined by Equation 5.11, becomes independent of the limitations of the PSA procedure.

$$F_A = \frac{[P_{SA}]_{MEA}}{[P_{SA}]_W} \qquad (Eq\ 5.11)$$

V.5.5. Interfacial area

The interfacial area was calculated with 0.1 N NaOH as the solvent. The CO_2 flux based on the composition changes in the gas is quantified as shown in Equation 5.12. The driving force for mass transfer is calculated using Equation 5.13. Since, the liquid and gas solutions are dilute; the equilibrium partial pressure of CO_2 in the liquid is negligible.

$$N_{CO2} = G_I \left(Y_{CO2,in} - Y_{CO2,out}\right) \quad (Eq\ 5.12)$$

$$\Delta p_{lm} = \frac{\left(p_{CO2,in} - p_{CO2,out}\right)}{\ln\left(p_{CO2,in}/p_{CO2,out}\right)} \quad (Eq\ 5.13)$$

Based on the CO_2 flux, the overall volumetric mass transfer coefficient is determined as showcased in Equation 5.14.

$$K_G a_e = \frac{N_{CO2}}{A_c\ Z\ \Delta p_{lm}} \quad (Eq\ 5.14)$$

Since the reaction between CO_2-0.1 N NaOH is fast, the gas side resistance is negligible. In this case, the overall volumetric coefficient ($K_G a_e$) approaches the liquid side coefficient ($k_g' a_e$).

$$\frac{1}{K_G a_e} \approx \frac{1}{k_g' a_e} \quad (Eq\ 5.15)$$

Based on the pseudo -1st order approximation, kg' can be determined analytically as shown in Equation 5.16 below.

$$\left(k_g'\right)_{analytical} = \frac{\sqrt{k_{OH^-} C_{NaOH} D_{CO2,l}}}{H_{CO2}} \quad (Eq\ 5.16)$$

The interfacial area is back calculated by dividing the value of Equation 5.15 with the value of Equation 5.16. In order to make a clear distinction between measured coefficients and those calculated analytically, appropriate suffixes are used in Equation 5.17.

$$a_e = \frac{\left(k_g{}' a_e\right)_{measured}}{\left(k_g{}'\right)_{analytical}} \qquad (Eq\ 5.17)$$

The constants in Equation 5.16 can be calculated from the correlations of Pohorecki and Moniouk (1988) as follows.

$$\log_{10}\left(\frac{k_{OH^-}}{k^{\infty}_{OH^-}}\right) = 0.221I - 0.016I^2 \qquad (Eq\ 5.18)$$

$$\log_{10}(k^{\infty}_{OH^-}) = 11.895 - \frac{2382}{T} \qquad (Eq\ 5.19)$$

$$\log_{10}\left(\frac{H_{CO2-PM}}{H_{CO2,w-PM}}\right) = \Sigma I_i h_i \qquad (Eq\ 5.20)$$

$$\Sigma I_i h_i = I_{NaOH}\left(h_{Na^+} + h_{OH^-} + h_{CO_2}\right) + I_{Na_2CO_3}\left(h_{Na^+} + h_{CO_3^{2-}} + h_{CO_2}\right) \qquad (Eq\ 5.21)$$

The contributions of ionic species in Equation 5.21 above to the Henry's constant calculation were evaluated using the work of Barett (1966). The diffusivity of CO_2 in NaOH was calculated from Dankwerts (1970) as shown in Equation 5.22.

$$log_{10}\, D_{CO2,l} = -8.1764 + \frac{712.5}{T} - \frac{2.59 * 10^5}{T^2} \qquad (Eq\ 5.22)$$

A summary of all the ionic constants and $k_g{}'$ values is presented in Appendix D.

CHAPTER VI

MONOETHANOLAMINE RESULTS

In the following section, results with 30 wt% MEA and 40 wt% MEA as test solvents will be presented. Results pertaining to the mass transfer coefficients, % CO_2 removal efficiency, Sauter mean diameter, and planar surface area will be showcased and discussed for both the solvents, respectively. Data regarding mass transfer coefficients and the % CO_2 removal efficiency will be combined and presented simply as mass transfer results. Detailed data are presented in Appendices A, B, and C.

VI.1. Mass transfer results

Mass transfer results are quantified in terms of the overall volumetric mass transfer coefficients (K_Ga_e), and the % CO_2 removal efficiency. K_Ga_e is a measure of how fast the solvent picks up CO_2, whereas the % CO_2 removal efficiency is a measure of how much of the incoming CO_2 gets removed from the gas inside the spray column.

VI.1.1. 30 wt% MEA

Figures 6.1 and 6.2 show the effect of inlet loading and L/G ratio on the measured mass transfer coefficients, and the % CO_2 removal efficiency with 30 wt% Monoethanolamine (MEA) as the test fluid, respectively.

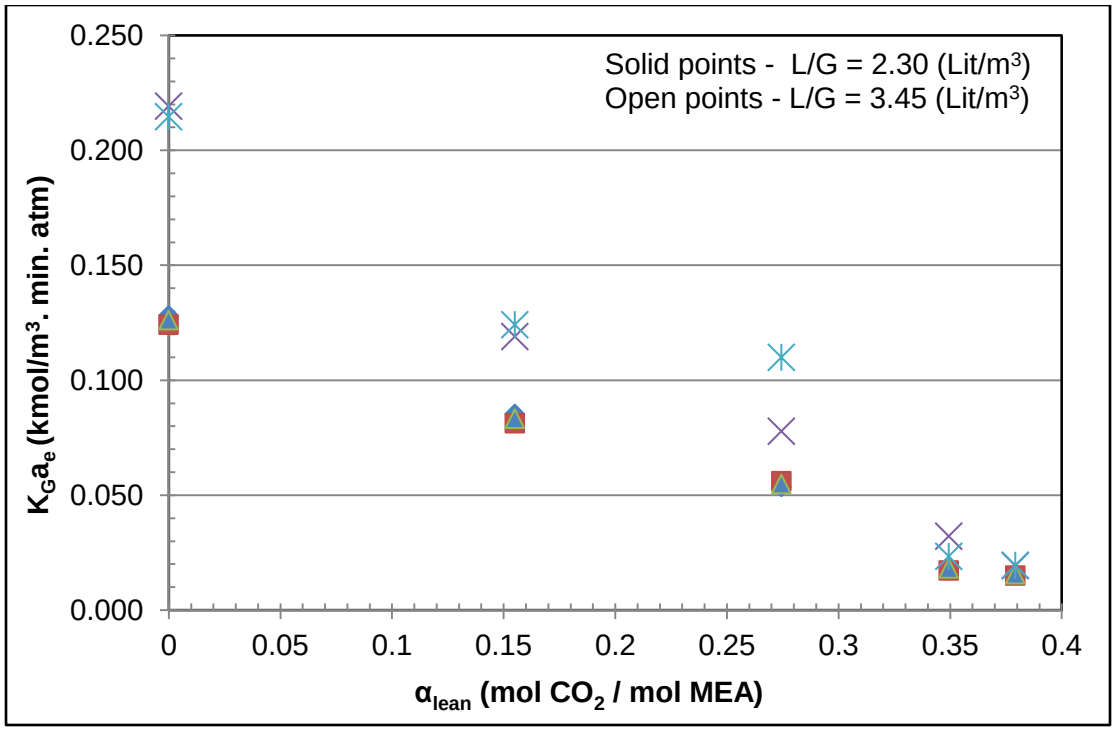

Figure 6.1. Effect of inlet loading and L/G ratio on mass transfer coefficients for 30wt% MEA

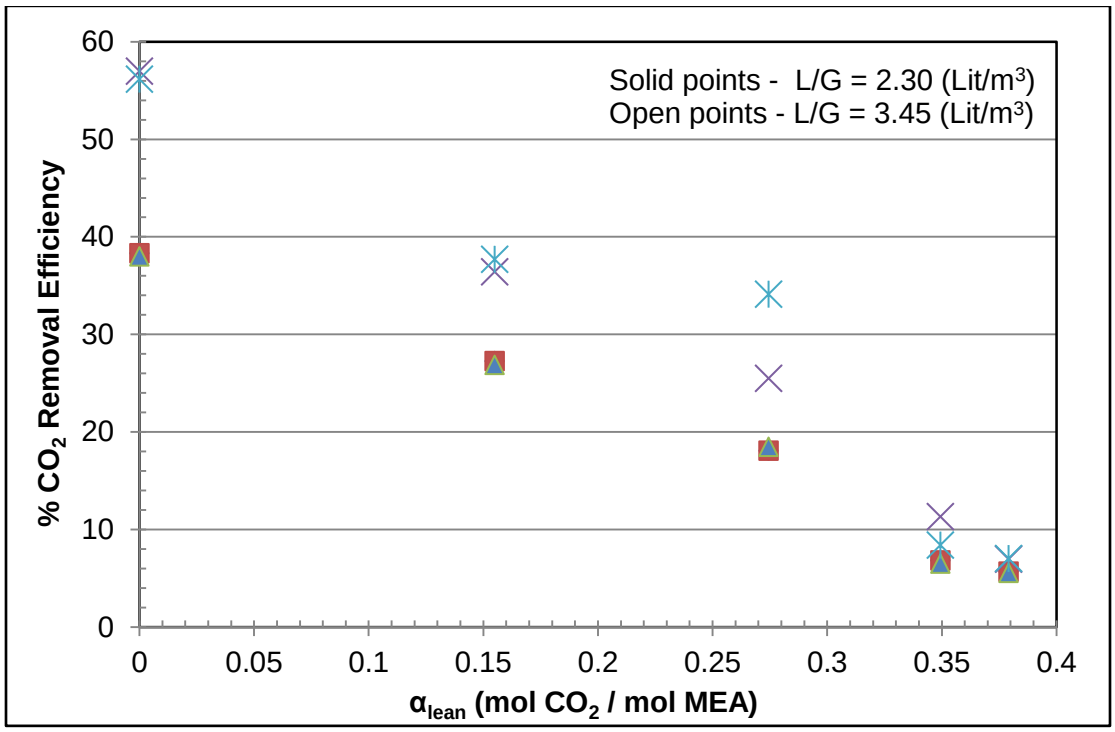

Figure 6.2. Effect of inlet loading and L/G ratio on %CO_2 removal efficiency for 30wt% MEA

Increasing the inlet loading of the solvent is found to decrease the mass transfer coefficients and the % CO_2 removal efficiency for both the L/G ratios, respectively. Increased inlet loading of the solvent results in lowering of the free MEA content and hence lower values of mass transfer coefficients and % CO_2 removal efficiency. Increasing the L/G ratio is found to increase the value of mass transfer coefficients and % CO_2 removal efficiency for all inlet loadings tested. Increasing the L/G ratio results in greater availability of free MEA for mass transfer. Further, increasing L/G ratio produces smaller drops and increasing surface area as seen in the following sections. It must be pointed out that in our tests the inlet gas rate was kept constant throughout. Higher L/G ratios were affected by simply increasing the liquid rate.

As seen in Figures 6.1 and 6.2, the benefit of increased L/G ratio on the mass transfer coefficients and the % CO_2 removal efficiency diminishes with increased loading, respectively. This can be explained by plotting the average HTU and average NTU (defined in Equation 2.33) against the inlet loading as below in Figures 6.3, and 6.4, respectively. With increasing loading, the HTU for both the L/G ratios is found to increase due to the lowering in $K_G a_e$ values. This trend in increasing HTU is comparable for both the L/G ratios employed. The NTU's are seen to decrease with increased loading due to the reduction in the CO_2 pickup, and the change in solvent loading. With increased loading, the NTU's for the two L/G ratios employed are seen to approach each other. This lowering of the change in solvent loading results in a smaller difference in the mass transfer coefficients for the two L/G ratios employed. At low initial loadings, both the increasing liquid rate and the change in loading contribute to the increased values of the mass transfer coefficient. Hence, a larger difference between the mass transfer coefficient values for the two L/G ratios employed is seen at low inlet loadings. With increased loading, the contribution of change in loading for the two L/G ratios diminishes. The improvement in the mass transfer coefficients is solely due to the higher liquid rate.

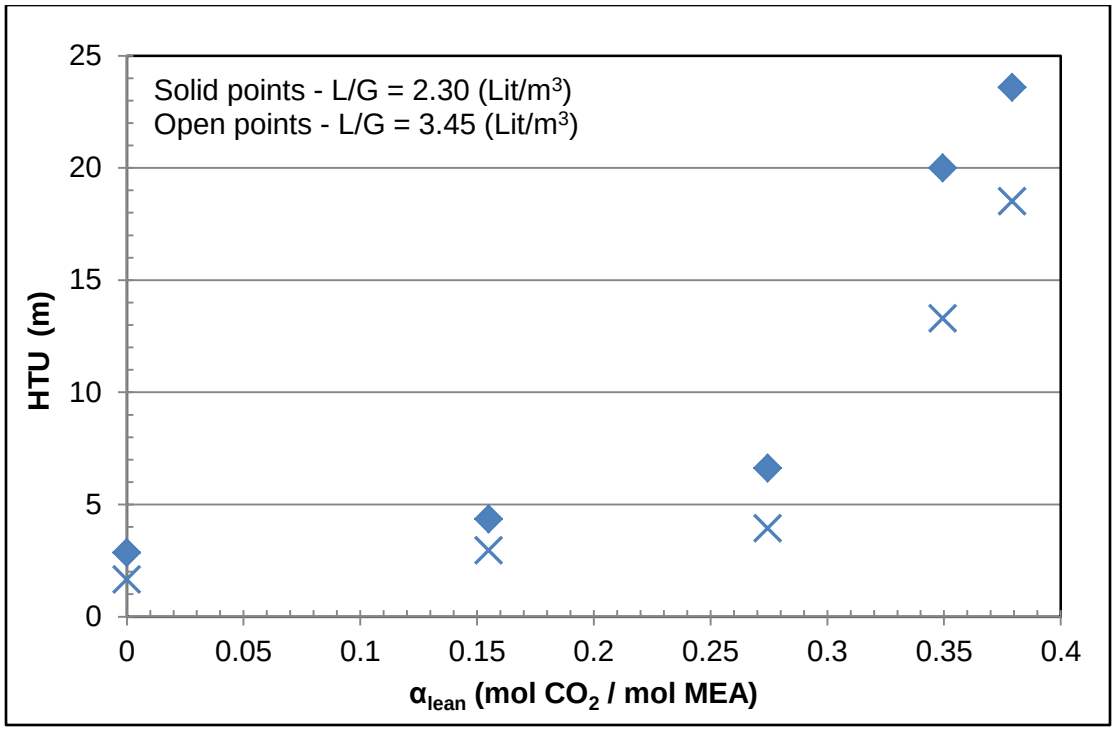

Figure 6.3. Effect of inlet loading on HTU for 30 wt% MEA

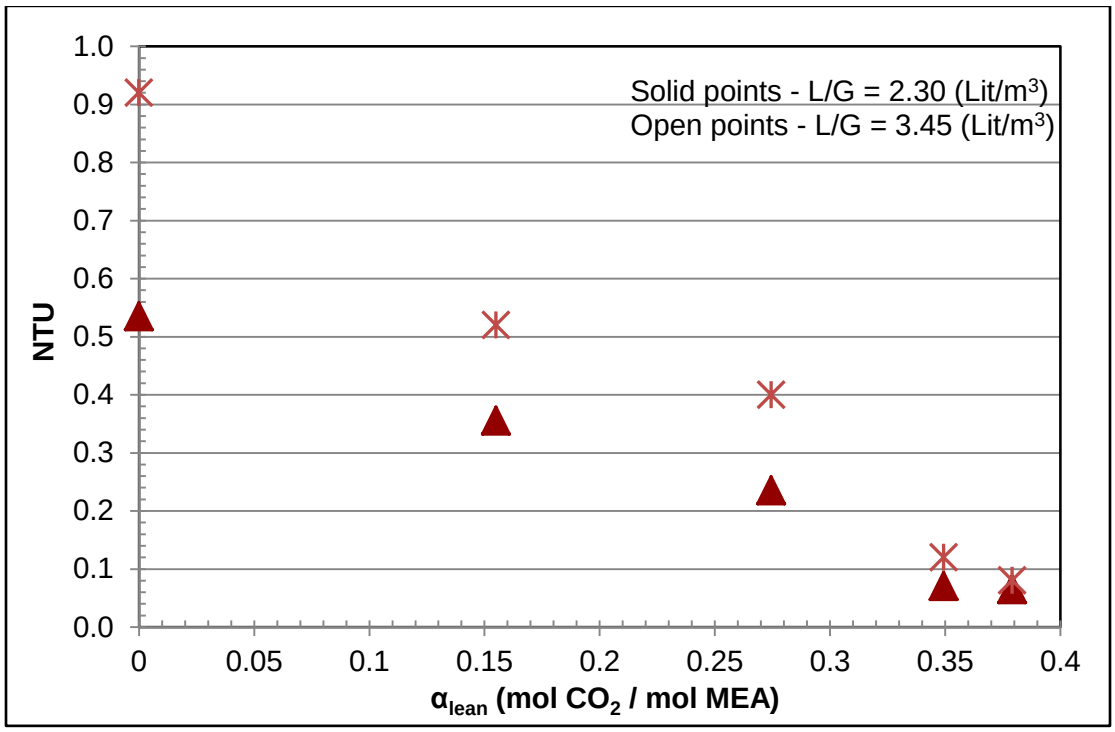

Figure 6.4. Effect of inlet loading on NTU for 30 wt% MEA

To evaluate the effect of column height, the spray nozzle was lowered to a height of 0.1017 m from the midpoint of the windows on the chimney tray. Figure 6.5 shows the effect of column height on the mass transfer coefficients with unloaded 30wt% MEA. The mass transfer coefficients are found to increase with lowering of the column height for both the L/G ratios tested, indicating that much of the spray mass transfer occurs in the region immediately downstream of the nozzle tip. A great deal of turbulence is seen in the region immediately downstream of the nozzle tip where drops are formed from breakup of liquid sheets and ligaments. This turbulent region contributes significantly to mass transfer rates (Lipp 2013a; Sherwood, Pigford *et.al.* 1975). Such findings can also be seen in the work of Yeh (2003).

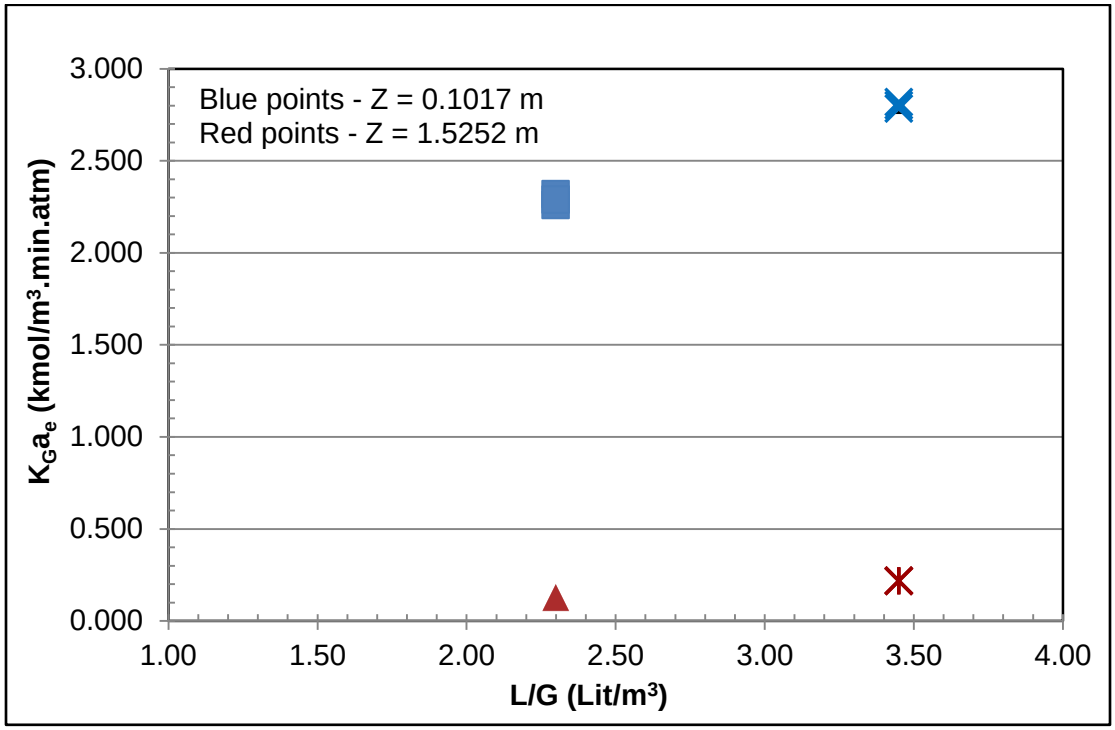

Figure 6.5. Effect of column height on mass transfer coefficients for unloaded 30wt% MEA

Figure 6.6 shows the effect of column height on the % CO_2 removal efficiency with unloaded 30wt% MEA. The % CO_2 removal efficiency is found to be comparable for both the heights and L/G ratios tested. The % CO_2 removal efficiency falls within the 15% difference lines for both the L/G ratios tested. The high values of mass transfer coefficient for the lower height, as seen in

Figure 6.5, negates the effect of lower residence time for drops or low gas-liquid contact time. The comparable % CO_2 removal efficiency for the two largely varying heights again points to the large mass transfer occurring in the region immediately downstream of the nozzle tip.

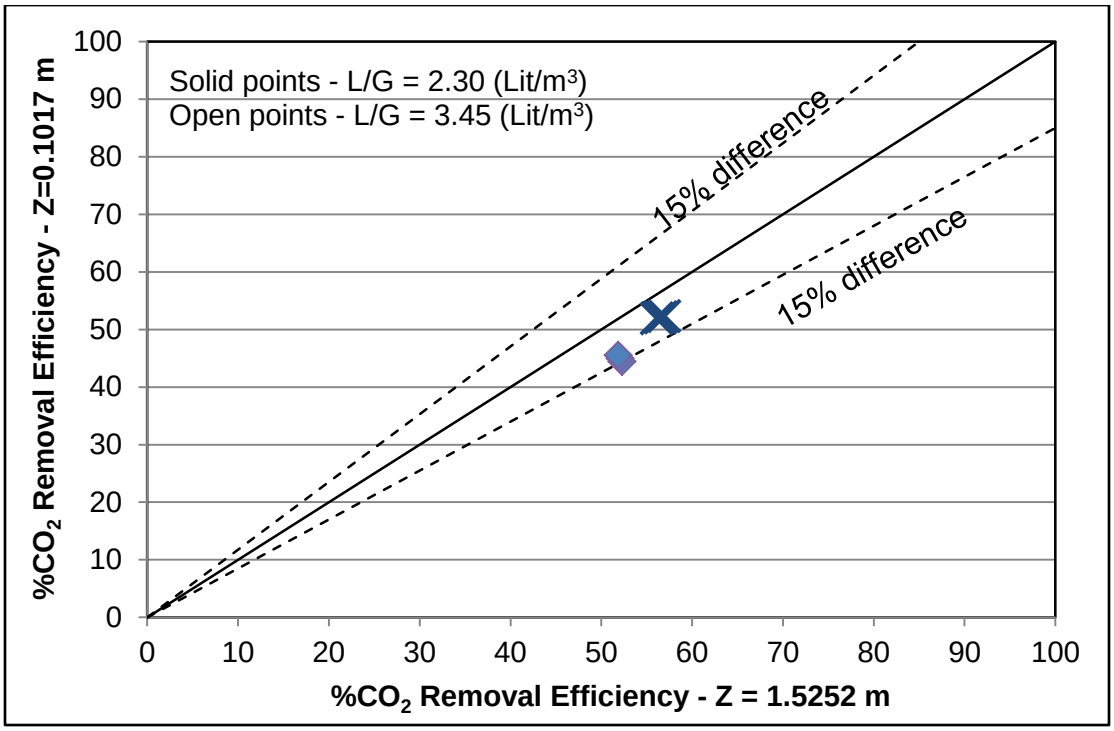

Figure 6.6. Effect of column height on % CO_2 removal efficiency for unloaded 30wt % MEA

It must be noted that at a contact height of 0.1017 m, no wall flow was observed. Some of the entrained liquid was seen to accumulate on the column wall above the roof of the chimney tray as seen in Figure 6.7. The gas exiting out of the chimney tray window was seen to push the spray plume towards the column wall. The comparable %CO_2 removal efficiency for the two L/G ratios employed indicates that the contribution of spray impact on the roof of the chimney tray was negligible.

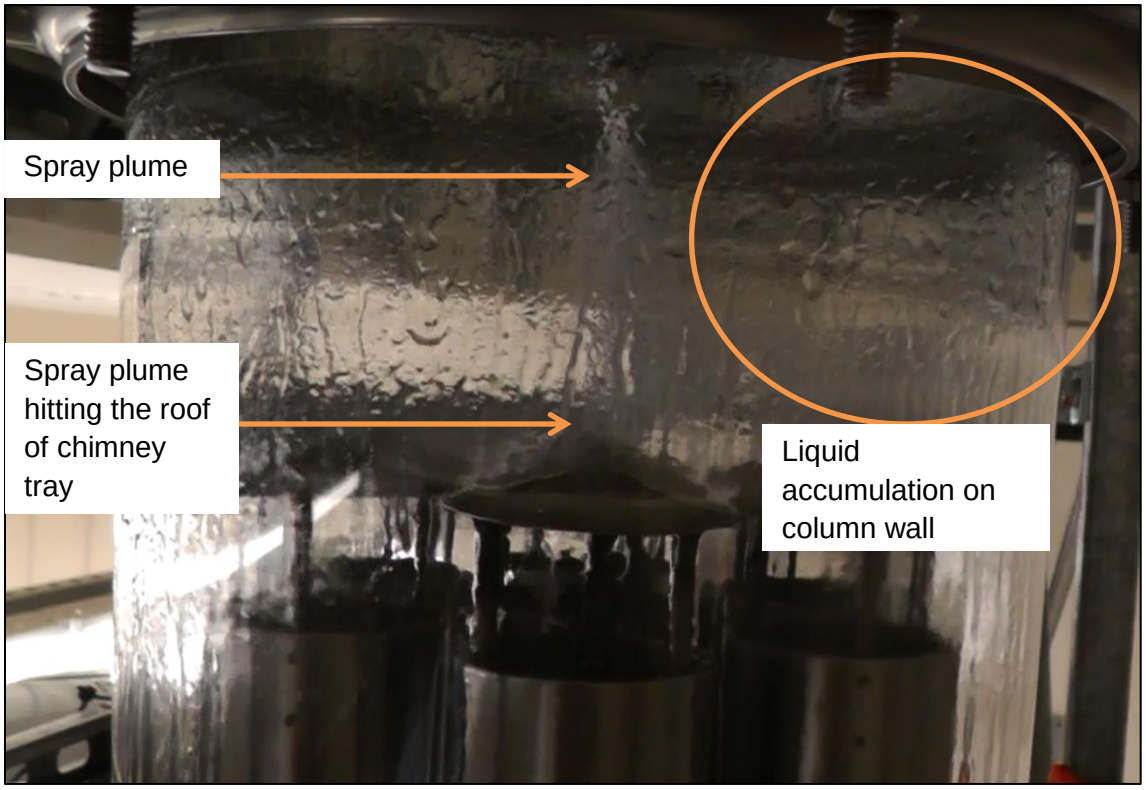

Figure 6.7. Accumulation of liquid on column wall at a height of 0.1017 m

VI.1.2. 40 wt% MEA

Figure 6.8 shows the effect of inlet loading and L/G ratio on the measured mass transfer coefficients with 40 wt% MEA as the test fluid. The mass transfer coefficients are seen to decrease with increased loading. With increasing inlet loading, the free MEA content decreases resulting in lowering of the mass transfer coefficients. Increased L/G ratio results in higher values of mass transfer coefficients due to the increased free MEA content inside the column. Further, increasing the liquid rate at a constant gas rate results in smaller drops, as discussed in the following sections. Smaller drops result in increased surface area per unit volume. However, unlike with 30wt% MEA, the values of mass transfer coefficients do not seem to approach each other at the two L/G ratios employed.

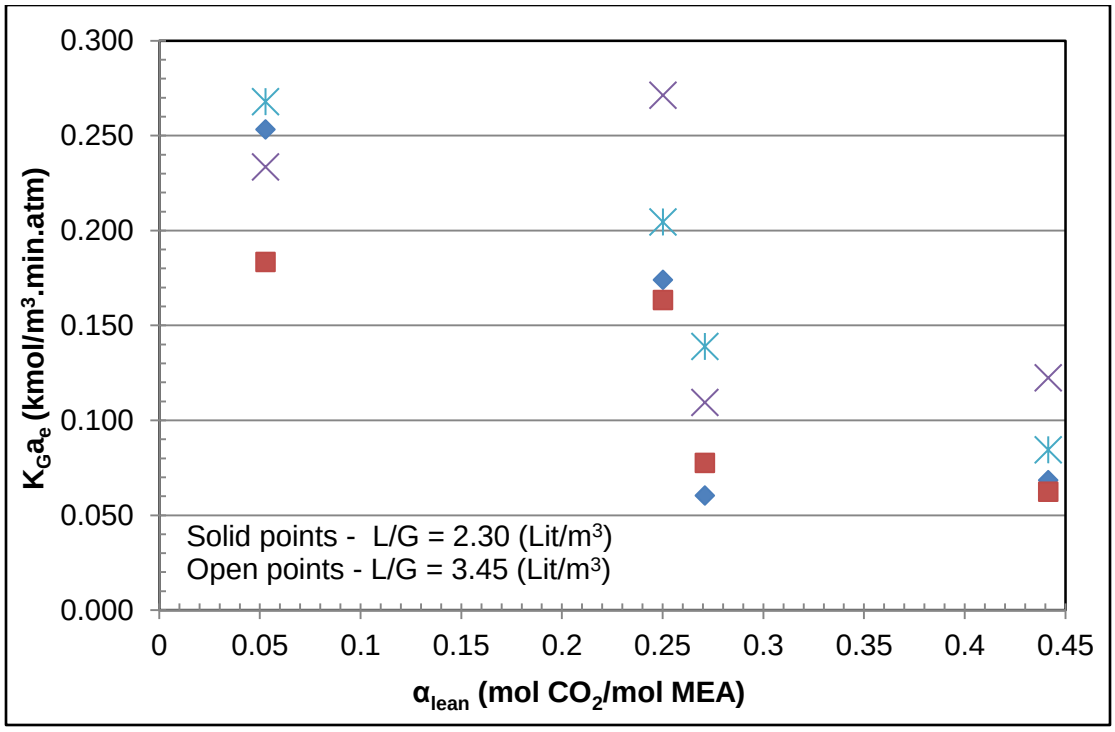

Figure 6.8. Effect on inlet loading and L/G ratio on mass transfer coefficients with 40 wt% MEA

The variation of % CO_2 removal efficiency with the inlet loading and L/G ratio is shown in Figure 6.9. As with 30 wt% MEA, increased inlet loading results in lowering of the % CO_2 removal efficiency on account of the lowering of the free MEA content. Conversely, increasing of the L/G ratio results in greater % CO_2 removal efficiency on account of the increased free MEA content.

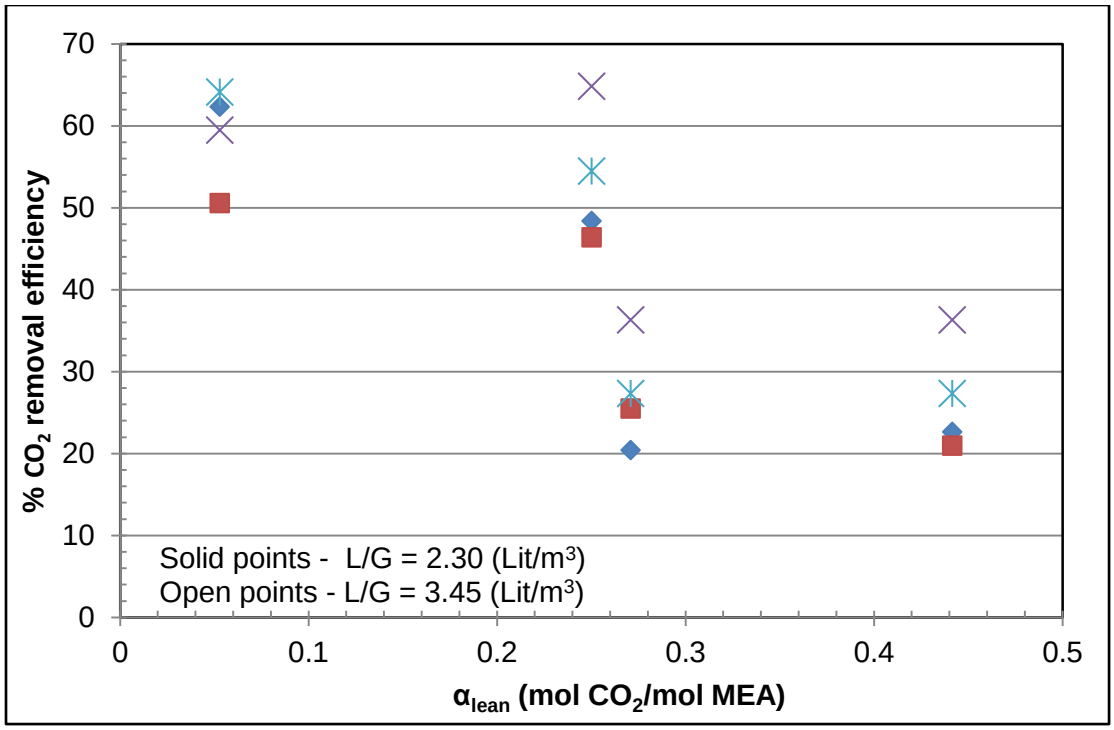

Figure 6.9. Effect of inlet loading and L/G ratio on % CO_2 removal efficiency with 40 wt% MEA

The effect of inlet loading on the HTU and NTU is showcased in Figures 6.10, and 6.11, respectively. HTU values for both the L/G ratios employed are seen to increase with inlet loading. The increasing values of HTU correspond to the lowering of the $K_G a_e$ values. The NTU's are found to decrease with the inlet loading on account of the lowering of the free MEA content, and the CO_2 pickup. Unlike 30 wt% MEA, the NTU values for the two L/G ratios do not seem to approach each other. The relative higher free MEA content availability for 40wt% MEA ensures that both the liquid rate and the change in solvent loading contribute to the mass transfer, even at high inlet loadings.

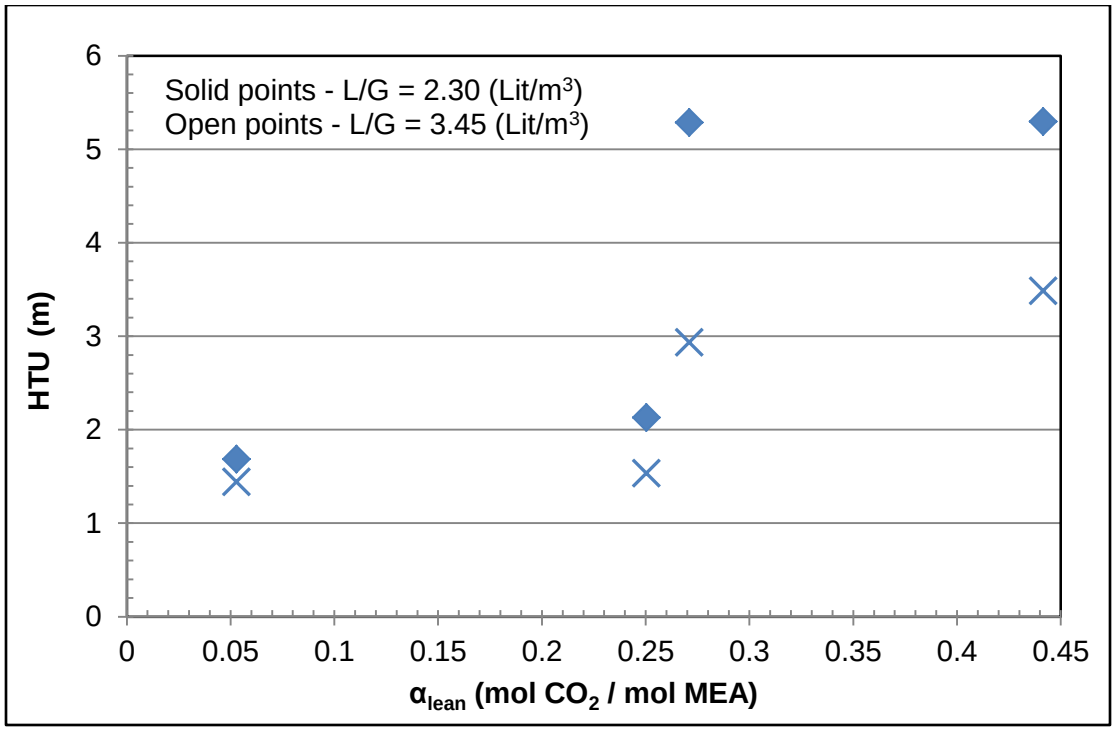

Figure 6.10. Effect of inlet loading on HTU for 40 wt% MEA

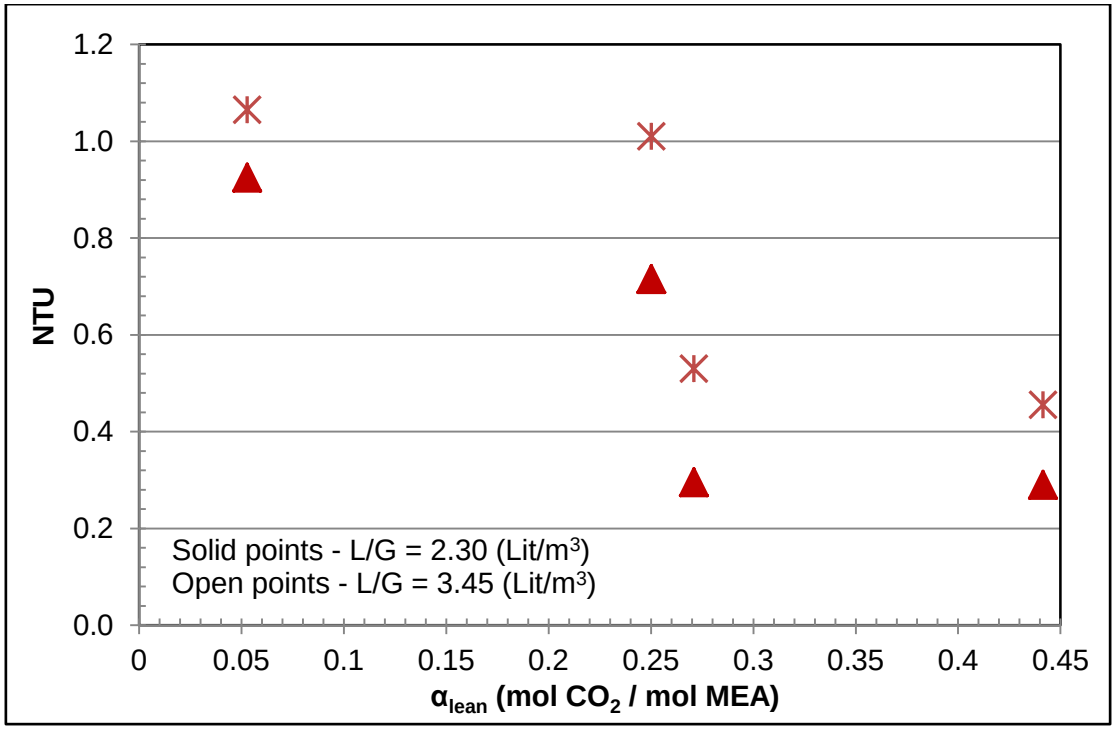

Figure 6.11. Effect of inlet loading on NTU for 40 wt% MEA

Figures 6.12 and 6.13 show the effect of column height on the mass transfer coefficients and % CO_2 removal efficiency with unloaded 40wt% MEA, respectively. As with 30 wt% unloaded MEA, the mass transfer coefficients are found to increase by an order of magnitude with lowering of the column height for both the L/G ratios tested. This large increase in mass transfer coefficients indicates the occurrence of a great degree of mass transfer in the region immediately downstream of the nozzle tip. The % CO_2 removal efficiency is again found to be comparable for the two heights and the two L/G ratios employed. The % CO_2 removal efficiency is seen to fall within 28% for all the conditions. The high rate of mass transfer negates the effect of reduction of droplet residence time inside the column. Again, as with 30 wt% MEA, at a height of 0.1017 m between the nozzle tip and mid-point of the window on the chimney tray, no wall flow was observed.

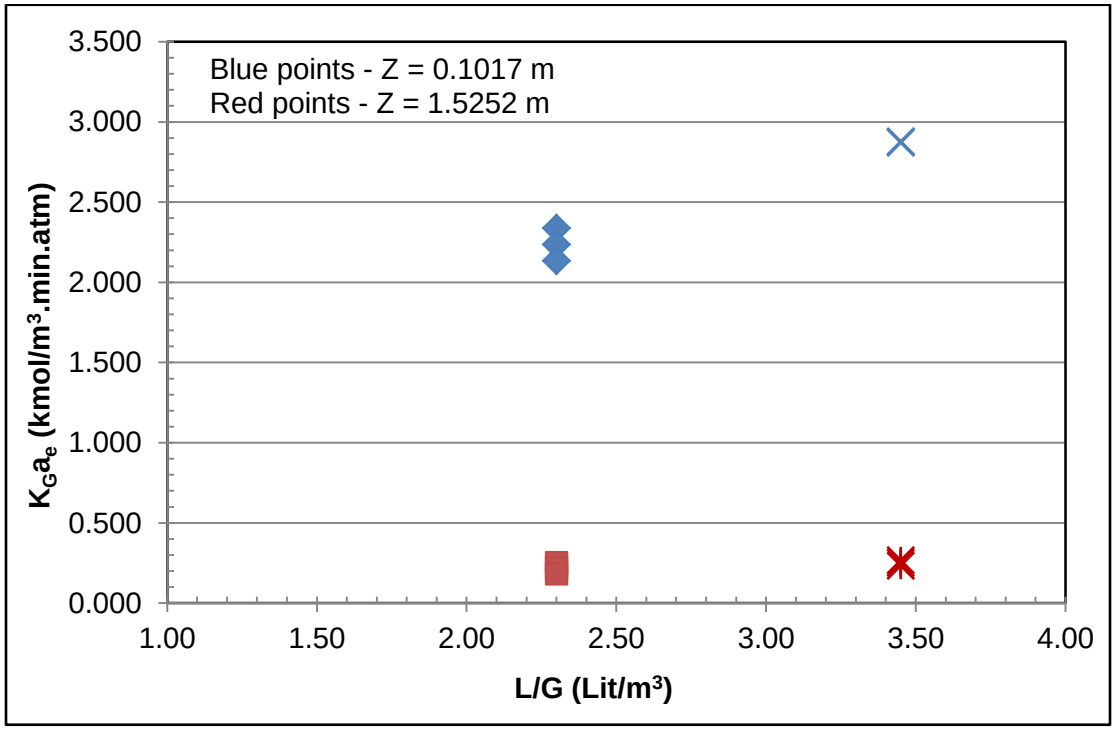

Figure 6.12. Effect of column height on mass transfer coefficients with unloaded 40 wt% MEA

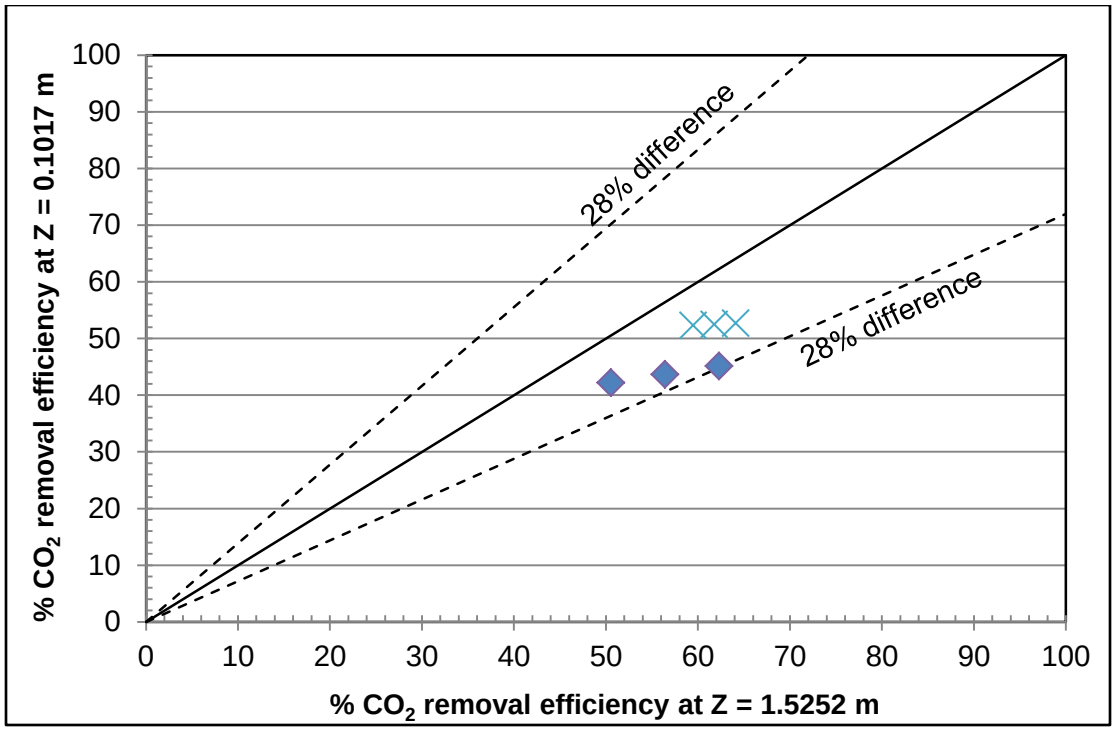

Figure 6.13. Effect of column height on the % CO_2 removal efficiency with 40 wt% MEA

VI.1.3. 30 wt% MEA vs. 40 wt% MEA

Figures 6.14, and 6.15 show the effect of MEA concentration on the measured K_Ga_e values for the L/G ratios of 2.30 Lit/m^3, and 3.45 Lit/m^3, respectively. For all the inlet loadings tested, KGae was found to increase with MEA concentration. Increasing concentration of MEA results in increased viscosity of the solvent which reduces the diffusion coefficient of CO_2 in MEA. This increase in the diffusive resistance with increasing MEA concentration reduces the absorption rates. Conversely, increasing MEA concentration results in greater availability of free MEA content which causes an increase in the absorption rates. Higher K_Ga_e values with increasing MEA concentration indicate that the contribution of free MEA content is greater than the reduction in the diffusion coefficient.

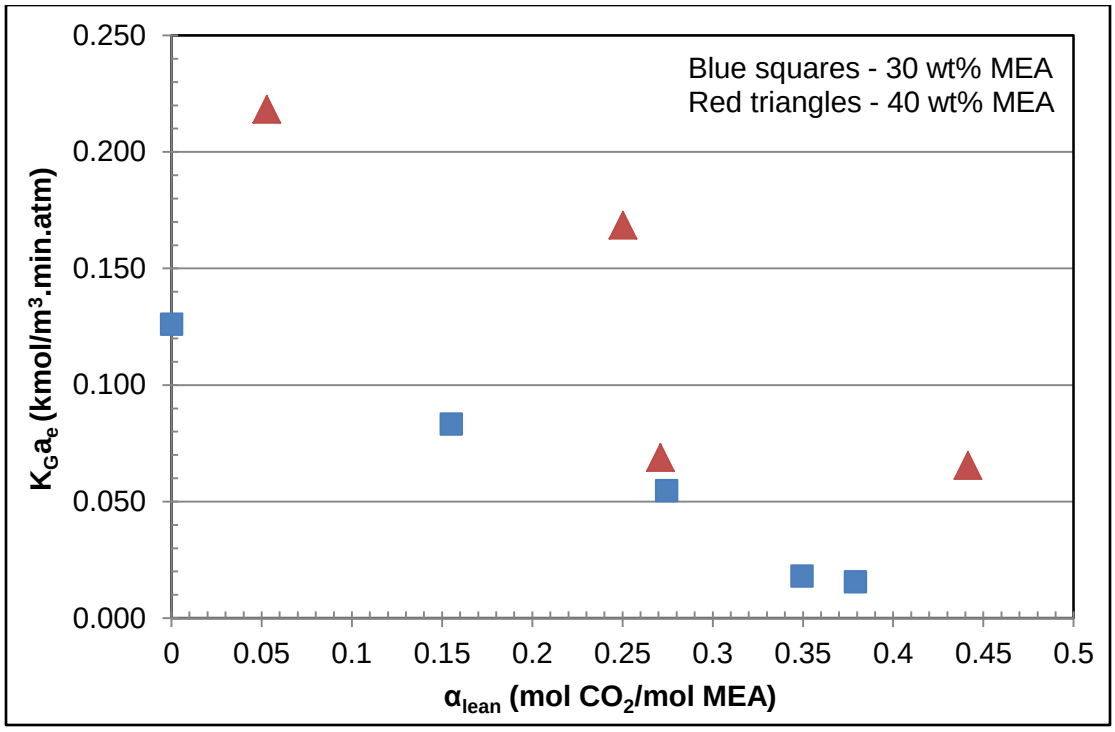

Figure 6.14. Effect of MEA concentration on mass transfer coefficients for L/G ratio of 2.30 Lit/m^3

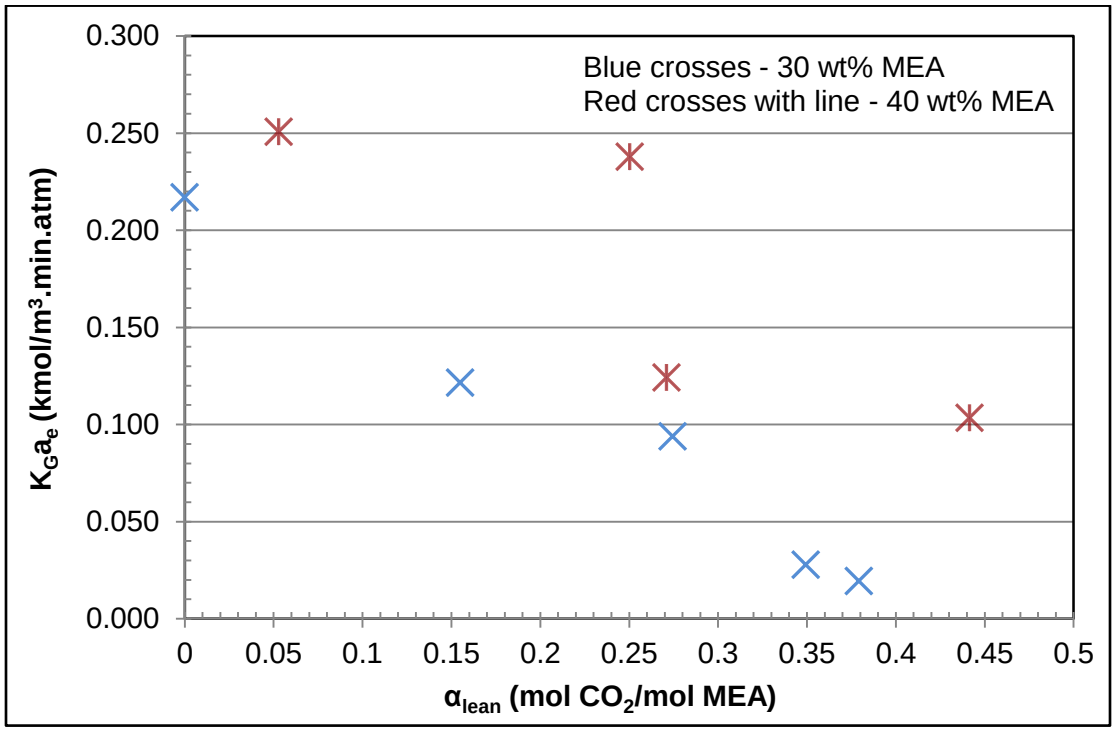

Figure 6.15. Effect of MEA concentration on mass transfer coefficients for L/G ratio of 3.45 Lit/m^3

In packed columns, $K_G a_e$ values are seen to decrease by about 5% for every molarity increase in the solvent concentration (Strigle 1994). This reduction can be attributed to both the increased diffusive resistance, and the lowering of the available area for gas-liquid contact. Dropsize measurements, and planar surface area quantification is performed to ascertain the effect of increasing MEA concentration on the available gas-liquid contact area in the spray column. The dropsize results, and planar surface area results are presented in Sections VI.2 and VI.3, respectively.

VI.2. Dropsize Results

Dropsize results are quantified in terms of the Sauter mean diameter (D_{32}). D_{32} is calculated at three radial locations within an axial plane based on the measured dropsize distributions by the PDI. The selection of radial locations in each axial plane was based on the theoretical calculation of the spray plume diameter, and the location of the axial plane downstream of the nozzle tip. PDI measurements were restricted to within the spray plume since the ultimate objective of dropsize distributions was to help compute the planar surface area of the spray plume at that axial location. Radial measurements of dropsize distributions were carried out at two axial planes or locations; 0.1524 m, and 0.3937 m downstream of the nozzle tip. At an axial distance of 0.1524 m the spray plume did not impact the column wall, whereas the axial distance of the 0.3937 m was located below the point where the spray plume was observed to hit the column wall.

To evaluate dropsizes and planar surface areas at two axial heights downstream of the nozzle tip, a separate campaign independent of the mass transfer runs was conducted for two reasons. In our present setup, the axial distance between the probe volume or PDI measurement point, and the nozzle tip is manipulated by moving the nozzle vertically or axially (up or down). Movement of the nozzle location vertically would have resulted in changing the gas-liquid contact height required for calculation of mass transfer coefficients. Second, dropsize measurement trial runs were conducted at each location (radial and axial) to fix the acquisition period (time for which

dropsize data is recorded by the PDI) in the PDI software to ensure reproducibility of data. An acquisition period of two minutes was found to be sufficient for all locations. A combined campaign of mass transfer rates, and dropsize data would not have permitted these trial runs due to the limited feed tank capacity, and solvent inventory.

VI.2.1. 30 wt% MEA

Figure 6.16 shows the variation of the average D_{32} with inlet loading for three radial locations at an axial plane 0.1524 m downstream of the nozzle tip for a L/G ratio of 2.30 Lit/m^3. The D_{32} is found to fall between ± 12% (flat long dotted lines) for all the inlet loadings, and radial locations for a L/G ratio of 2.30 Lit/m^3. In fact, most of the measured D_{32} fall within ± 6% (round dotted lines) of each other. According to Schick (2014), dropsize measurements within ±6 % are considered to be the same.

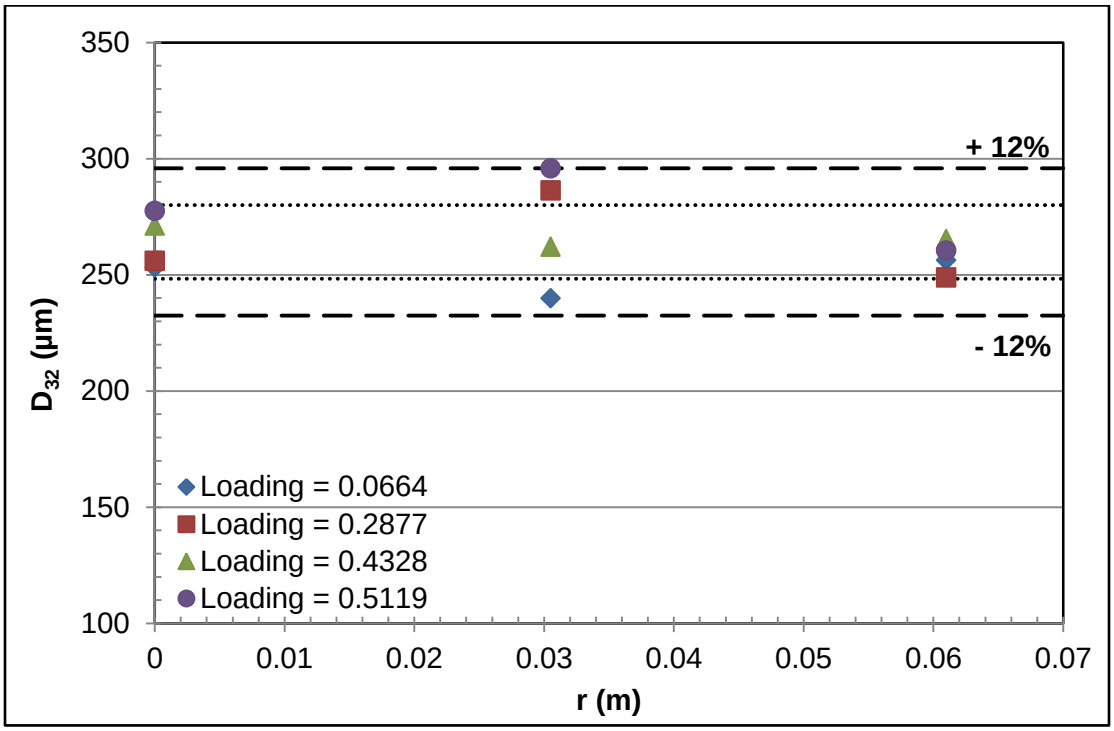

Figure 6.16. Variation of D_{32} with radial distance from column center, and inlet loading for 30 wt% MEA with a L/G ratio of 2.30 Lit/m^3 at an axial distance of 0.1524 m

The variation of average D_{32} with radial location and inlet loading for the L/G ratio of 3.45 Lit/m^3 is shown in Figure 6.17 below. Similar to Figure 6.16, the D_{32} is found to be practically independent of inlet loading and radial location. All the D_{32} measurements are seen to lie within ± 10% of each other. Most of the data is seen to fall within ±6% lines.

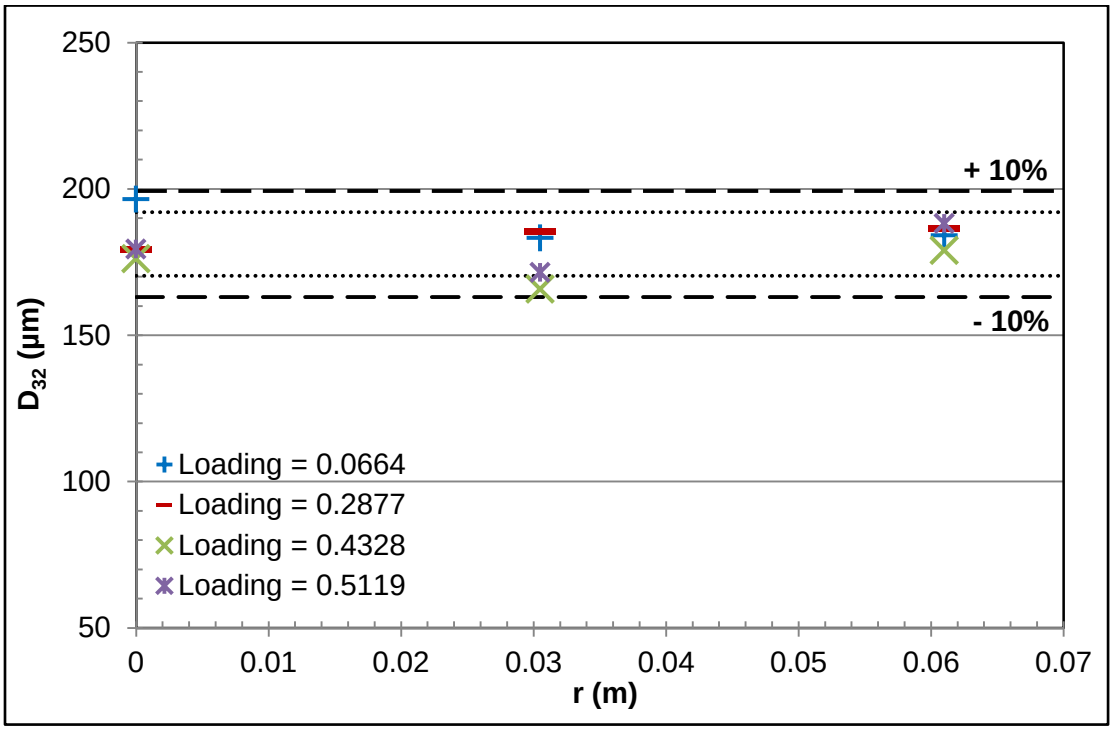

Figure 6.17. Variation of D_{32} with radial distance from column center, and inlet loading for 30 wt% MEA with a L/G ratio of 3.45 Lit/m^3 at an axial distance of 0.1524 m

The effect of L/G ratio on the average D_{32} at all three radial locations with varying inlet loading is shown in Figure 6.18 below. The increasing L/G ratio is found to reduce the average D_{32} by about 30%. In all our experiments, the L/G ratio was manipulated by varying the liquid rate, while the gas rate was kept constant. The increased L/G ratio was thus achieved by merely increasing the liquid rate by applying a larger differential pressure across the nozzle orifice or opening. The differential pressure across the nozzle was increased from 1.26 atm (g) to about 3.4 atm (g) to affect the change in the L/G ratio. This increased pressure energy results in smaller dropsizes as more energy is available to compress the drop (Lipp 2013a; Liu 1999).

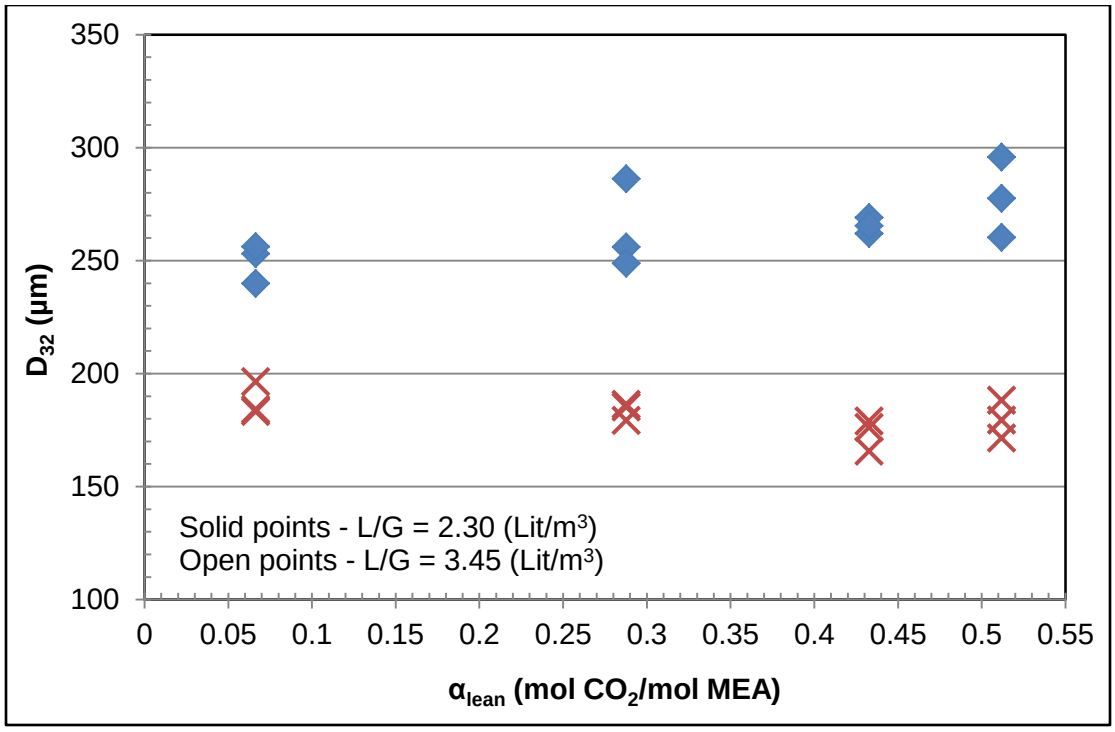

Figure 6.18. Effect of L/G ratio on D_{32} for 30 wt% MEA at 0.1524 m

Figure 6.19 shows the variation of average D_{32} with inlet loading for all three radial locations with a L/G ratio of 2.30 (Lit/m^3) at an axial distance of 0.3937 m below the nozzle tip. As seen in Figure 6.16, no appreciable trend in D_{32} is seen with varying inlet loading. All of the measurements are seen to fall within ±22% (long, flat dotted lines), with most measurements lying within the ±6% lines (short, round dotted lines).

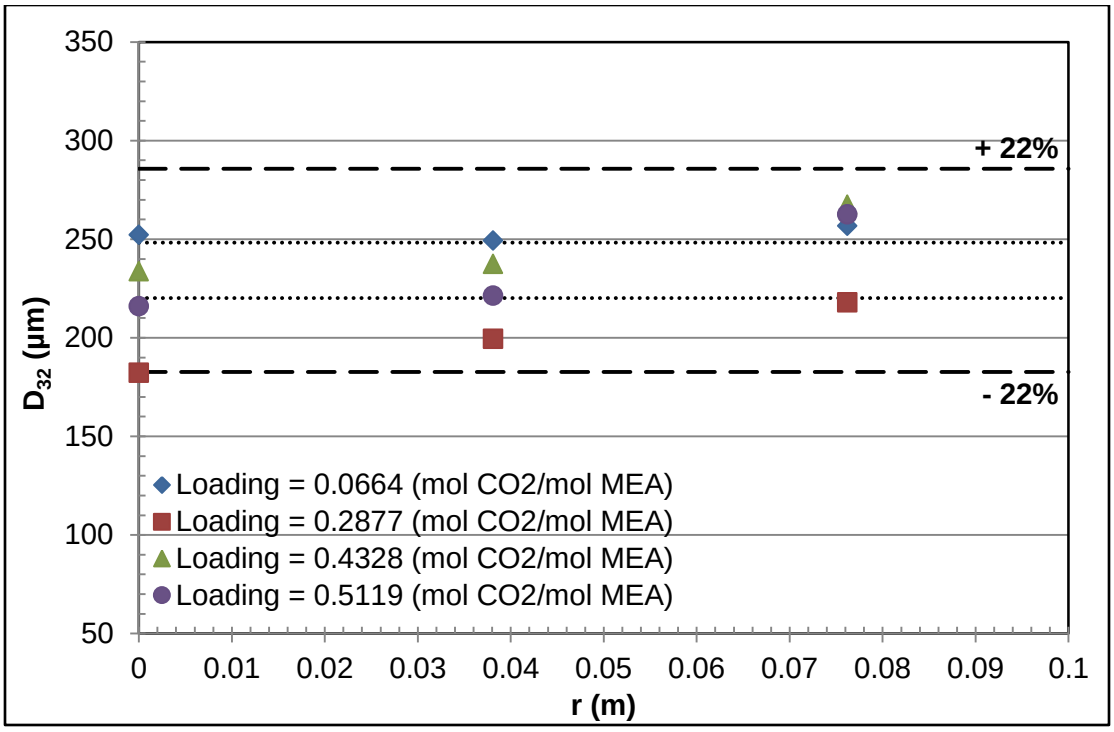

Figure 6.19. Variation of D_{32} with radial distance from column center, and inlet loading for 30 wt% MEA with a L/G ratio of 2.30 Lit/m^3 at an axial distance of 0.3937 m

The variation of the average D_{32} with radial distance, and inlet loading for 30 wt% MEA at an axial distance of 0.3937 m for a L/G ratio of 3.45 Lit/m^3 is shown in Figure 6.20. The D_{32} is found to be practically independent of the inlet loading. All the measured D_{32}'s are found to lie within ±8% of each other.

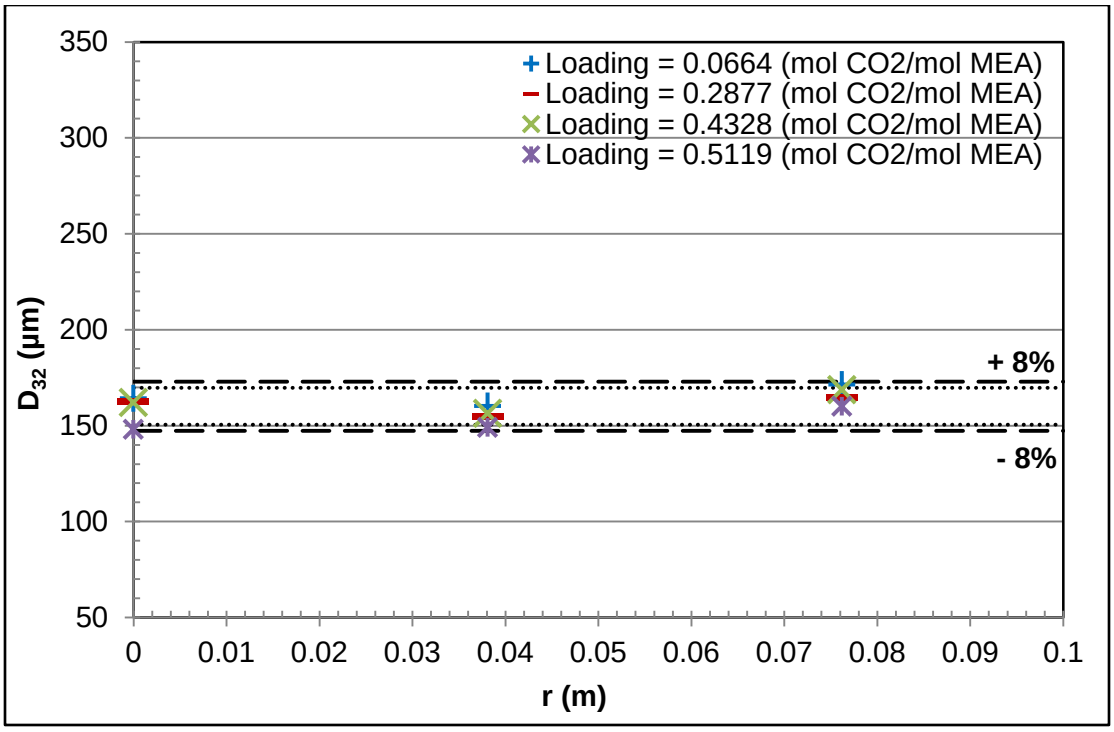

Figure 6.20. Variation of D_{32} with radial distance from column center, and inlet loading for 30 wt% MEA with a L/G ratio of 3.45 Lit/m^3 at an axial distance of 0.3937 m

The effect of L/G ratio on the average D_{32} at all three radial locations with varying inlet loading is shown in Figure 6.21 below. The increasing L/G ratio is found to reduce the average D_{32} by about 30%. The reduction in the drop size with increased L/G ratio is a result of the greater pressure energy available to compress to smaller drop sizes.

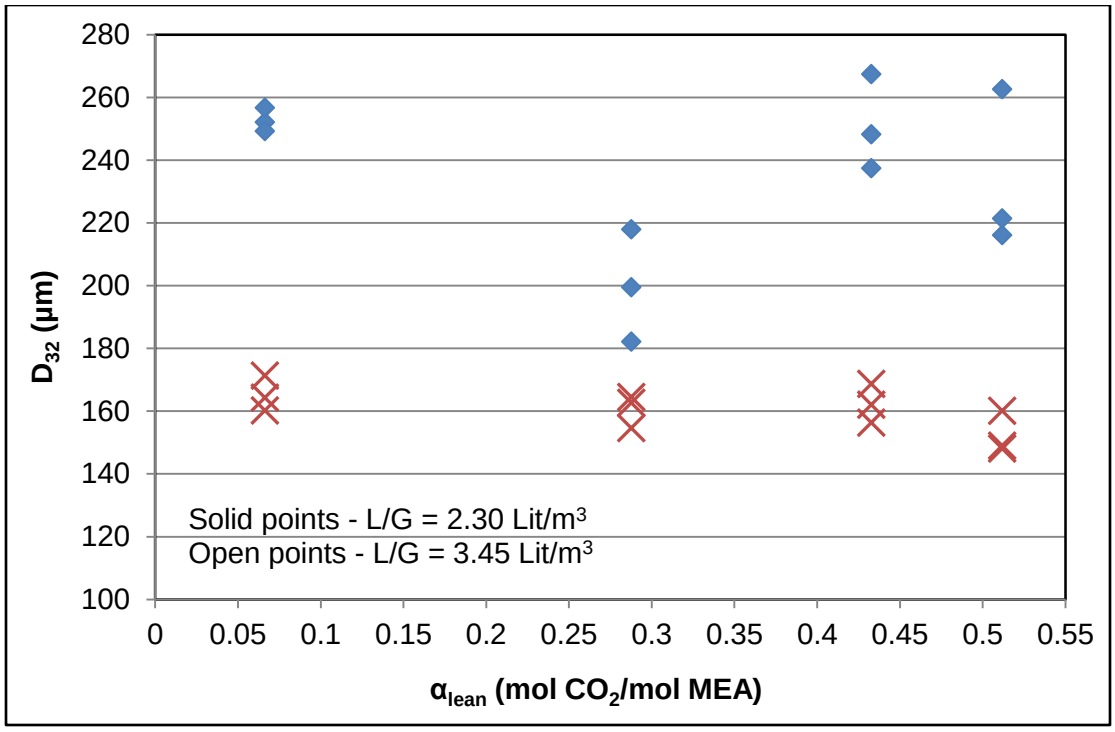

Figure 6.21. Effect of L/G ratio on D_{32} for 30 wt% MEA at 0.3937 m

Figures 6.22, and 6.23 show the comparison of measured D_{32} against established correlations of Mugele (1960), and Lefebvre (1988) for the two L/G ratios employed, respectively. Density and viscosity data from Weiland, Dingman *et. al.* (1998), and surface tension data from Vazquez, Alvarez *et. al.* (1997) were utilized to calculate the D_{32} for both the correlations. The D_{32} is found to increase marginally with increasing α_{lean}. Again, as with the PDI measurements, the calculated D_{32} from each correlation are found to fall within ±6%. The correlation of Lefebvre (1988) matches all the PDI measurements to within 15%. The D_{32} PDI measurements at an axial plane 0.3937 m downstream of the nozzle were found to be smaller than at an axial plane 0.1524 m for both the L/G ratios employed. In between the two axial planes of interest, the spray plume impacted the wall resulting in breakup of drops.

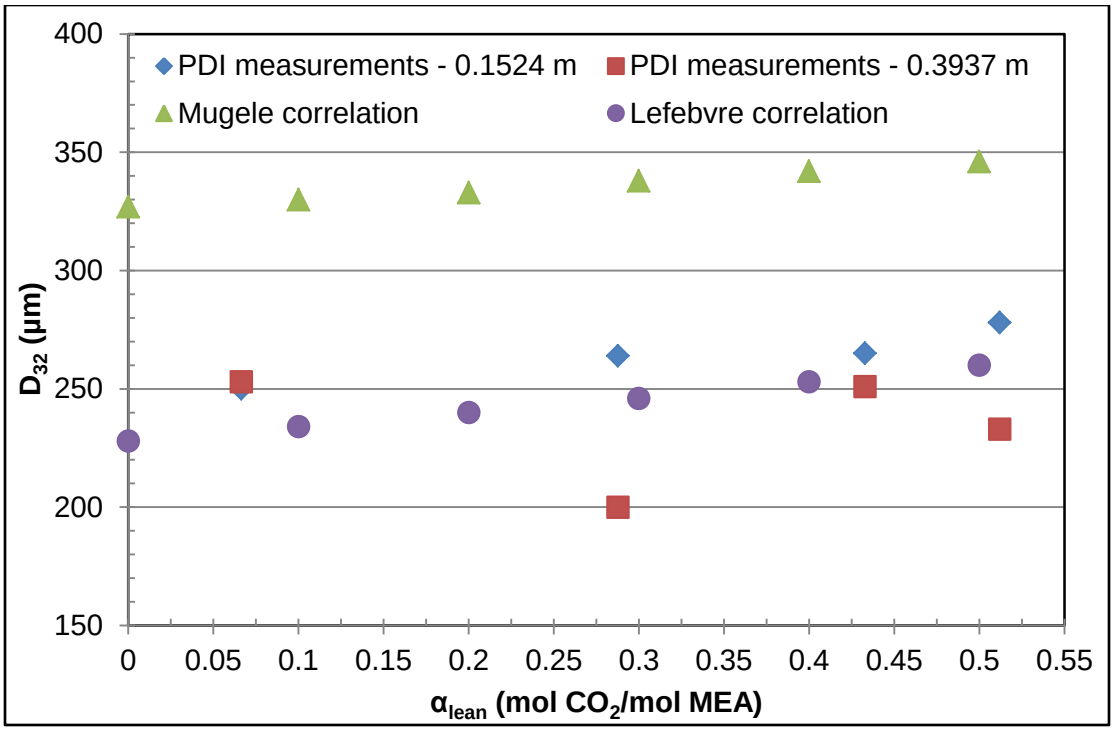

Figure 6.22. Comparison of PDI measurements with correlations for 30 wt% MEA with L/G = 2.30 Lit/m^3

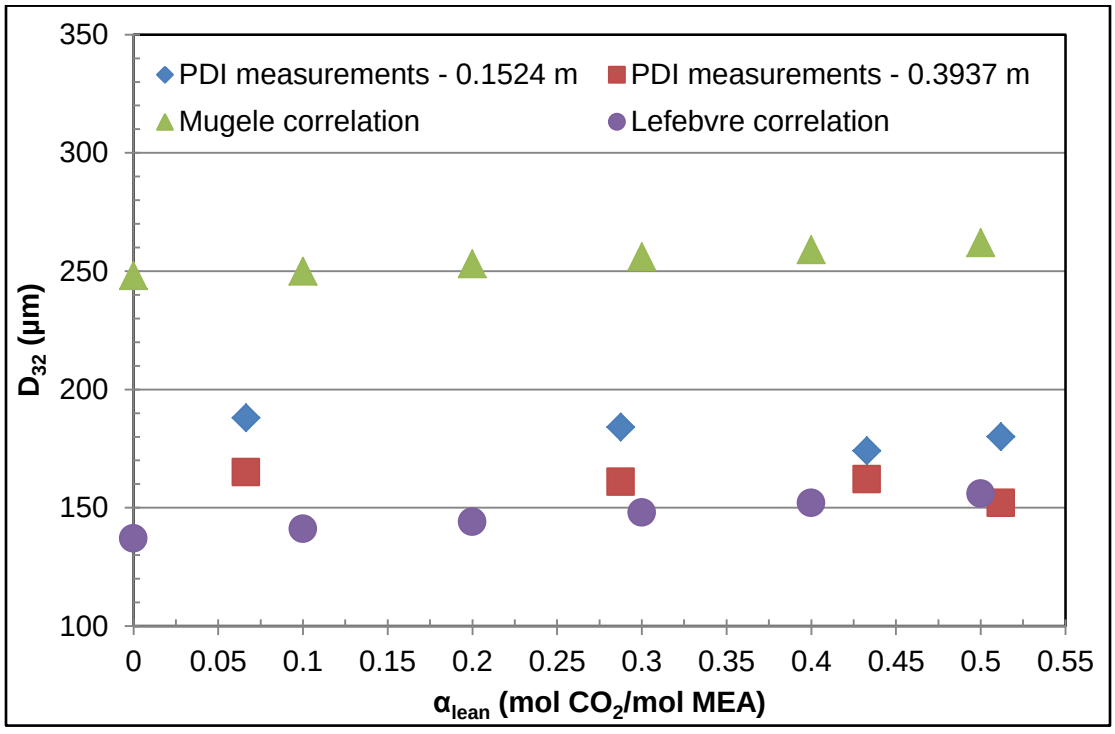

Figure 6.23. Comparison of PDI measurements with correlations for 30 wt% MEA with L/G = 3.45 Lit/m^3

VI.2.2. 40 wt% MEA

Figures 6.24, and 6.25 show the variation of the average D_{32} with inlet loading, and radial distance at an axial distance of 0.1524 m with 40 wt% MEA as the test fluid for L/G ratio of 2.30 Lit/m^3, and 3.45 Lit/m^3. As with 30 wt% MEA, the measured D_{32} is found to be independent of the inlet loading and radial distance for both the L/G ratios employed. In both the plots, all measurements are seen to lie within ±12% of each other.

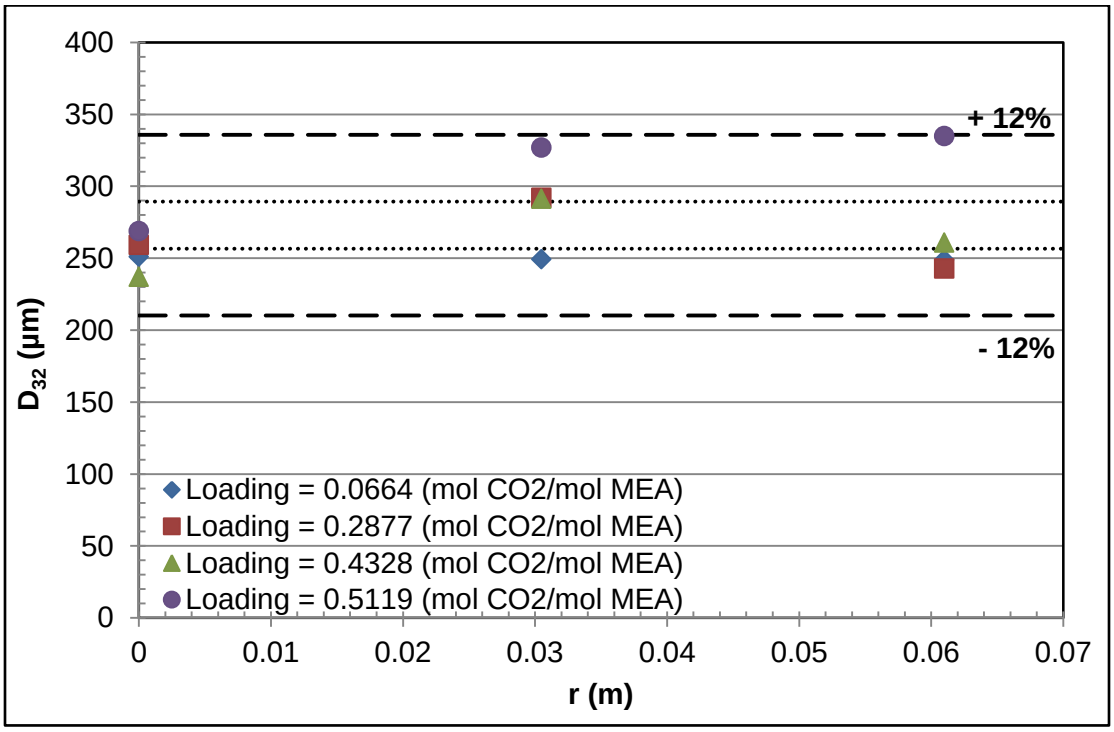

Figure 6.24. Variation of D_{32} with radial distance from column center, and inlet loading for 40 wt% MEA with a L/G ratio of 2.30 Lit/m^3 at an axial distance of 0.1524 m

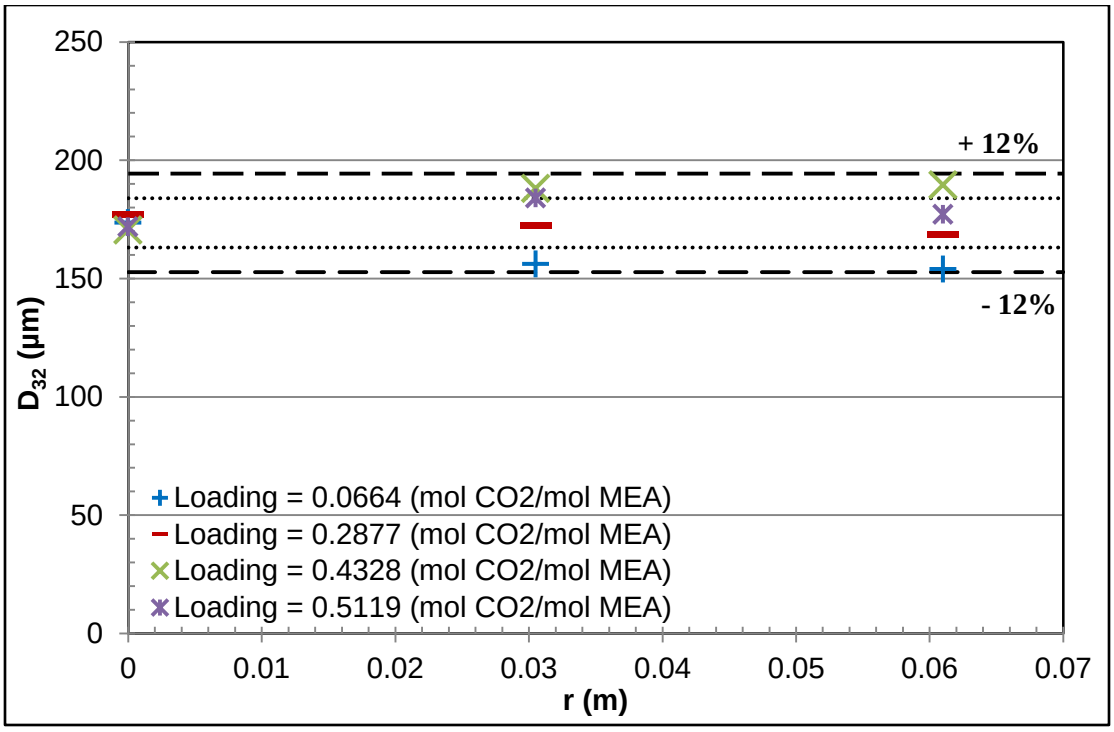

Figure 6.25. Variation of D_{32} with radial distance from column center, and inlet loading for 40 wt% MEA with a L/G ratio of 3.45 Lit/m^3 at an axial distance of 0.1524 m

The effect of L/G ratio on the average D_{32} at all three radial locations with varying inlet loading for 40 wt% MEA is shown in Figure 6.26 below. The increasing L/G ratio is found to reduce the average D_{32} by about 36%. Increased pressure resulted in greater availability of atomization energy (Lefebvre 1988; Liu 1999).

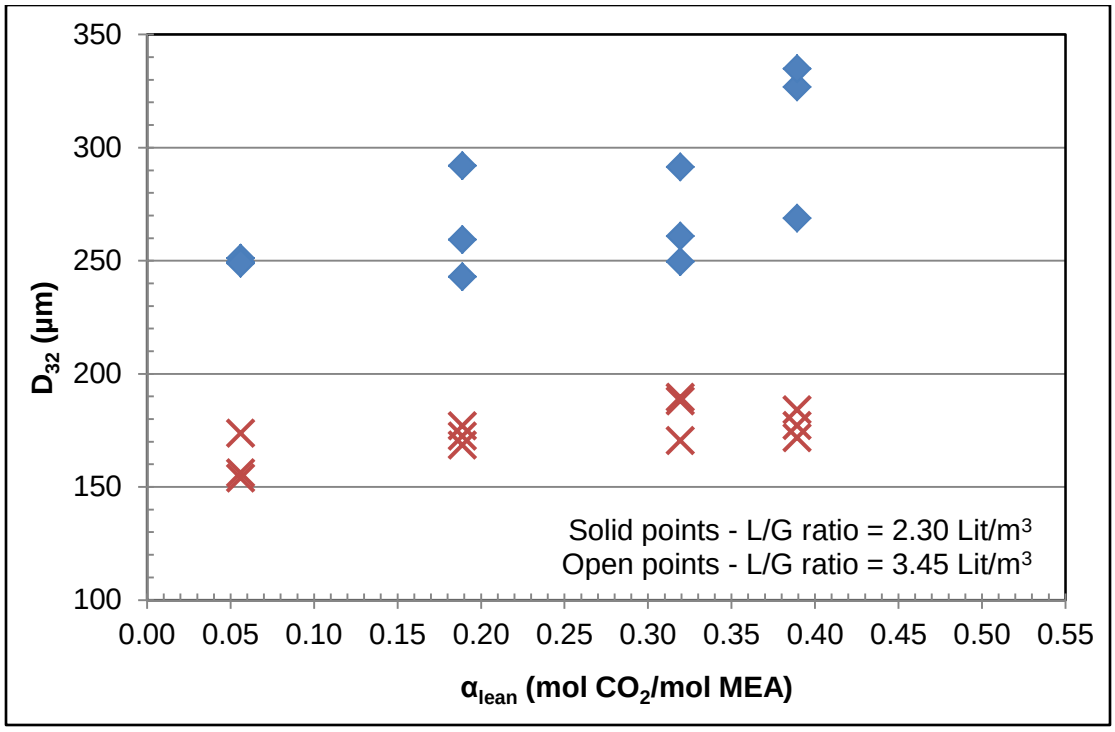

Figure 6.26. Effect of L/G ratio on D_{32} for 40 wt% MEA at 0.1524 m

Figure 6.27 shows the variation of average D_{32} with inlet loading for all three radial locations with a L/G ratio of 2.30 (Lit/m^3) at an axial distance of 0.3937 m below the nozzle tip. No appreciable trend in D_{32} is seen with varying inlet loading. All of the measurements are seen to fall within ±30% (long, flat dotted lines).

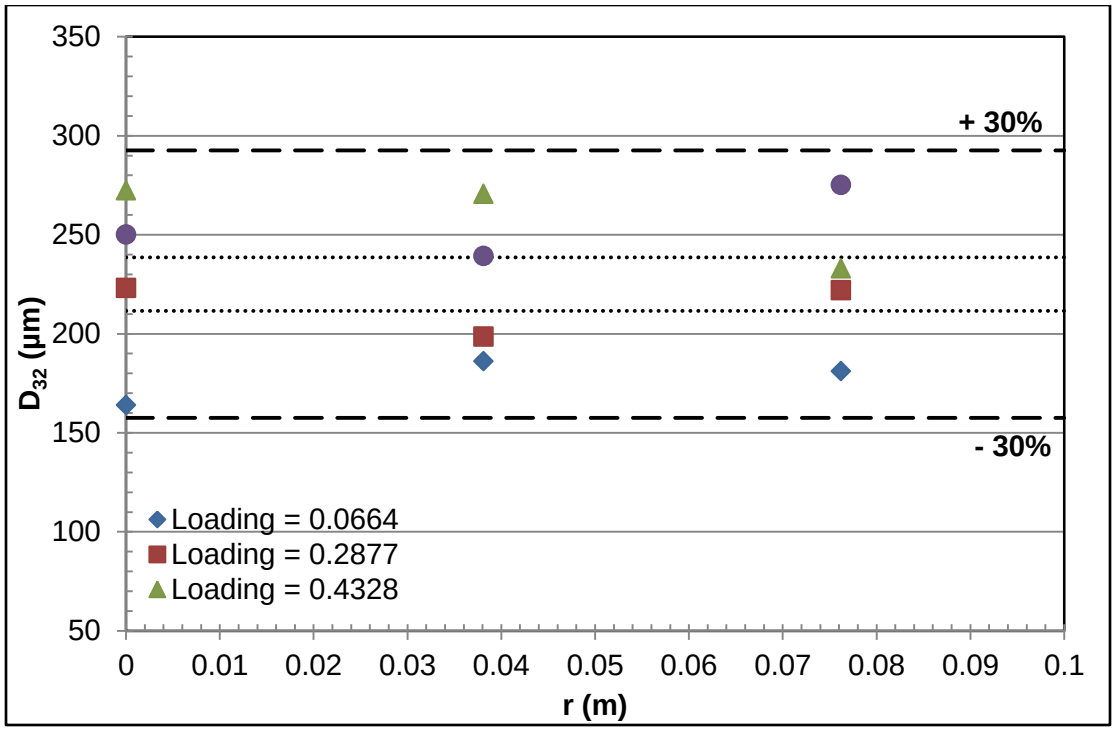

Figure 6.27. Variation of D_{32} with radial distance from column center, and inlet loading for 40 wt% MEA with a L/G ratio of 2.30 Lit/m^3 at an axial distance of 0.3937 m

The variation of the average D_{32} with radial distance, and inlet loading for 40 wt% MEA at an axial distance of 0.3937 m for a L/G ratio of 3.45 Lit/m^3 is shown in Figure 6.28. The D_{32} is found to be practically independent of the inlet loading. All the measured D_{32}'s are found to lie within ±10 % of each other.

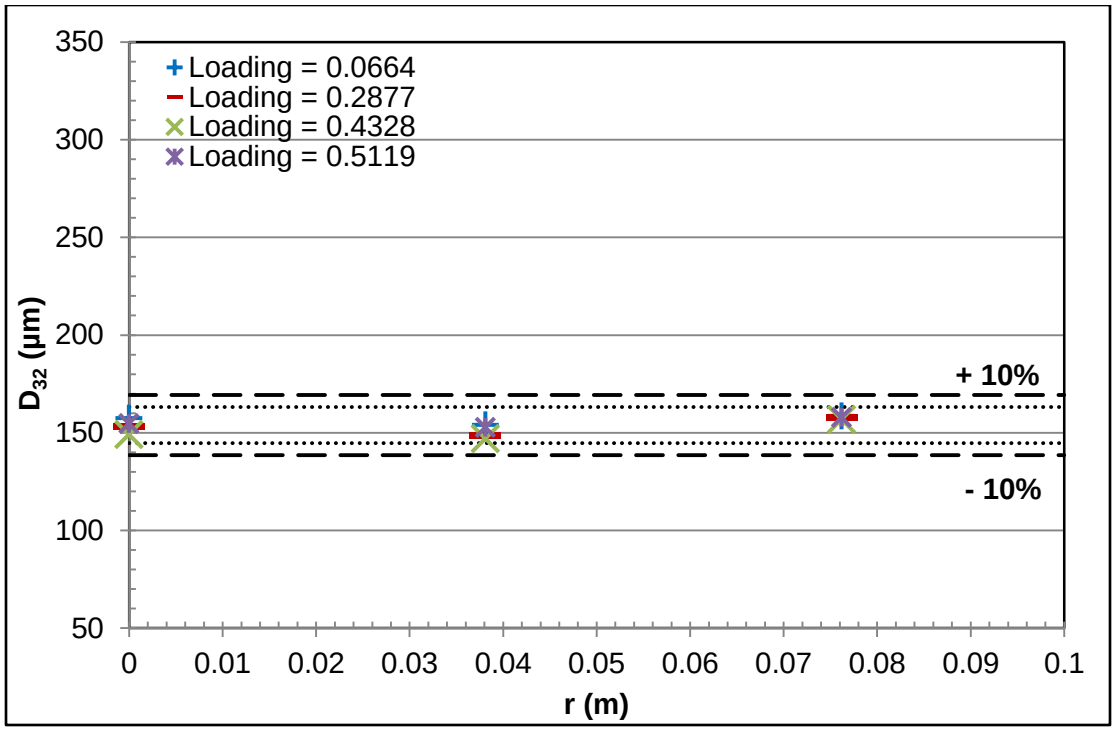

Figure 6.28. Variation of D_{32} with radial distance from column center, and inlet loading for 40 wt% MEA with a L/G ratio of 3.45 Lit/m^3 at an axial distance of 0.3937 m

The effect of L/G ratio on the average D_{32} for radial locations, and inlet loadings at an axial distance of 0.3937 m is shown in Figure 6.29. The average D_{32} is found to reduce by about 30% due to increased supply pressure.

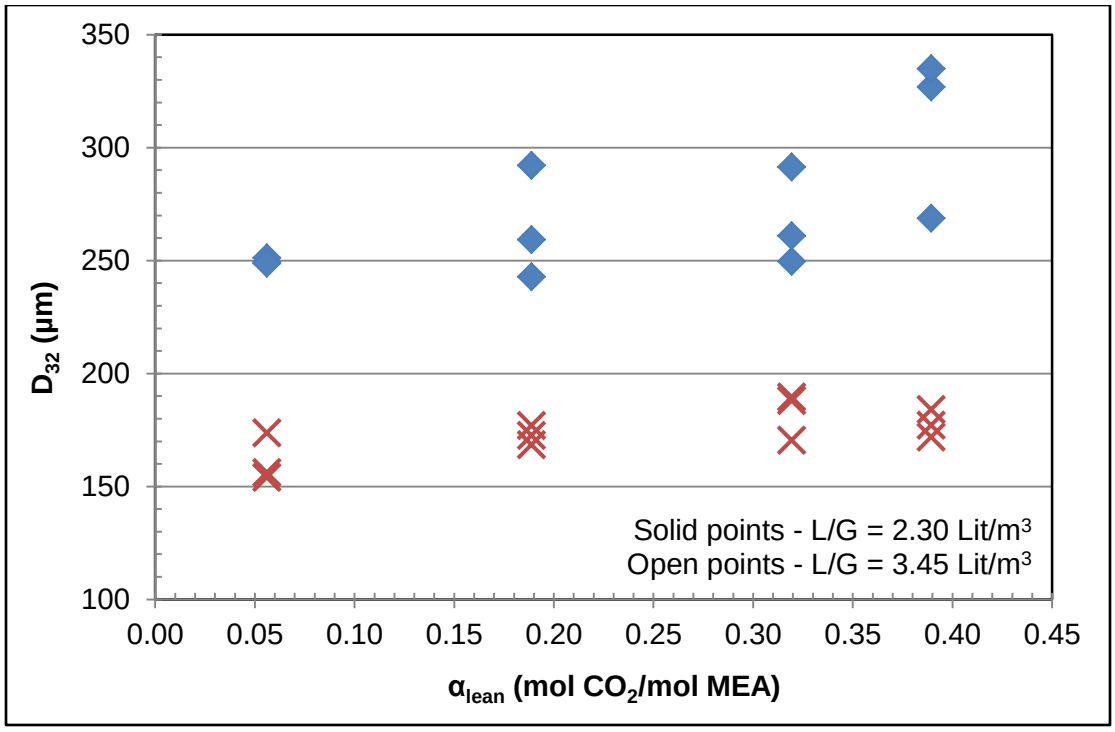

Figure 6.29. Effect of L/G ratio on D_{32} for 40 wt% MEA at 0.3937 m

Figures 6.30, and 6.31 show the comparison of measured D_{32} against established correlations of Mugele (1960), and Lefebvre (1988) for the two L/G ratios employed, respectively. Density and viscosity data from Weiland, Dingman *et. al.* (1998), and surface tension data from Vazquez, Alvarez *et. al.* (1997) were utilized to calculate the D_{32} for both the correlations. As with 30 wt% MEA, the calculated D_{32} from each correlation are found to fall within ±6%. The correlation of Lefebvre (Lefebvre 1988) matches all the PDI measurements to within 15%. The D_{32} PDI measurements at an axial plane 0.3937 m downstream of the nozzle were found to be smaller than at an axial plane 0.1524 m for both the L/G ratios employed because of the spray plume impacting the column wall at an intermediate height.

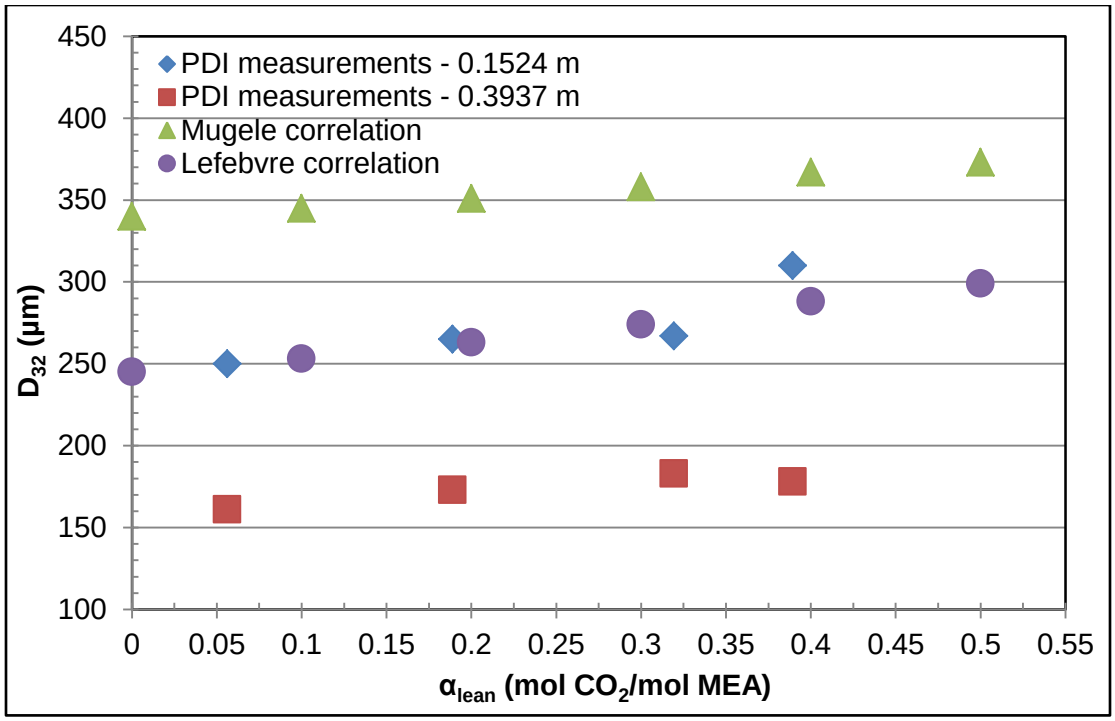

Figure 6.30. Comparison of PDI measurements with correlations for 40 wt% MEA with L/G = 2.30 Lit/m^3

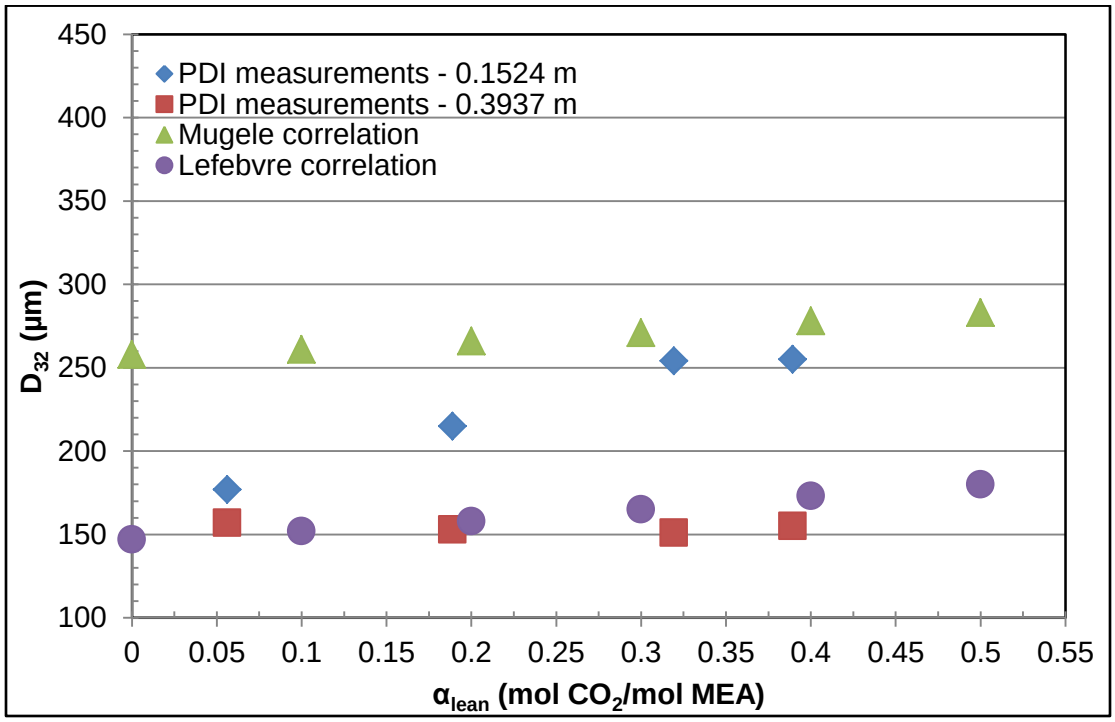

Figure 6.31. Comparison of PDI measurements with correlations for 40 wt% MEA with L/G = 3.45 Lit/m^3

VI.2.3. 30 wt% MEA vs. 40 wt% MEA

Figures 6.32, and 6.33 show the variation of the average planar D_{32} with MEA concentration at two axial distances, at comparable α_{lean} values, respectively. All of the D_{32} measurements are seen to lie within 30%, and 25% of each other, for the two axial distances, respectively. Most of the D_{32} measurements predict a marginal increase in drop size with MEA concentration. This trend of increasing D_{32} with MEA concentration is also predicted by the correlations of Mugele (1960) and Lefebvre (1988).

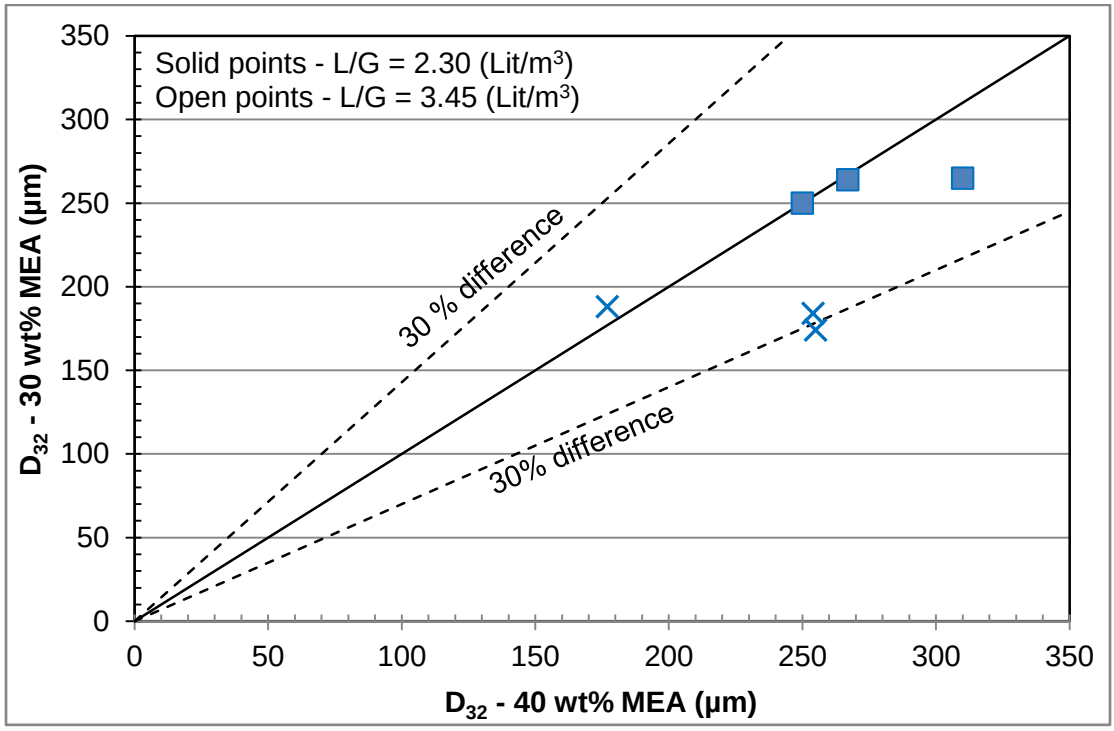

Figure 6.32. Variation of D_{32} with MEA concentration at 0.1524 m

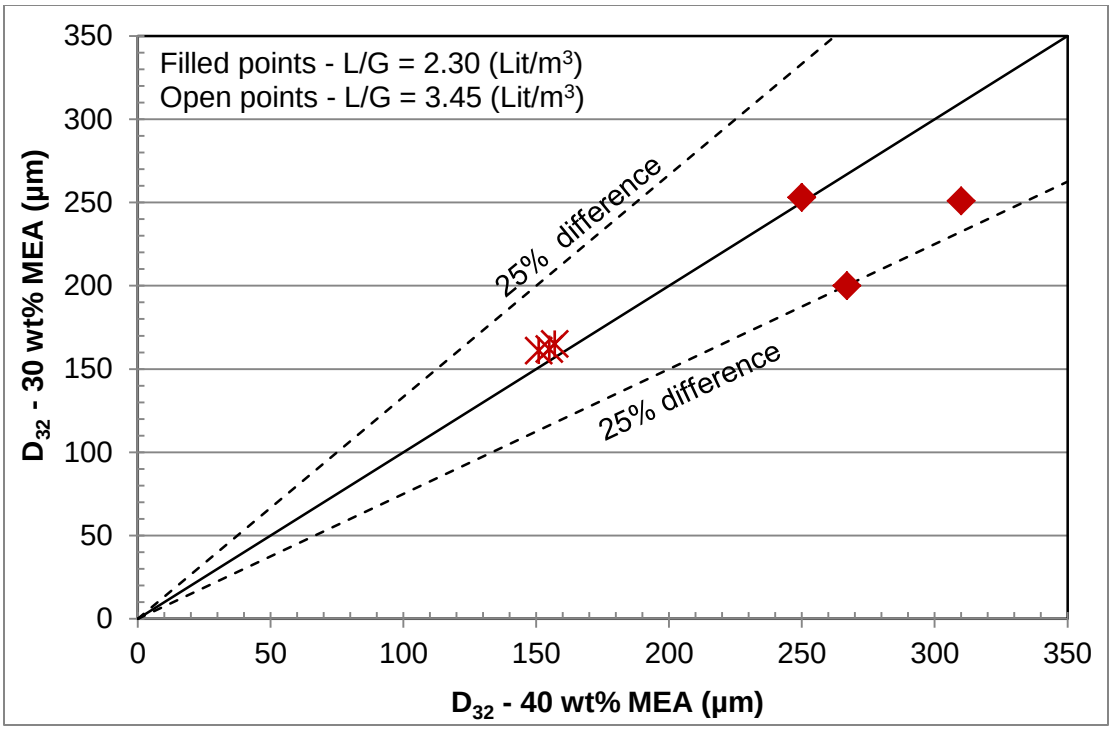

Figure 6.33. Variation of D_{32} with MEA concentration at 0.3937 m

VI.3. Surface Area Results

Planar Surface Areas (P_{SA}) are calculated at two axial planes; 0.1524 m, and 0.3937 m downstream of the nozzle tip. P_{SA}'s are calculated based on the measured dropsize distributions showcased in Section IV.2. Detailed P_{SA} results are presented in Appendix C.

VI.3.1. 30 wt% MEA

Figures 6.34, and 6.35 show the variation of P_{SA} with inlet loading, and L/G ratio for 30 wt% MEA at an axial height of 0.1524 m, and 0.3937 m downstream of the nozzle tip, respectively. P_{SA} for both the L/G ratios is found to be independent of the inlet loading, since the measured drop sizes were found to be practically independent of inlet loading. Increasing L/G ratio is found to increase P_{SA} for all inlet loading conditions. Increasing L/G ratio has been shown to reduce dropsize, thereby resulting in a greater surface area per unit volume of the liquid sprayed.

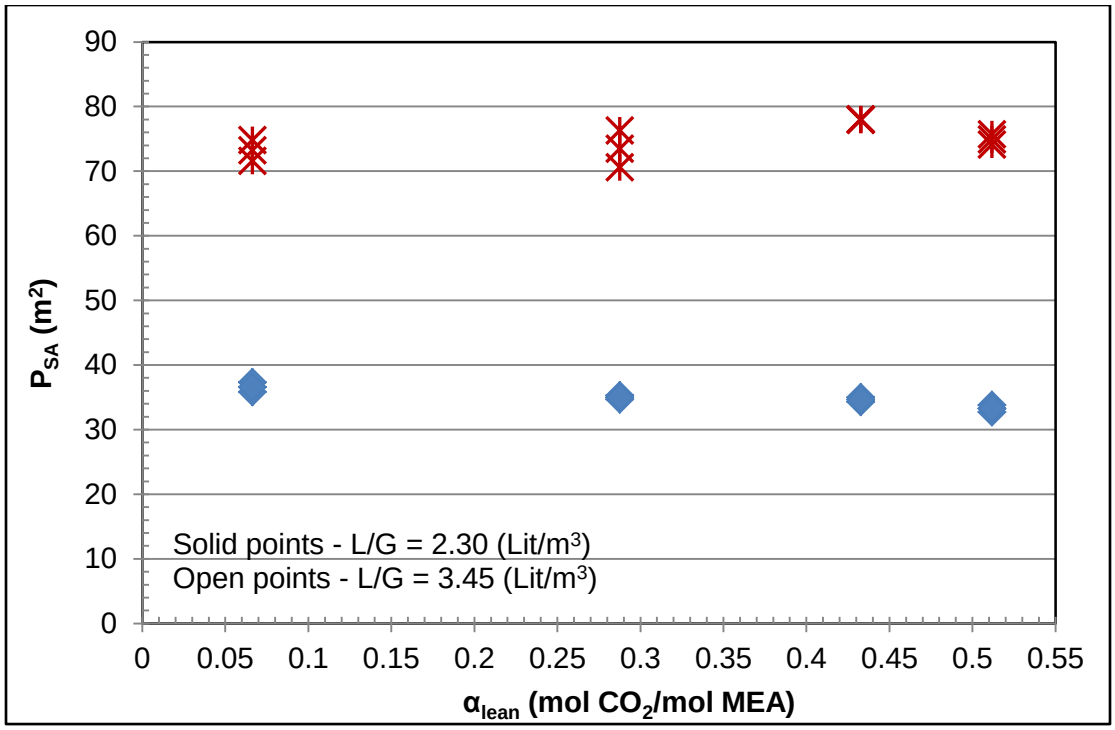

Figure 6.34. Variation of P_{SA} for 30 wt% MEA with inlet loading, and L/G ratio at 0.1524 m

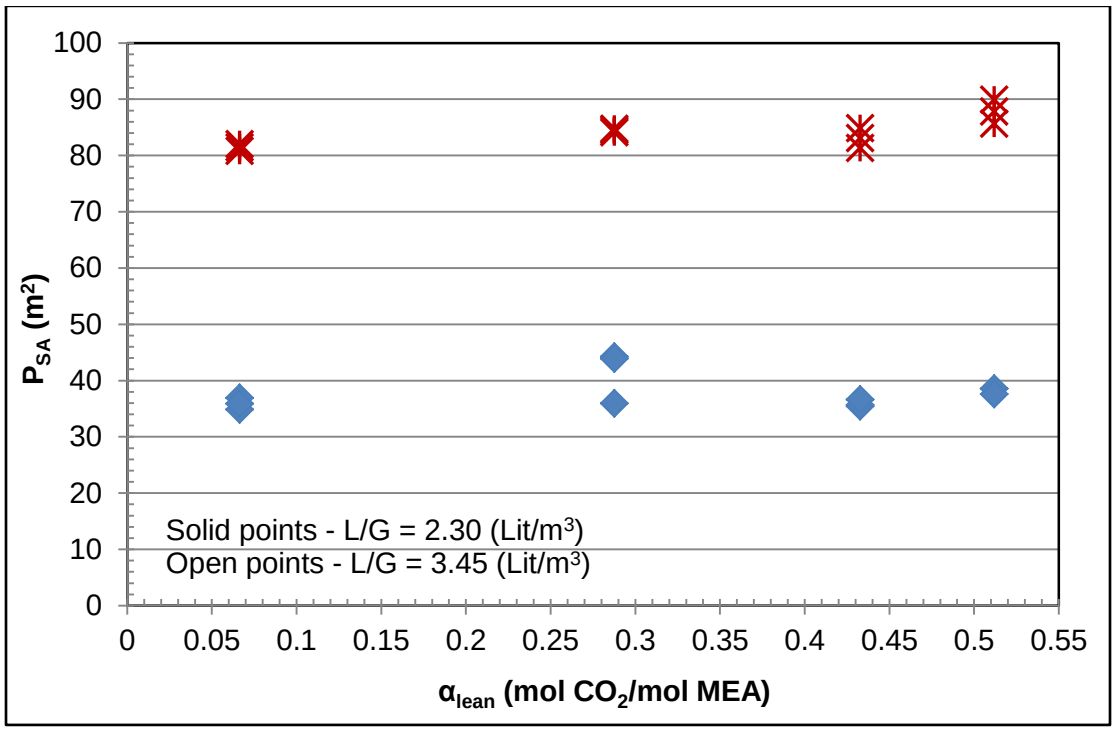

Figure 6.35. Variation of P_{SA} for 30 wt% MEA with inlet loading, and L/G ratio at 0.3937 m

VI.3.2. 40 wt% MEA

Figures 6.36, and 6.37 show the variation of P_{SA} with inlet loading, and L/G ratio for 40 wt% MEA at axial heights of 0.1524 m, and 0.3937 m, respectively. As with 30 wt% MEA, P_{SA}'s are found to be independent of the inlet loading. Increasing L/G ratio is found to result in larger P_{SA}'s. Increasing L/G ratio results in smaller drops and consequently larger P_{SA}.

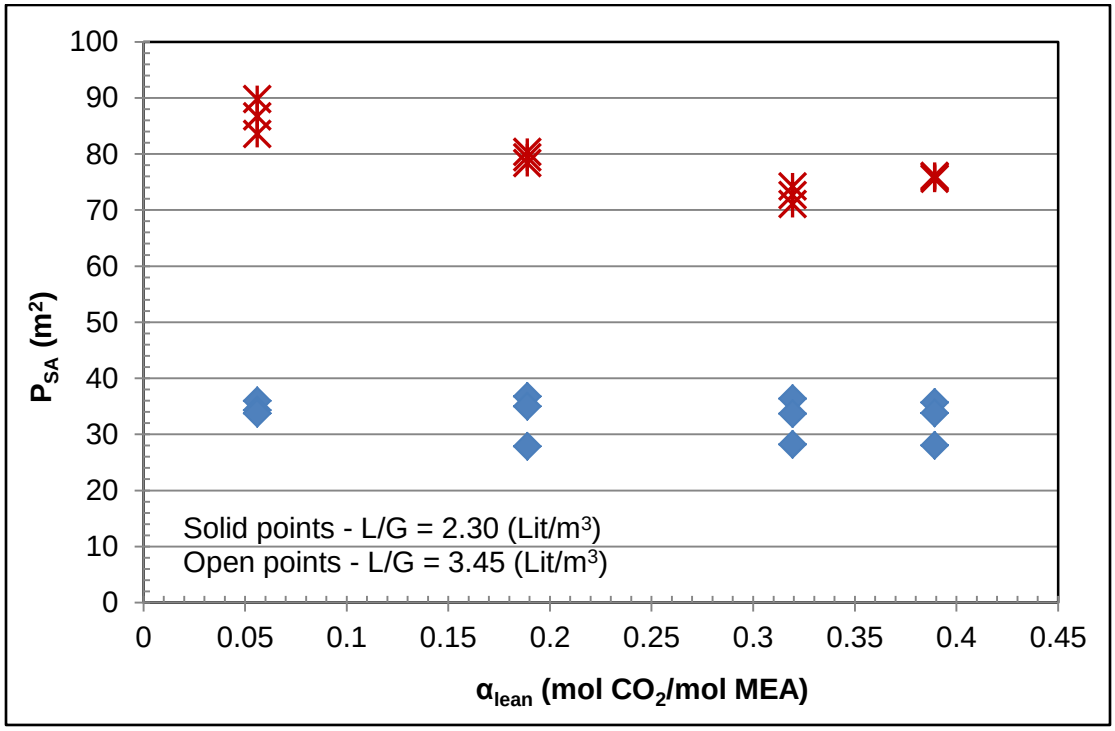

Figure 6.36. Variation of P_{SA} for 40 wt% MEA with inlet loading, and L/G ratio at 0.1524 m

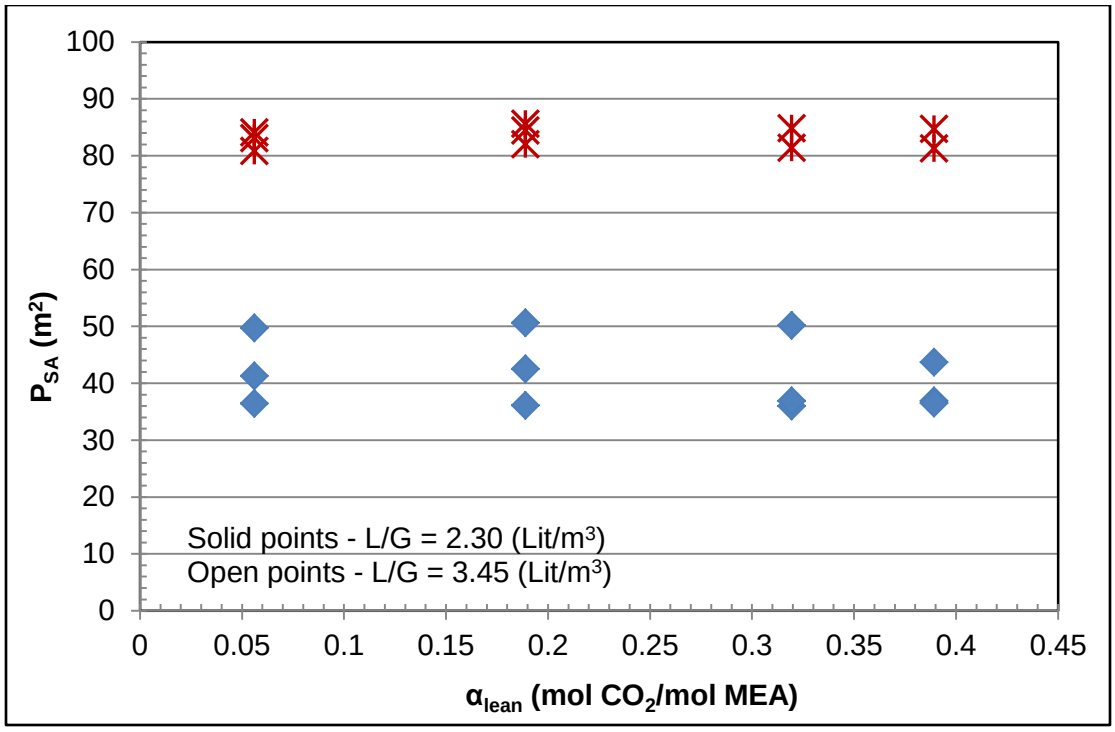

Figure 6.37. Variation of P_{SA} for 40 wt% MEA with inlet loading, and L/G ratio at 0.3937 m

VI.3.3. 30 wt% MEA vs. 40 wt% MEA

Figure 6.38 shows the relative difference between the Fractional Area (F_A) for 30 wt% MEA, and 40 wt% MEA at an axial height of 0.1524 m. The F_A's are found to lie within 20% for comparable inlet loadings, and L/G ratio. The F_A represents the change in P_{SA} for the two MEA concentrations with P_{SA} for water as the baseline.

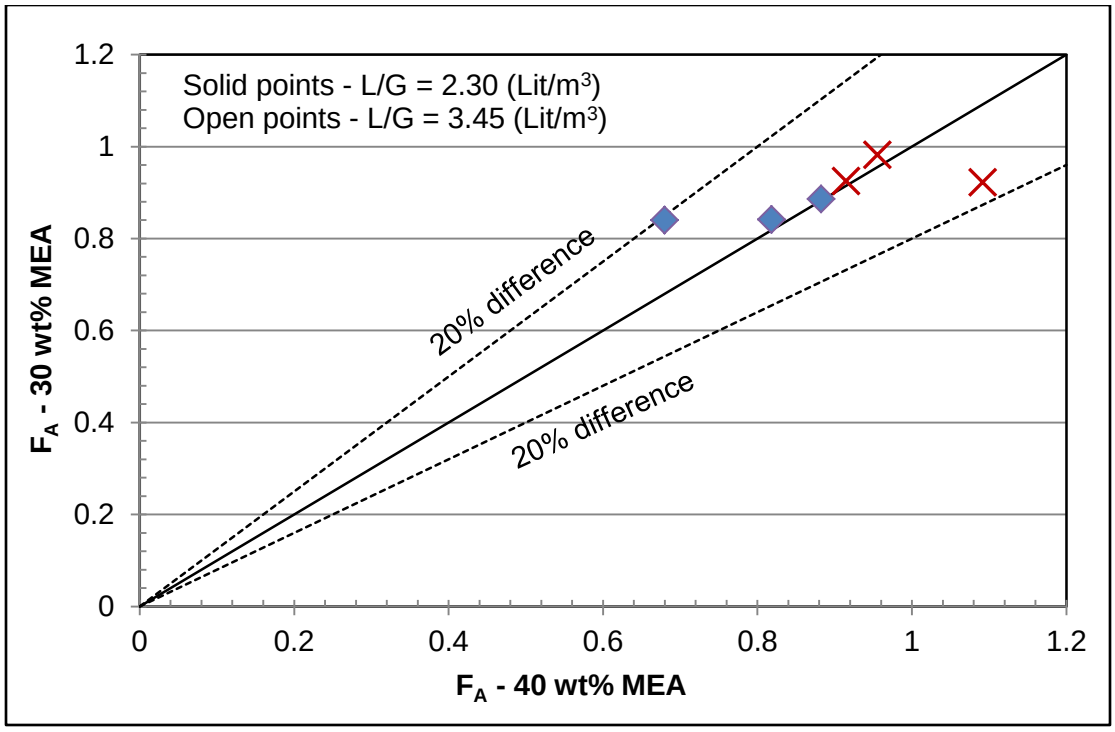

Figure 6.38. Comparison of F_A for 30 wt% MEA and 40 wt% MEA at 0.1524 m

Figure 6.39 shows the comparison of F_A for 30 wt% MEA, and 40 wt% MEA at an axial height of 0.3937 m. The F_A's are found to lie within 30% of each other for comparable inlet loading and L/G ratio.

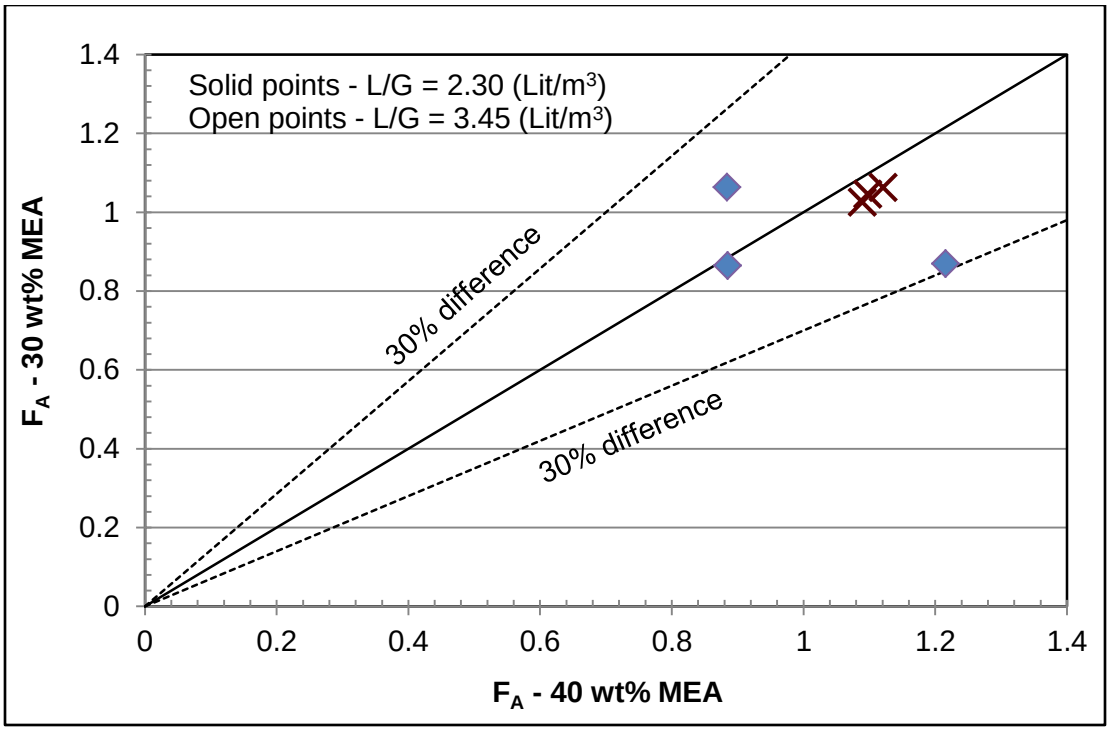

Figure 6.39. Comparison of F_A for 30 wt% MEA and 40 wt% MEA at 0.3932 m

The small difference in F_A for 30 wt% MEA, and 40 wt% MEA at both the axial planes is an indication that the increase in $K_G a_e$ values with MEA concentration seen in Figures 6.14 and 6.15 are not attributable to increasing surface area. The interfacial area (a_e) will likely be a fraction of the available surface area of all drops. The increasing $K_G ae$ values with MEA concentration are a result of the increasing in free MEA content. Free MEA content seems to dominate the spray absorption process.

CHAPTER VII

SODIUM HYDROXIDE RESULTS

NaOH results pertain to interfacial area (a_e) measurements inside the spray column. Interfacial area is the measure of the effective gas-liquid contact area. The interfacial area measurement provides a convenient basis to compare the efficiency of a spray contactor with another spray contactor (with a different nozzle), or a packed column.

The interfacial area measurements were made for two L/G ratios, 2.30 Lit/m^3 and 3.45 Lit/m^3, and two gas-liquid contact heights, 1.5252 m and 0.1778 m. The two L/G ratios and the gas-liquid contact height of 1.5252 m utilized for interfacial area measurements were consistent with the conditions for MEA work.

Figures 7.1, and 7.2 show the effect of L/G ratio on the two gas-liquid contact heights employed. With increasing L/G ratio, the interfacial area was found to increase by about 36% and 50% for the gas-liquid contact heights of 1.5252 m and 0.1778 m, respectively.

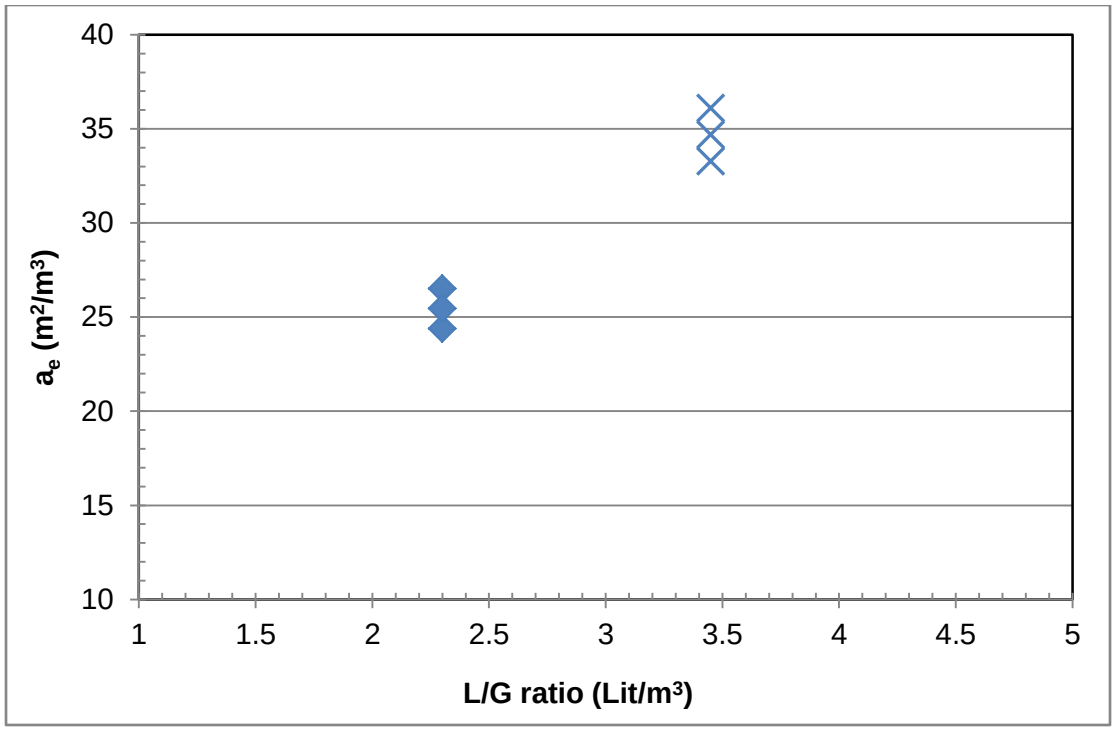

Figure 7.1. Effect of L/G ratio on interfacial area at a height of 1.5252 m

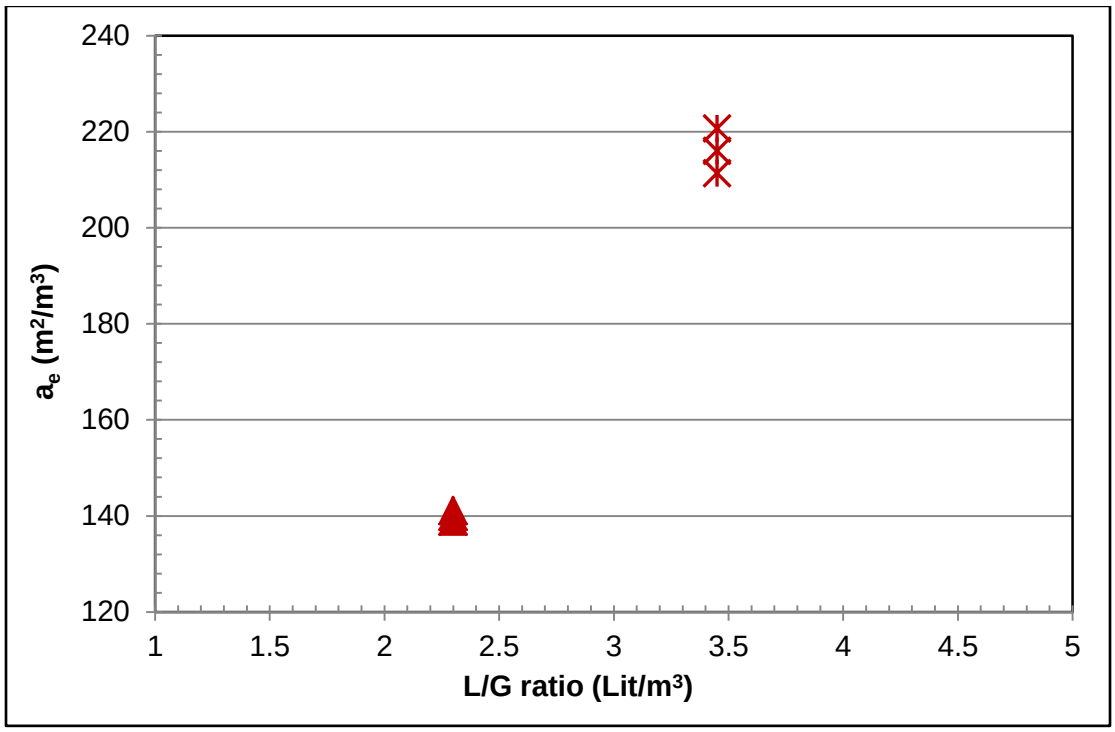

Figure 7.2. Effect of L/G ratio on interfacial area at a height of 0.1778 m

The effect of gas-liquid contact height on the average interfacial area is showcased in Figure 7.3. The measured a_e is found to increase with lowering of the gas-liquid contact height. The average a_e for a L/G ratio of 2.30 Lit/m^3 is found to increase from about 25 m^2/m^3 to about 140 m^2/m^3 by lowering the contact height from 1.5252 m to 0.1778 m, respectively. Similarly, the average a_e for the L/G ratio of 3.45 Lit/m^3 is found to increase from 35 m^2/m^3 to 216 m^2/m^3 with a reduction in the gas-liquid contact height from 1.5252 m to 0.1778 m, respectively.

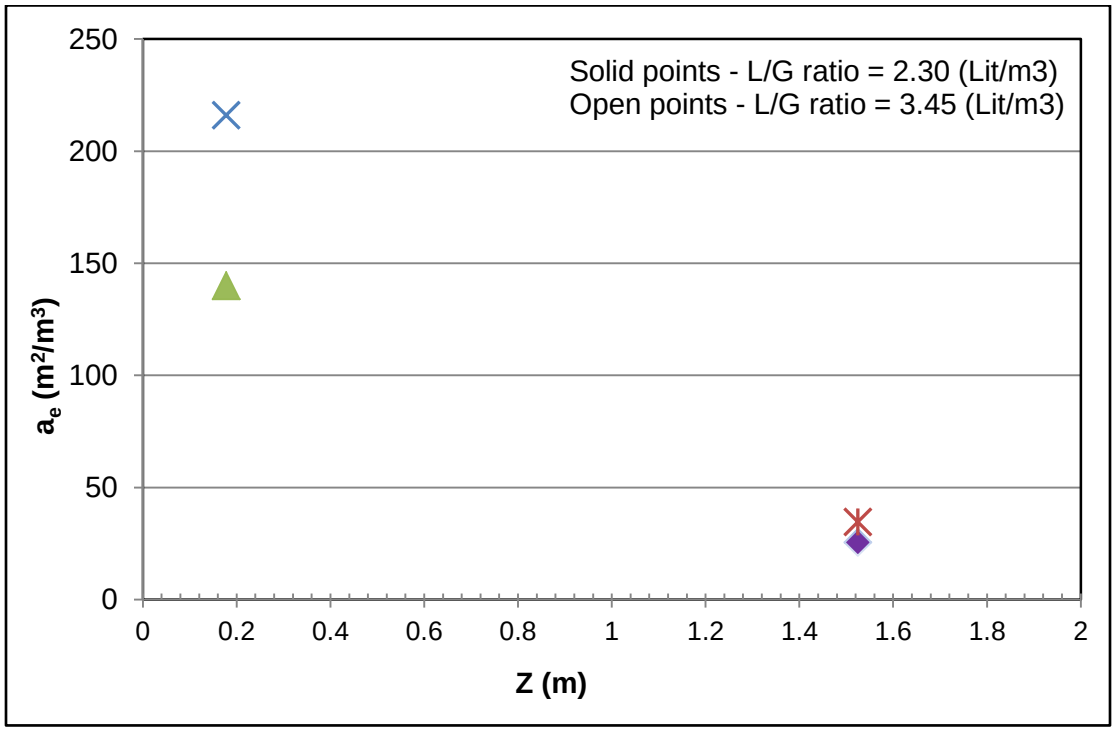

Figure 7.3. Effect of gas-liquid contact height on interfacial area

The large increase in a_e with reduction is an indication of a large amount of mass transfer occurring in the immediate vicinity of the spray nozzle. The areas in the immediate vicinity of the nozzle tip are characterized by a high degree of turbulence and rapid liquid sheet or jet break-up (Lipp 2013a). The lowering of the mass transfer coefficients due to large contact height is more rapid than the improvement expected from an increase in the residence time of the drops.

The increase in a_e with low contact height is consistent with the results obtained with MEA, wherein the mass transfer coefficients and % CO_2 removal efficiency was found to be comparable for the two gas-liquid contact heights employed. The interfacial area in spray columns is highly sensitive to the gas-liquid contact height. The large interfacial areas measured in the small contact height point to the use of squat spray columns for absorption applications.

CHAPTER VIII

CONCLUSIONS & RECOMMENDATIONS

In this work, spray mass transfer rates, drop size data, and planar surface area data for a CO_2-MEA system were presented. Further, interfacial area inside the spray column was ascertained using a CO_2-NaOH system. These measurements were made inside a newly built spray column facility. In this chapter the key findings of this work, limitations of the present study, and recommendations for future work are highlighted.

VIII.1. Conclusions

Based on the MEA results, the following conclusions can be made:

1. A spray column with associated equipment and methods capable of measuring mass transfer rates, dropsize, and surface area, has been successfully built at Oklahoma State University.
2. Coupling of mass transfer data, dropsize data, and surface area quantification can provide better insight in understanding spray absorption.
3. The mass transfer coefficients for CO_2-MEA are found to increase with MEA concentration. Free MEA content of the solvent dominates the spray absorption process.
4. The dropsize distribution and planar surface area were found to be comparable for the two MEA concentrations tested.

5. Increasing MEA concentration for spray absorption of CO_2 may be a feasible option.
6. A large amount of mass transfer was found to occur in the immediate vicinity of the nozzle (before the spray plume impacted the column wall).
7. Impact of wall flow to mass transfer is found to be negligible.

The key conclusions from the interfacial area measurements with NaOH are:

1. Sprays can offer comparable interfacial areas to packings over a limited height.
2. The interfacial area in sprays is strongly dependent on the gas-liquid contact height.
3. The large interfacial areas measured in the spray column for a small gas-liquid contact height point to the use of short contact spray columns.
4. The contribution of wall flow to interfacial area is negligible.

VIII.2. Limitations

Before proceeding to list the recommendations from this work, the following limitations of the present study need to be pointed out. The limitations of the present study are:

1. In this work, the inlet gas was not saturated because of the limitations imposed by the volume of water required to saturate the gas. Saturation of gas will greatly help in matching the mass balance on the gas and liquid side.
2. The L/G ratios employed in this work are at the lower end of the operational range of commercial spray contactors. Spray contactors are found to operate at an L/G ratio of 10 Lit/m^3 (U.S. EPA 1982) and above.
3. In the present study, low gas velocities were utilized for all runs. Increasing the gas velocity at constant inlet CO_2 gas composition was not feasible due to the practical limits of the CO_2 cylinder bank heating manifold. The gas velocity was kept low to avoid freezing the CO_2 injection piping.

4. The mass transfer rates could not be reported at fixed increments of inlet loading for the MEA work. In absence of a stripper to regenerate the MEA solvent, solvent cost and disposal were found to be a substantial hindrance. Measuring rates at fixed increments of inlet solvent loading would have resulted in a large inventory of MEA solvent.
5. Dropsize and mass transfer runs had to be carried out separately. Solvent inventory limitations and lack of automation were the prime reasons for this.
6. For this work, the interfacial area measurements were made solely to compliment the MEA work. Effect of gas rate and quantification of the contribution of drop surface area to interfacial area were never attempted.
7. No attempt was made in the work to ascertain the gas side mass transfer coefficients.

VIII.3. Recommendations

Primary recommendations from this work are:

1. Saturation of inlet gas prior to column entry is needed.
2. The present study needs to be repeated with higher L/G ratios. Effect of nozzle type, gas rate, and varying inlet CO_2 gas concentration on mass transfer rates need to be evaluated.
3. A shorter column could be utilized to reduce space. Further, co-flow and cross flow spray columns need to be tested. Multiple stages (each spray column being a stage) with interstate cooling could be utilized.
4. The local gas side mass transfer coefficient needs to be ascertained. Unloaded, 15 wt% MEA solutions could be utilized to measure the gas side mass transfer coefficient with indoor air (Pacheco 1998). Use of unloaded, 15 wt% MEA solution ensures that the reaction between CO_2 and MEA is fast and all of the resistance to mass transfer is on the gas side. A form of the Equation 2.10 could then be utilized to measure the local gas side mass transfer coefficient.

5. More radial and axial measurements for dropsize should be made. More radial and axial measurements of the PDI will help improve the planar surface area calculations. The change in surface across the height of the column could then be ascertained. This will provide added insight into surface area effects inside spray columns.
6. Development of a robust interfacial area correlation for spray columns is needed. The developed correlation needs to be scalable with changing nozzle geometry and column height.
7. Measurement of solvent physical properties (density, viscosity, and surface tension) with mass transfer and dropsize measurements will greatly reduce any uncertainties in the calculations.
8. Blends of MEA-MDEA (Methyldiethanolamine) solvents should be tested. The analytical procedures developed and highlighted in this work can be easily extended to MEA-MDEA blends.

REFERENCES

Abu-Zahra, M. R. M., L. H. J. Schneiders, J. P. M. Niederer, P. H. M. Feron and G. F. Versteeg (2007). "CO_2 capture from power plants: Part I. A parametric study of the technical performance based on monoethanolamine." International Journal of Greenhouse Gas Control **1**(1): 37-46.

Albrecht, H.-E., Borys, M., Damaschke, N., and C. Tropea (2003). Laser Doppler and phase Doppler measurement techniques, Springer.

Astarita, G., Savage, D. W. and A. Bistro (1983). Gas treating with chemical solvents, John Wiley & Sons.

Bachalo, W. D. (1980). "Method for measuring the size and velocity of spheres by dual-beam light-scatter interferometry." Applied Optics **19**(3): 363-370.

Bachalo, W. D. and M. J. Houser (1984). "Phase/Doppler spray analyzer for simultaneous measurements of drop size and velocity distributions." Optical Engineering **23**(5): 235583-235583-.

Bade, K. and R. Schick (2008). "Volume distribution comparison methods for 1D, 2D, and point measurement techniques." ILASS Americas.

Bade K. (2014). Personal communication. Y. Tamhankar. Stillwater, OK.

Bandyopadhyay, A. and M. N. Biswas (2012). "CO_2 capture in a spray column using a critical flow atomizer." Separation and Purification Technology **94**(0): 104-114.

Barrett PVL. (1966). Gas absorption on a sieve plate. Cambridge, UK, University of Cambridge. Ph.D. Dissertation.

Blauwhoff, P., Versteeg, G., and W. Van Swaaij (1983). "A study on the reaction between CO_2 and alkanolamines in aqueous solutions." Chemical Engineering Science **38**(9): 1411-1429.

Bonilla, C. F., Mottes, J. R., and M. Wolf (1950). "Air humidification coefficients in spray towers - gas-film mass transfer coefficients at low air velocities for use in scrubber Design." Industrial and Engineering Chemistry **42**(12): 2521-2525.

Bose, A. K. and D. C. T. Pei (1964). "Evaporation rates in spray drying." The Canadian Journal of Chemical Engineering **42**(6): 259-262.

Bys, B. (2012). Personal communication. Y. Tamhankar. Stillwater, OK

Critchfield, J. (1998). CO_2 absorption/desorption in methyldiethanolamine solutions promoted with monoethanolamine and diethanolamine: mass transfer and reaction kinetics. Austin, TX, The University of Texas at Austin. Ph.D. Dissertation.

Carslaw, H. S. and J. C. Jaeger (1959). Conduction of heat in solids. Clarendon Press.

Closmann, F. B. (2011). Oxidation and thermal degradation of methyldiethanolamine/piperazine in CO_2 capture. Austin, TX, The University of Texas at Austin. Ph.D. Dissertation.

Crank, J. (1957). The mathematics of diffusion. Clarendon Press.

Danckwerts PV. (1951). "Significance of liquid-film coefficients in gas absorption." Industrial and Engineering Chemistry **43**(6):1460-1467.

Danckwerts PV (1970). Gas-liquid reactions. McGraw-Hill.

Dimiccoli, A., Di Serio, M., and E. Santacesaria (2000). "Mass transfer and kinetics in spray-tower-loop absorbers and reactors." Industrial & Engineering Chemistry Research **39**(11): 4082-4093.

Dodge, L. G. (1987). "Comparison of performance of drop-sizing instruments." Applied Optics **26**(7): 1328-1341.

Dugas, R. E. (2009). Carbon dioxide absorption, desorption & diffusion in aqueous piperzine & monoethanolamine. Austin, TX, The University of Texas at Austin. Ph.D. Dissertation.

Feng, B., Du, M., Dennis, T. J., Anthony, K., and M.J. Perumal (2009). "Reduction of energy requirement of CO_2 desorption by adding acid into CO_2-loaded solvent." Energy & Fuels **24**(1), 213-219.

Freeman, S. (2011). Thermal degradation and oxidation of aqueous piperazine for carbon dioxide capture. Austin, TX, The University of Texas at Austin. PhD. Dissertation.

Frossling, N. (1938). "The evaporation of falling drops." Gerland Beitrage Zur Geophysik **52**: 170-216.

Haubrock J, Hogendoorn JA, and G. Versteeg (2005). "The applicability of activities in kinetic expressions: a more fundamental approach to represent the kinetics of the system CO_2-OH^- in terms of activities." International Journal of Chemical Reaction Engineering **3**(1): 1-17.

Higbie, R. (1935). "The rate of absorption of pure gas into a still liquid during short periods of exposure." Transactions of the American Institute of Chemical Engineers **31**: 365-389.

Hilliard, M. (2008). A predictive thermodynamic model for an aqueous blend of potassium carbonate, piperazine, and monoethanolamine for carbon dioxide capture from flue gas. Austin, TX, The University of Texas at Austin. Ph.D. Dissertation.

Hixson, A. W. and C. E. Scott (1935). "Absorption of gases in spray towers." Industrial and Engineering Chemistry **27**(3): 307-314.

Javed, K. H., Mahmud, T., and E. Purba (2010). "The CO_2 capture performance of a high-intensity vortex spray scrubber." Chemical Engineering Journal **162**(2): 448-456.

Kohl, A. L. and R. Nielsen (1997). Gas purification, Gulf Professional Publishing.

Koller, M., Wappel, D., Trofaier, N., and G. Gronald (2011). "Test results of CO_2 spray scrubbing with monoethanolamine." Energy Procedia **4**(0): 1777-1782.

Kuntz, J. (2006). Absorption of carbon dioxide in a spray column. Saskatchewan, University of Regina. M.A.S. Thesis.

Lefebvre, A. (1988). Atomization and sprays, CRC press.

Levenspiel, O. (1999). Chemical reaction engineering, John Wiley & Sons.

Lewis W.K. and W.G. Whitman (1924). "Principles of gas absorption." Industrial and Engineering Chemistry **16**(12):1215-1220.

Lipp, C. (2013a). Practical spray technology. Lake Innovation LLC.

Lipp, C. (2013b). Personal communication. Y. Tamhankar. Kemah, TX.

Lipp, C. (2014). "Spray nozzle 101: spray nozzle selection." Chemical Engineering Progress **110**(8): 51- 58.

Liu, H. (1999). Science and engineering of droplets: fundamentals and applications, William Andrew.

Maddox, R. N. (1974). Gas and liquid sweetening. John M. Campbell (Campbell Petroleum Series).

Marshall, W. R., Jr. and W. E. Ranz (1955). "Heat and mass transfer in spray drying." Transactions of the American Society of Mechanical Engineers **77**: 1377-1385.

Mehta, K. C. and M. M. Sharma (1970). "Mass transfer in spray columns." British Chemical Engineering **15**(11): 1440-1442.

Mugele, R. A. (1960). "Maximum stable droplets in dispersoids." AIChE Journal **6**(1): 3-8.

Mycock, J. C., McKenna, J. D., and L. Theodore (1995). Handbook of air pollution control engineering and technology, CRC Press.

Oexmann, J. and A. Kather (2010). "Minimising the regeneration heat duty of post-combustion CO_2 capture by wet chemical absorption: the misguided focus on low heat of absorption solvents." International Journal of Greenhouse Gas Control **4**(1): 36-43.

Oyenekan, B. A. and G. T. Rochelle (2009). "Rate modeling of CO_2 stripping from potassium carbonate promoted by piperazine." International Journal of Greenhouse Gas Control **3**(2): 121-132.

Pacheco, M.A. (1998). Mass transfer, kinetics, and rate-based modelling of reactive absorption. Austin, TX, University of Texas at Austin. Ph.D. Dissertation.

Pagcatipunan, C., and R. Schick (2005). "Maximize the performance of spray nozzle systems." Chemical Engineering Progress **101**(12): 38-44.

Pigford, R. L. and C. Pyle (1951). "Performance characteristics of spray-type absorption equipment." Industrial and Engineering Chemistry **43**(7): 1649-1662.

Pinilla, E. A., Diaz, J. M., and J. Coca (1984). "Mass transfer and axial dispersion in a spray tower for gas-liquid contacting." Canadian Journal of Chemical Engineering **62**(5): 617-622.

Pohorecki R, and W. Moniuk (1988). "Kinetics of reaction between carbon dioxide and hydroxyl ions in aqueous electrolyte solutions." Chemical Engineering Science **43**(7): 1677-1684.

Rousseau, R. W. (1987). Handbook of separation process technology, John Wiley & Sons.

Rochelle, G. T. (2009a). "Amine scrubbing for CO_2 capture." Science **325**: 1652-1654.

Rochelle, G. T. (2009b). "CO_2 Capture by aqueous absorption: summary of 2nd quarterly progress reports 2009." http://www.che.utexas.edu/rochelle_group/Pubs/Rochelle_Q2_Report_2009.pdf." Retrieved 1/14/2015, 2015.

Rochelle, G.T., Chen, E., Freeman, S., Wagener, D.V., Xu, Q., and A. Voice (2011). "Aqueous piperazine as the new standard for CO_2 capture technology." Chemical Engineering Journal **171**(3): 725-733.

Sardar, H., Sivasubramanian, M.S., and R. Weiland (1985). "Simulation of absorbers and strippers in commercial amine treating units." Houston, TX, AIChE Conference.

Schick R. (2014). Personal communication. Y. Tamhankar. Stillwater, OK.

Seader, J.D., and E.J. Henley (2006). Separations process principles. John Wiley and Sons.

Sherwood, T.K., Shipley, G.H., and F.A.L. Holloway (1938). "Flooding velocities in packed columns." Industrial and Engineering Chemistry **30**(7): 765-769.

Sherwood, T. K., R. L. Pigford and C. R. Wilke (1975). Mass transfer, McGraw-Hill.

Siperley, C. (2013). Personal communication. Y. Tamhankar. Stillwater, OK.

Srinivasan, V. and R. C. Aiken (1988). "Mass transfer to droplets formed by the controlled breakup of a cylindrical jet-physical absorption." Chemical Engineering Science **43**(12): 3141-3150.

Strigle, R. F. (1994). Packed tower design and applications: random and structured packings. Gulf Publishing Company.

Tamhankar, Y. S., Whiteley, J. R., Resetarits, M. R., & Aichele, C. P. (2014a). "Spray droplet characterization inside a glass column through dense wall flow." Atomization and Sprays, **24**(2): 115-128.

Tamhankar, Y., B. King, R. Whiteley, M. Resetarits, T. Cai and C. Aichele (2014b). "Aqueous amine spray absorption and droplet distribution data for CO_2 capture applications." Energy Procedia **63**(0): 293-300.

Taniguchi, I., Takamura, Y., and K. Asano (1997). "Experimental study of gas absorption with a spray column." Journal of Chemical Engineering of Japan **30**(3): 427-433.

Taniguchi, I., Yokoyama, H., and K. Asano (1999). "Mass transfer in absorption of lean gas using small spray column." Journal of Chemical Engineering of Japan **32**(1): 145-150.

Treybal, R. E. (1980). Mass-transfer operations. McGraw-Hill.

Tsai, R. E. (2010). Mass transfer area of structured packing. Austin, TX, The University of Texas at Austin. Ph.D. Dissertation.

Turpin, A., Couvert, A., Laplanche, A., & Paillier, A. (2008). "Experimental study of mass transfer and H_2S removal efficiency in a spray tower." Chemical Engineering and Processing: Process Intensification **47**(5): 886-892.

U.S. Energy Information Administration (USEIA 2011). Net generation by energy source and type of Producer.

U.S. Energy Information Administration (USEIA 2014). U.S. energy-related carbon dioxide emissions, 2013.

U.S. Evironmental Protection Agency (USEPA 1982). Control techniques for particulate emissions from stationary sources- Volume 1. EPA-450/3-81-005a

U.S. Department of Energy (USDOE 2008). Annual Energy Outlook.

Van Wagener, D. H. (2011). Stripper modeling for CO_2 removal using monoethanolamine and piperazine solvents. Austin, TX, The University of Texas at Austin. Ph.D. Dissertation.

Vazquez, G., E. Alvarez, J. M. Navaza, R. Rendo and E. Romero (1997). "Surface tension of binary mixtures of water+ monoethanolamine and water+ 2-amino-2-methyl-1-propanol and tertiary mixtures of these amines with water from 25 C to 50 C." Journal of Chemical & Engineering Data **42**(1): 57-59.

Vivian, J.E., and D.W. Peaceman (1956). “Liquid-side resistance in gas absorption.” AIChE Journal **2**(4): 437-443.

Weber, C. (1931). “Disintegration of liquid jets.” Zeitschrift für Angewandte Mathematik und Mechanik **11**(2), 136-159.

Weiland, R. H., Rawal, M., & Rice, R. G. (1982). "Stripping of carbon dioxide from monoethanolamine solutions in a packed column." AIChE Journal **28**(6): 963-973.

Weiland, R. H., Dingman, J. C., Cronin, D. B., and G. J. Browning (1998). "Density and viscosity of some partially carbonated aqueous alkanolamine solutions and their blends." Journal of Chemical & Engineering Data **43**(3): 378-382.

Whiteley, R. (2012). Personal communication. Y. Tamhankar. Stillwater, OK.

Winter, W. E. (1974). Mass Transfer in a Liquid-Gas Spray Column. College Park, MD, University of Maryland. Ph.D. Dissertation.

Yeh, N. K. and G. T. Rochelle (2003). "Liquid-phase mass transfer in spray contactors." AIChE Journal **49**(9): 2363-2373.

APPENDICES

APPENDIX A – MEA MASS TRANSFER DATA

30 wt % MEA; L/G = 2.30 Lit/m^3; Z=1.5252 m

	G_{total}	G_I	$y_{CO2,in}$	$N_{CO2,g}$	L_{MEA}	α_{lean}	α_{rich}	$N_{CO2,l}$	Δp_{lm}	$K_G a_e$	% CO_2 Removal
	kmol/min	kmol/min	-	kmol/min	kmol/min	mol CO_2/mol MEA	mol CO_2/mol MEA	kmol/min	atm	kmol/m^3.min.atm	
Run 1	0.01457	0.00181	0.124	0.000772	0.00377	0	0.18343	0.000692	0.10951	0.12814	38.30
Run 2	0.01440	0.00179	0.124	0.000748	0.00377	0	0.17836	0.000673	0.10999	0.12405	37.66
Average										0.12609	37.98
Run 1	0.01462	0.00175	0.12	0.000544	0.00389	0.15504	0.27794	0.000478	0.11370	0.08523	27.23
Run 2	0.01440	0.00179	0.124	0.000584	0.00389	0.15504	0.27673	0.000473	0.11806	0.08127	26.48
Average										0.08325	26.86
Run 1	0.01457	0.00182	0.125	0.000351	0.00398	0.27448	0.35700	0.000329	0.12469	0.05348	18.05
Run 2	0.01457	0.00181	0.124	0.000436	0.00398	0.27448	0.35982	0.000340	0.12317	0.05599	18.82
Average										0.05473	18.44
Run 1	0.01451	0.00181	0.125	0.000292	0.00404	0.34942	0.38003	0.000124	0.13175	0.01904	6.82
Run 2	0.01453	0.00182	0.125	0.000229	0.00404	0.34942	0.37709	0.000112	0.13211	0.01716	6.15
Average										0.01810	6.49
Run 1	0.01440	0.00173	0.120	0.000098	0.00406	0.37914	0.40318	0.000098	0.12688	1.5611E-02	5.65
Run 2	0.01453	0.00177	0.122	0.000131	0.00406	0.37914	0.40271	0.000096	0.12916	1.50E-02	5.40
Average										1.53E-02	5.53

30 wt % MEA; L/G = 3.45 Lit/m^3; Z=1.5252 m

	G_{total}	$Gco_{2,in}$	$y_{CO2,in}$	$N_{CO2,g}$	L_{MEA}	α_{lean}	α_{rich}	$N_{CO2,l}$	Δp_{lm}	$K_G a_e$	% CO_2 Removal
	kmol/min	kmol/min	-	kmol/min	kmol/min	mol CO_2/mol MEA	mol CO_2/mol MEA	kmol/min	atm	kmol/m^3.min.atm	
Run 1	0.01440	0.00177	0.123	0.000821	0.00583	0.15504	0.26564	0.000645	0.11001	0.11890	36.40
Run 2	0.01440	0.00173	0.120	0.000789	0.00583	0.15504	0.26668	0.000651	0.10636	0.12414	37.66
Average										0.12152	37.03
Run 1	0.01440	0.00177	0.123	0.000613	0.00598	0.27448	0.34999	0.000451	0.11770	0.07776	25.47
Run 2	0.01440	0.00179	0.124	0.000629	0.00598	0.27448	0.40281	0.000609	0.11235	0.10995	34.10
Average										0.09386	29.79
Run 1	0.01440	0.00176	0.122	0.000414	0.00606	0.34942	0.38221	0.000199	0.12575	0.03205	11.31
Run 2	0.01440	0.00174	0.121	0.000398	0.00606	0.34942	0.37351	0.000146	0.12653	0.02340	8.38
Average										0.02772	9.84
Run 1	0.01440	0.00176	0.122	0.000414	0.00609	0.37914	0.42299	0.000122	0.12805	0.01935	6.95
Run 2	0.01440	0.00174	0.121	0.000398	0.00609	0.37914	0.39919	0.000122	0.12715	0.01949	7.01
Average										0.01942	6.98

Unloaded, 30 wt % MEA; Z=0.1017 m

	G_{total}	$Gco_{2,in}$	$y_{CO2,in}$	$N_{CO2,g}$	L_{MEA}	α_{lean}	α_{rich}	$N_{CO2,l}$	Δp_{lm}	$K_G a_e$	% CO_2 Removal
	kmol/min	kmol/min	-	kmol/min	kmol/min	mol CO_2/mol MEA	mol CO_2/mol MEA	kmol/min	atm	kmol/m^3.min.atm	
Run 1	0.01411	0.00171	0.121	0.000600	0.00385	0.09355	0.29067	0.000758	0.10217	2.25792	44.40
Run 2	0.01401	0.00168	0.120	0.000638	0.00385	0.09355	0.29235	0.000765	0.10045	2.31615	45.49
Average										2.28703	44.94
Run 1	0.01401	0.00168	0.120	0.000710	0.00577	0.09355	0.24595	0.000879	0.09498	2.81680	52.31
Run 2	0.01401	0.00169	0.121	0.000754	0.00577	0.09355	0.24595	0.000879	0.09615	2.78233	51.88
Average										2.79956	52.09

40 wt % MEA; L/G = 2.30 Lit/m^3; Z=1.5252 m

	G_{total}	G_l	$y_{CO2,in}$	$N_{CO2,g}$	L_{MEA}	α_{lean}	α_{rich}	$N_{CO2,l}$	Δp_{lm}	$K_G a_e$	% CO_2 Removal
	kmol/min	kmol/min	-	kmol/min	kmol/min	mol CO_2/mol MEA	mol CO_2/mol MEA	kmol/min	atm	kmol/m^3.min.atm	
Run 1	0.01438	0.00174	0.121	0.000760	0.00384	0.0529	0.3352	0.001085	0.08692	0.25313	62.31
Run 2	0.01438	0.00181	0.126	0.000866	0.00384	0.0529	0.2914	0.000916	0.10138	0.18336	50.56
Average										0.21824	56.44
Run 1	0.01438	0.00173	0.12	0.000640	0.00403	0.2503	0.4576	0.000835	0.09743	0.17385	48.38
Run 2	0.01433	0.00172	0.120	0.000653	0.00403	0.2503	0.4483	0.000798	0.09909	0.16327	46.38
Average										0.16856	47.38
Run 1	0.01433	0.00173	0.121	0.000488	0.00405	0.2710	0.3583	0.000354	0.11912	0.06022	20.39
Run 2	0.01433	0.00172	0.120	0.000479	0.00405	0.2710	0.3791	0.000438	0.11473	0.07742	25.46
Average										0.06882	22.93
Run 1	0.01386	0.00168	0.121	0.000323	0.00423	0.4415	0.5312	0.000379	0.11244	0.06844	22.62
Run 2	0.01381	0.00168	0.122	0.000337	0.00423	0.4415	0.5249	0.000353	0.11481	0.06232	20.94
Average										0.06538	21.78
Run 1	0.01388	0.00168	0.121	0.000233	0.00427	0.5158	0.6082	0.000395	0.04397	1.8204E-01	23.49
Run 2	0.01378	0.00167	0.121	0.000231	0.00427	0.5158	0.59	0.000317	0.07258	8.85E-02	19.01
Average										1.35E-01	21.25

40 wt % MEA; L/G = 3.45 Lit/m^3; Z=1.5252 m

	G_{total}	G_l	$y_{CO2,in}$	$N_{CO2,g}$	L_{MEA}	α_{lean}	α_{rich}	$N_{CO2,l}$	Δp_{lm}	$K_G a_e$	% CO_2 Removal
	kmol/min	kmol/min	-	kmol/min	kmol/min	mol CO_2/mol MEA	mol CO_2/mol MEA	kmol/min	atm	kmol/m^3.min.atm	
Run 1	0.01433	0.00176	0.123	0.001087	0.00576	0.0529	0.2348	0.001048	0.09110	0.23344	59.47
Run 2	0.01451	0.00176	0.121	0.001042	0.00576	0.0529	0.2482	0.001126	0.08526	0.26778	64.10
Average										0.25061	61.79
Run 1	0.01433	0.00172	0.12	0.000872	0.00604	0.2503	0.4348	0.001115	0.08341	0.27112	64.83
Run 2	0.01433	0.00172	0.120	0.000886	0.00604	0.2503	0.4053	0.000937	0.09293	0.20442	54.46
Average										0.23777	59.64
Run 1	0.01433	0.00176	0.123	0.000744	0.00608	0.2710	0.3700	0.000602	0.11157	0.10936	34.12
Run 2	0.01446	0.00173	0.120	0.000703	0.00608	0.2710	0.3879	0.000710	0.10376	0.13886	40.94
Average										0.12411	37.53
Run 1	0.01393	0.00170	0.122	0.000490	0.00634	0.4415	0.5388	0.000617	0.10234	0.12235	36.31
Run 2	0.01393	0.00169	0.121	0.000504	0.00634	0.4415	0.5141	0.000461	0.11077	0.08434	27.32
Average										0.10335	31.82
Run 1	0.01440	0.00176	0.122	0.000414	0.00641	0.5158	0.5567	0.000262	0.10353	0.05133	14.91
Run 2	0.01440	0.00174	0.121	0.000398	0.00641	0.5158	0.5608	0.000288	0.09961	0.05870	16.54
Average										5.501E-02	15.72

Unloaded, 40 wt % MEA; Z=0.1017 m

	G_{total}	$Gco_{2,in}$	$y_{CO2,in}$	$N_{CO2,g}$	L_{MEA}	α_{lean}	α_{rich}	$N_{CO2,l}$	Δp_{lm}	$K_G a_e$	% CO_2 Removal
	kmol/min	kmol/min	-	kmol/min	kmol/min	mol CO_2/mol MEA	mol CO_2/mol MEA	kmol/min	atm	kmol/m^3.min.atm	
Run 1	0.01429	0.00174	0.122	0.000682	0.00384	0.04796	0.25279	0.000787	0.10247	2.33716	45.13
Run 2	0.01429	0.00182	0.127	0.000760	0.00384	0.04796	0.24719	0.000765	0.10918	2.13345	42.17
Average										2.23530	43.65
Run 1	0.01429	0.00177	0.124	0.000888	0.00576	0.04796	0.20879	0.000927	0.09826	2.87059	52.30
Run 2	0.01419	0.00176	0.124	0.000895	0.00576	0.04796	0.20872	0.000926	0.09793	2.87881	52.67
Average										2.87470	52.48

APPENDIX B – MEA DROPSIZE DATA

30 wt% MEA	Axial Height (m)	Inlet Loading	L/G ratio	Radial location 0 (m)			Radial location 0.0381 (m)			Radial location (m) 0.0762		
				Run 1	Run 2	Average	Run 1	Run 2	Average	Run 1	Run 2	Average
	0.3937	0.0664	2.30	261.7	242.5	252.1	254.3	244.1	249.2	265.3	248	256.65
	0.3937	0.2877	2.30	178.6	185.7	182.15	195.1	203.8	199.45	217.8	218.1	217.95
	0.3937	0.4328	2.30	262.7	233.7	248.2	232.9	241.9	237.4	263.4	271.4	267.4
	0.3937	0.5119	2.30	205	227.1	216.05	230.6	212.2	221.4	270.7	254.4	262.55

30 wt% MEA	Axial Height (m)	Inlet Loading	L/G ratio	Radial location 0 (m)			Radial location 0.03181 (m)			Radial location (m) 0.0762		
				Run 1	Run 2	Average	Run 1	Run 2	Average	Run 1	Run2	Average
	0.3937	0.0664	3.45	164.6	163.9	164.25	159.4	160.9	160.15	174.1	168.6	171.4
	0.3937	0.2877	3.45	159.7	165.5	162.6	152.2	156.9	154.55	165.8	163.2	164.5
	0.3937	0.4328	3.45	159.4	164.6	162	156.7	156	156.35	162.7	174.6	168.7
	0.3937	0.5119	3.45	150.8	145.4	148.1	149.6	148.4	149	151.6	168.5	160.1

30 wt% MEA	Axial Height (m)	Inlet Loading	L/G ratio	Radial location 0 (m)			Radial location 0.0305 (m)			Radial location 0.061(m)		
				Run 1	Run 2	Average	Run 1	Run 2	Average	Run 1	Run 2	Average
	0.1504	0.0664	2.30	256.9	249.2	253.05	236.5	243.2	239.85	263.7	248.7	256.2
	0.1504	0.2877	2.30	255.3	256.6	255.95	286.2	286.2	286.2	248.8	248.8	248.8
	0.1504	0.4328	2.30	267	271.1	269.05	262.7	261.3	262	266	264.6	265.3
	0.1504	0.5119	2.30	279.3	275.7	277.5	292.6	299	295.8	254.3	266.3	260.3

30 wt% MEA	Axial Height (m)	Inlet Loading	L/G ratio	Radial location 0 (m)			Radial location 0.0305 (m)			Radial location 0.061(m)		
				Run 1	Run 2	Average	Run 1	Run 2	Average	Run 1	Run 2	Average
	0.1504	0.0664	3.45	202.1	190.8	196.45	187.8	178.6	183.2	187.6	180.5	184.1
	0.1504	0.2877	3.45	170.9	187.6	179.25	200.9	169.6	185.25	181.4	191.4	186.4
	0.1504	0.4328	3.45	171.8	180.4	176.1	165.4	166	165.7	180.4	177.4	178.9
	0.1504	0.5119	3.45	179.8	178.9	179.35	173.1	169.7	171.4	190.7	185.6	188.2

40 wt% MEA	Axial Height (m)	Inlet Loading	L/G ratio	Radial location 0 (m)			Radial location 0.0305 (m)			Radial location 0.061 (m)		
				Run 1	Run 2	Average	Run 1	Run 2	Average	Run 1	Run 2	Average
	0.1504	0.0561	2.30	249.3	253	251.15	249.8	248.9	249.35	254	243.6	248.8
	0.1504	0.1889	2.30	263.7	254.9	259.3	290.8	293.3	292.05	234.6	251.1	242.85
	0.1504	0.3194	2.30	262.2	237	249.6	292.2	290.5	291.35	258.9	262.9	260.9
	0.1504	0.3893	2.30	261.4	276.2	268.8	329.7	323.9	326.8	339.5	330.3	334.9

40 wt% MEA	Axial Height (m)	Inlet Loading	L/G ratio	Radial location 0 (m)			Radial location 0.0305 (m)			Radial location 0.061 (m)		
				Run 1	Run 2	Average	Run 1	Run 2	Average	Run 1	Run 2	Average
	0.1504	0.0561	3.45	172.8	174.5	173.65	155.2	157.1	156.15	164.5	143.4	154.0
	0.1504	0.1889	3.45	177.4	176.4	176.9	170.3	174.7	172.5	166	170.9	168.5
	0.1504	0.3194	3.45	167.1	173.8	170.45	180.4	195.7	188.05	187.7	191.4	189.6
	0.1504	0.3893	3.45	168.7	174.9	171.8	182.3	185.8	184.05	176.4	177.8	177.1

40 wt% MEA	Axial Height (m)	Inlet Loading	L/G ratio	Radial location 0(m)			Radial location 0.0381 (m)			Radial location 0.0762 (m)		
				Run 1	Run 2	Average	Run 1	Run 2	Average	Run 1	Run 2	Average
	0.3937	0.0561	2.30	168.5	159.3	163.9	186.5	185.7	186.1	183.3	178.9	181.1
	0.3937	0.1889	2.30	229.2	217	223.1	197	200.2	198.6	209.6	234.2	221.9
	0.3937	0.3194	2.30	244	272.4	258.2	280.3	261	270.65	232.9	232.9	232.9
	0.3937	0.3893	2.30	258.2	242.1	250.15	232.6	245.8	239.2	262.1	288.1	275.1

40 wt% MEA	Axial Height (m)	Inlet Loading	L/G ratio	Radial location 0(m)			Radial location 0.0381 (m)			Radial location 0.0762 (m)		
				Run 1	Run 2	Average	Run 1	Run 2	Average	Run 1	Run 2	Average
	0.3937	0.0561	3.45	158.1	156.9	157.5	153.2	154.7	153.95	158.8	158.2	158.5
	0.3937	0.1889	3.45	154.6	151.4	153	147.3	150.3	148.8	160.6	154.5	157.6
	0.3937	0.3194	3.45	147.3	151	149.15	145.3	148.7	147	159.8	153.7	156.8
	0.3937	0.3893	3.45	154.3	155.1	154.7	149.4	156.1	152.75	157.3	158.1	157.7

APPENDIX C- MEA PLANAR SURFACE AREA DATA

Planar Surface Area					
30 wt % MEA; 0.1524 m; L/G= 2.3Lit/m^3					
	Inlet Loading	Zone 1 (m^2)	Zone 2 (m^2)	Zone 3 (m^2)	PSA (m^2)
Run 1	0.0664	3.9221	12.7413	19.1495	35.8
Run 2	0.0664	4.0414	12.3924	20.8287	37.3
Average					36.55
Run 1	0.2877	3.9411	10.5193	20.2818	34.7
Run 2	0.2877	3.9411	10.5193	20.2818	34.7
Average					34.7
Run 1	0.4328	3.7724	11.5174	18.9861	34.3
Run 2	0.4328	3.7151	11.5328	19.7035	35.0
Average					34.65
Run 1	0.5119	3.6076	10.2979	19.8558	33.8
Run 2	0.5119	3.6528	10.0779	18.9624	32.7
Average					33.25

Planar Surface Area					
30 wt % MEA; 0.1524 m; L/G= 3.45 Lit/m^3					
	Inlet Loading	Zone 1 (m^2)	Zone 2 (m^2)	Zone 3 (m2)	P_{SA} (M^2)
Run 1	0.0664	7.4511	24.0214	40.1564	71.6
Run 2	0.0664	7.8936	25.2480	41.7055	74.8
Average					73.2
Run 1	0.2877	8.8163	22.4556	39.3424	70.6
Run 2	0.2877	8.0841	26.6771	41.5509	76.3
Average					73.45
Run 1	0.4328	8.7414	27.3167	41.8255	77.9
Run 2	0.4328	8.3416	27.1940	42.4838	78.0
Average					77.95
Run 1	0.5119	8.3833	26.1311	39.5766	74.1
Run 2	0.5119	8.4169	26.6343	40.6366	75.7
Average					74.9

Planar Surface Area					
30 wt % MEA; 0.3937 m; L/G= 2.3 Lit/m^3					
	Inlet Loading	Zone 1 (m^2)	Zone 2 (m^2)	Zone 3 (m2)	P_{SA} (M^2)
Run 1	0.0664	3.7978	11.8940	19.1366	34.8
Run 2	0.0664	4.1522	12.4641	20.3164	36.9
Average					35.85
Run 1	0.2877	5.6205	15.4766	23.1400	44.2
Run 2	0.2877	5.4063	15.0403	23.1011	43.5
Average					43.85
Run 1	0.4328	3.8023	12.9862	19.1421	35.9
Run 2	0.4328	4.2789	12.5056	18.5766	35.4
Average					35.65
Run 1	0.5119	4.8900	13.1048	18.6204	36.6
Run 2	0.5119	4.4057	14.2431	19.8143	38.5
Average					37.55

Planar Surface Area					
30 wt % MEA; 0.3937 m; L/G= 3.45 Lit/m^3					
	Inlet Loading	Zone 1 (m^2)	Zone 2 (m^2)	Zone 3 (m2)	P_{SA} (M^2)
Run 1	0.0664	9.1840	28.4115	43.2401	80.8
Run 2	0.0664	9.2516	28.1326	44.6485	82.0
Average					81.4
Run 1	0.2877	9.4695	29.7358	45.4952	84.7
Run 2	0.2877	9.1671	28.8460	46.1129	84.1
Average					84.4
Run 1	0.4328	9.4883	28.9169	46.4079	84.8
Run 2	0.4328	9.1855	29.0142	43.1329	81.3
Average					83.05
Run 1	0.5119	10.0144	30.2405	49.6733	89.9
Run 2	0.5119	10.3792	30.4833	44.7334	85.6
Average					87.75

Planar Surface Area					
40 wt % MEA; 0.1524 m; L/G= 2.30 Lit/m^3					
	Inlet Loading	Zone 1 (m^2)	Zone 2 (m^2)	Zone 3 (m2)	P_{SA} (M^2)
Run 1	0.0561	4.0380	12.0651	19.8769	36.0
Run 2	0.0561	3.9791	12.1076	20.7188	36.8
Average					36.4
Run 1	0.1889	3.8188	10.3630	21.5287	35.7
Run 2	0.1889	3.9514	10.2257	20.1154	34.3
Average					35
Run 1	0.3194	3.8423	10.3197	19.5051	33.7
Run 2	0.3194	4.2422	10.3730	19.1940	33.8
Average					33.75
Run 1	0.3893	3.8513	9.1387	14.8799	27.9
Run 2	0.3893	3.6427	9.2998	15.2816	28.2
Average					28.05

Planar Surface Area					
40 wt % MEA; 0.3937 m; L/G= 2.30 Lit/m^3					
	Inlet Loading	Zone 1 (m^2)	Zone 2 (m^2)	Zone 3 (m2)	P_{SA} (M^2)
Run 1	0.0561	5.9549	16.1961	27.5105	49.7
Run 2	0.0561	6.2977	16.2212	28.1230	50.6
Average					50.15
Run 1	0.1889	4.3570	15.3323	24.0239	43.7
Run 2	0.1889	4.6283	15.1183	21.5116	41.3
Average					42.5
Run 1	0.3194	3.6063	10.7853	21.6354	36.0
Run 2	0.3194	3.6557	11.5840	21.6423	36.9
Average					36.45
Run 1	0.3893	3.8867	12.9949	19.2343	36.1
Run 2	0.3893	4.1403	12.3014	17.5084	34.0
Average					35.05

Planar Surface Area					
40 wt % MEA; 0.3937 m; L/G= 3.45 Lit/m^3					
	Inlet Loading	Zone 1 (m^2)	Zone 2 (m^2)	Zone 3 (m2)	P_{SA} (M^2)
Run 1	0.0561	9.5600	29.5596	47.3881	86.5
Run 2	0.0561	9.6534	29.2696	47.5772	86.5
Average					86.5
Run 1	0.1889	9.7793	30.7357	46.9106	87.4
Run 2	0.1889	10.0050	30.1222	48.6968	88.8
Average					88.1
Run 1	0.3194	10.0114	31.1550	47.1429	88.3
Run 2	0.3194	10.2646	30.4444	48.9851	89.7
Average					89
Run 1	0.3893	9.7448	30.3154	47.8592	87.9
Run 2	0.3893	9.7967	29.0102	47.6308	86.4
Average					87.15

APPENDIX D- NaOH INTERFACIAL AREA DATA

CONSTANTS USED:

Parameter	Symbol	Unit	Value
Solvent Temperature	T	K	303
Ionic Strength of NaOH	I_{NaOH}	mol/L	0.10
Log of Hydroxide Solubility at Infinite Dilution	$\log_{10} k^{\infty}_{OH^-}$	m^3/ kmol .s	4.03
Log of Solubiity Ratio	$\log_{10} [k_{OH^-}/k^{\infty}_{OH^-}]$	m^3/ kmol .s	0.022
Second Order Rate Constant	k_{OH^-}	m^3/ kmol .s	11364.59
Diffusivity of CO_2 in 0.1 N NaOH	$D_{CO2\text{-}NaOH}$	m^2/s	2.25E-09
Ionic Strength of Sodium Carbonate	I_{Na2CO3}	mol/L	0.30
Barrett Contributions to Henry's Constant	h_{Na^+}	L/mol	0.091
	h_{OH^-}	L/mol	0.066
	$h_{CO3^{2-}}$	L/mol	0.021
	h_{CO2}	L/mol	-0.021
Total Barrett Contributions to Ionic Strength	$\sum I_i h_i$	-	0.041
Log of Henry's Constant for CO_2-Water	$\log10\ H_{CO2,W\text{-}PM}$	kmol/m^3.bar	-1.53
Log of Henry's Constant for CO_2-0.1 N NaOH	$\log10\ H_{CO2,NaOH\text{-}PM}$	kmol/m^3.bar	-1.57
Henry's Constant for CO_2-0.1 N NaOH	$H_{CO2,NaOH\text{-}PM}$	kmol/m^3.bar	0.027
	$H_{CO2,NaOH}$	m3.atm/kmol	36.51
Liquid film MTC (chemical)	k_g'	kmol/m^2.s.atm	4.38391E-05

DATA:

Axial Height	L/G (lit/m^3)	Run #	G_{Total} (kmol/min)	$y_{CO2,in}$ (PPM)	$y_{CO2,out}$ (PPM)	N_{CO2} (kmol/sec)	ΔP_{lm} (atm)	$K_g a_e$ (sec)	a_e (m^2/m^3)
1.5252 (m)	2.3	1	0.01403	620	480	0.000002	0.00059	0.001161	26.51
		2	0.01408	600	470	0.000002	0.00058	0.001068	24.39
		Avg							25.45
	3.45	1	0.01408	600	430	0.000002	0.00056	0.087439	33.27
		2	0.01408	610	430	0.000003	0.00056	0.094847	36.09
		Avg							34.68
0.1778 (m)	2.3	1	0.01406	480	390	0.000001	0.00047	0.010646	138.89
		2	0.01406	460	390	0.000001	0.00046	0.010815	141.09
		Avg							139.9
	3.45	1	0.01401	460	360	0.000001	0.00044	0.016911	220.61
		2	0.01401	460	360	0.000001	0.00044	0.016198	211.31
		Avg							215.96

APPENDIX E- TOTAL ALKALINITY

Total Alkalinity Analysis Procedure:

1. Dispense 60 ml of DI water into a 100 ml beaker using a pipet aid.
2. Record the weight of the DI water and tare the scale.
3. Use a graduated syringe to transfer 0.5 ml of sample into the beaker
4. Record the weight of the sample.
5. Arrange the beaker on a stir plate and place a small stir bar in the solution.
    a. Set the stir plate to a reasonable setting as to not disturb the surface of the solution.
6. Suspend a pH probe into the solution, being careful not to contact the bulb with the stir bar or walls of the beaker.
    a. It is recommended to rinse the pH probe with DI water prior to starting the titration.
7. Use 0.1 M H_2SO_4 to titrate the solution using a graduated syringe.
    a. Record the initial pH of the solution.
    b. Add 0.5 ml H_2SO_4 and allow the solution to equilibrate.
    c. Record the pH.
    d. Repeat steps 7.b-7.c until a pH of ~2.8 is reached.
8. Plot the titration curve.

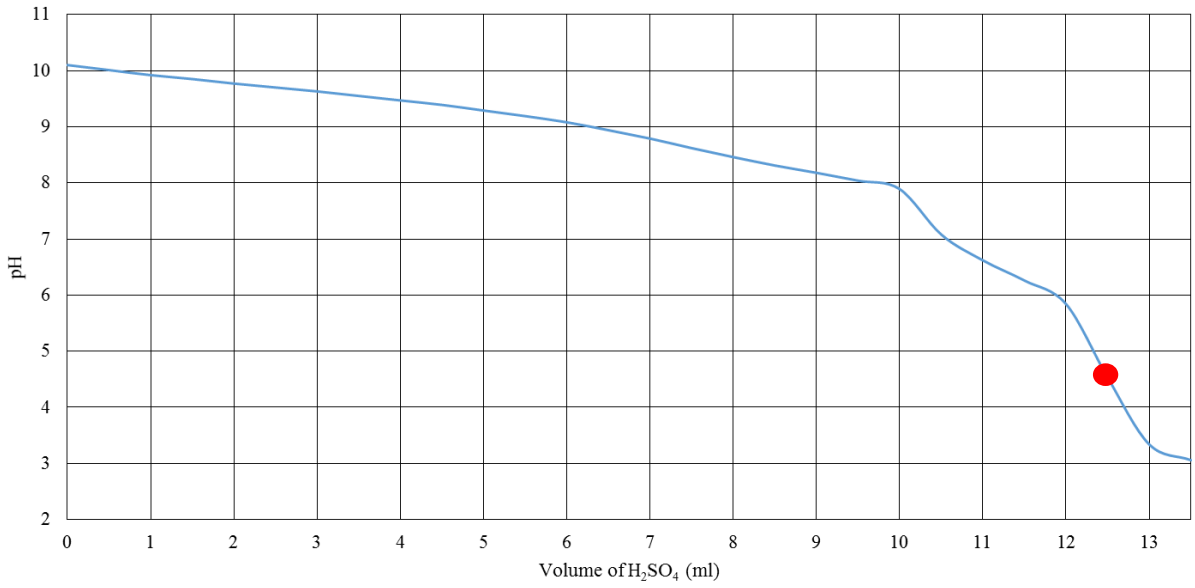

Example titration curve for unloaded 30 wt% MEA.

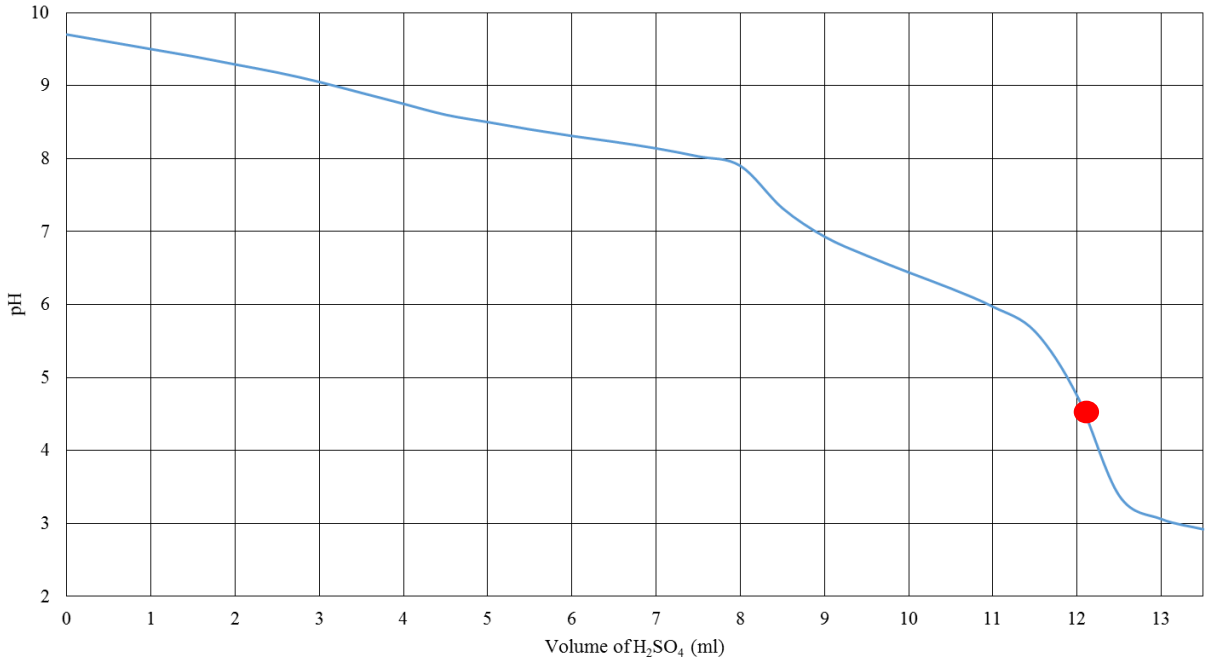

Example titration curve for loaded 30 wt% MEA.

Using the volume of H_2SO_4 found at the red dot in the figures above, the following equation can be used to calculate total alkalinity (TA) of a loaded and unloaded sample:

$$TA\left(\frac{mol}{kg-soln}\right)=\frac{H_2SO_4(ml)\cdot 0.2}{Sample\ (gm)}$$

APPENDIX F- TOTAL INORGANIC CARBON

TIC Preparation/MEA Dilution

1. Prepare a clean 25 ml volumetric flask
2. Record the weight and tare the flask on the scale.
3. Dispense 25 ml of DI water into the volumetric flask using a pipette aid.
4. Record the weight of the DI water on the scale.
5. Dispense 0.1 ml of sample into the flask using a graduated syringe.
6. Record the weight of the sample on the scale.
7. Use a stopper to seal the flask.

The following equation is used to determine the dilution factor for a sample:

$$F = \frac{m_{H_2O}}{m_{sample}}$$

8. Prepare the glass injection beds as shown in TIC section of the main document.
    a. Wash and dry each tube.
    b. For the first bed, use a septum to seal the glass-T.
    c. The second bed should remain empty except for the frit near the inlet side of the bed.
    d. Fill the third bed with magnesium perchlorate flakes by placing a small plug of glass wool near one end of the tube, inserting the crystals through the open end, and then plugging the open end of the tube with a small amount of glass wool.
    e. Attach all necessary tubing.
9. Open the nitrogen (N_2) cylinder and set the pressure regulator to no more than 40 psi into the injection beds.
10. Start the Horiba injection pump.
11. Open the needle valve on the Horiba to allow gas to flow through the unit at the flow rate marked on the middle of the Horiba's internal rotameter.
12. Inject 1 ml 30 wt% phosphoric acid (H_3PO_4) into the septum of the first injection bed using a clean graduated syringe.
13. Allow the CO_2 reading on the Horiba to reach zero before beginning sample analysis.
14. Prepare the data collection from the Horiba using PicoLog software.
    f. Open the PicoLog program on a computer linked to the Horiba output board.
    g. Save the data file.
    h. Press the "Graph" icon to open the time vs mV signal plot window.
    i. Press the "Record" icon to begin recording data. I
15. Inject a 0.1 ml diluted sample into the H_3PO_4 pool through the septum of the first injection bed using a clean graduated syringe.
    j. Draw 0.1 ml sample into the syringe and discard as waste twice before injecting the sample.
16. Allow the Horiba reading to peak and go back down to zero.
17. Repeat step 15 and 16 two more times for a total of 3 peaks recorded.
18. If the three peaks lie within < 2% error, press the "Stop Recording" icon and copy the plotted data curve to a spreadsheet.
19. Integrate the peak area under each curve using the trapezoid rule, shown below:

$$A = \sum_{i=1}^{n} a_i = \frac{h}{2}\sum_{i=1}^{n}(f_i + f_{i+1})$$

where n is total data point recorded, h is the length of the interval (1 sec.), and f_i is the voltage recorded at data point i. Calculate the average area for the three curves.

20. Compare the average area with the calibration curve to determine the ppm_v carbon contained in the diluted sample.
21. Use the following equation to convert ppm_v of carbon to mol CO_2/kg-soln:

$$n_{CO2}\left(\frac{mol\ CO_2}{kg - soln}\right) = \frac{ppm_v\ of\ carbon}{12.0107 \cdot 1000}$$

22. Use the following equation to determine the concentration of total CO_2 in the concentrated sample using the dilution factor of the concentrated sample:

$$n_{CO2}\left(\frac{mol\ CO_2}{kg - soln}\right) = n_{CO2} \cdot F$$

TIC Calibration procedure

1. Make 5 samples of varying concentration of Carbon Standard (Ricca Chemical; 1 mg = 1000 ppmv). Concentrations of 30, 50, 80, 100, and 150 ppmv of C.
2. Inject 1 ml of 30 wt% H3PO4 into the tee, start the N2 purge. Ensure that the rotameter on the ES-510 reads a minimum flowrate of 0.5 ml/min (recommended by Horiba).
3. Start Pico Log, specify the file name, and save the file in the appropriate folder.
4. Inject 0.1ml of diluted standard in triplicates into the acid bath through the septum. Thus, for 5 concentrations of standard C solution, 15 injections will be made.
5. Calculate the area under the curve for each individual injection using the Trapezoidal rule.
6. Plot a the Integrates area response against the ppmv of C injected as seen in the Figure below

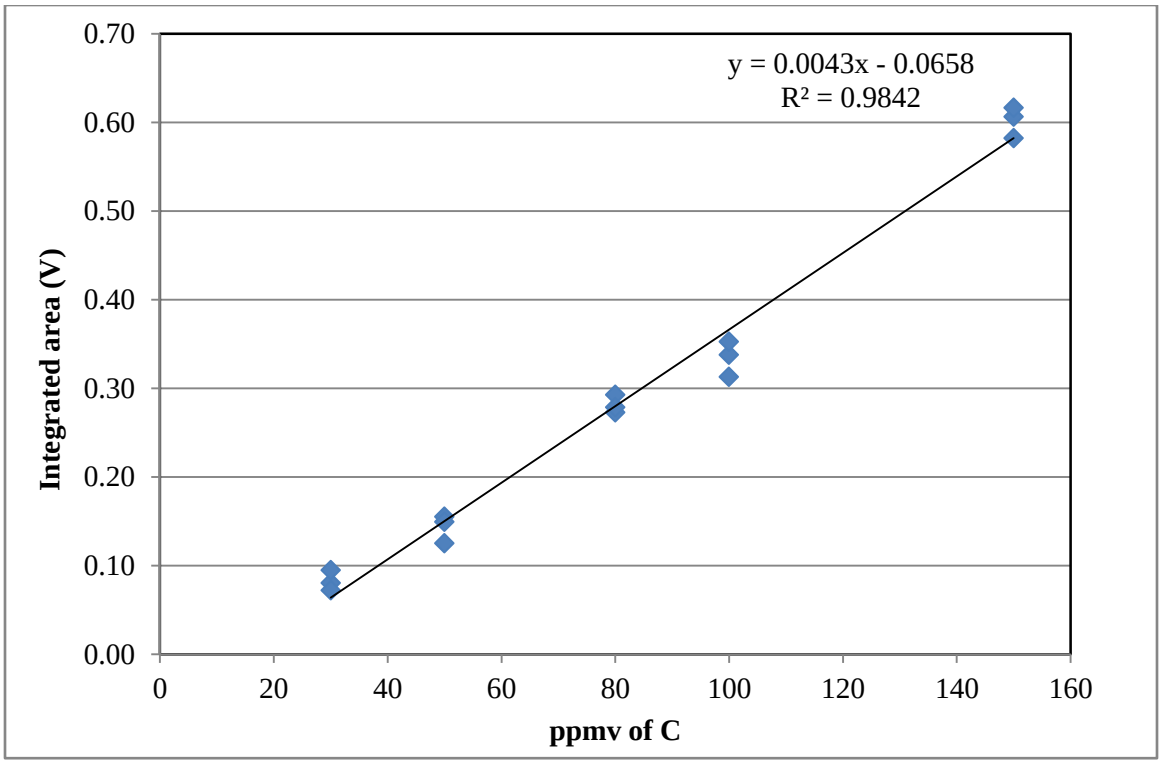

Typical Integrated area vs. ppmv of C curve

7. Use the above calibration curve to estimate the ppmv of C in the unknown sample to be analyzed.

APPENDIX G- EQUIPMENT STANDARD OPPERATING PROCEDURES

Blower- Atlantic Blowers AB800

General Notes

Blower On/Off:

- Blower is ready to use immediately after power is supplied to the system.
- Blower/control panel do not have power down setting; external (manual) on/off switch controls system power.
- Following a complete power off and power on procedure, the controller will retain the last frequency setting.
    - Once power is restored the frequency display will flash, indicating the frequency may be adjusted using the directional arrow buttons.

Important Precautions:

- **Always make sure column gas exit is clear;** prolonged blower dead-head can result in damage to glass column and/or blower.
- In order overcome water head pressure in scrubber, blower must reach 18 Hz to begin gas flow.
- Butterfly valve downstream of the blower should remain partially or fully open during blower operation.

Blower Start-Up/Operation with Scrubber Installed

Starting with system power off:

1. Flip the power supply breaker to the "ON" position (Frequency display will flash, indicating the frequency can be set without adjusting the current blower operation).
2. Use control panel to set initial blower frequency to **12.00 Hz** (blower with be at dead head until 18 Hz).
    1. Use left arrow button [<] to toggle between frequency digits (xx.xx) and the up/down arrows [^] [v] to set each digit to the desired frequency.
3. Press the red colored "Start/Stop" button to engage blower (Frequency will cease flashing, indicating current operating blower frequency).
4. Ramp up frequency to 18.00 Hz by increments of 3.00 Hz.
    1. Press left arrow button [<] to exit current operating frequency (frequency display will flash).
    2. Use up/down arrows [^] [v] to set desired frequency.
    3. Press red colored "Start/Stop" to set blower frequency to adjusted setting.
5. Once 18.00 Hz is reached allow 10 seconds for scrubber to purge liquid from scrubber pipes and bubbling action to equilibrate.
6. Once scrubber is bubbling, blower frequency can be lowered or raised to desired flow rate (lowest frequency is dependent on liquid level in scrubber; highest frequency is 60.00 Hz).
7. Allow 5 minutes for gas exiting blower to reach a peak temperature.

Blower Shut-Down

Starting from normal blower operation:

1. Press red colored "Start/Stop" button (blower will ramp down to 0 Hz and frequency display will flash).
2. Flip power supply breaker to "OFF" position (controller retains residual power for approximately 10 seconds until complete shut-down).

Brooks CO_2 Mass Flow Meter Controller

0254/SLA5853S; Controller/Mass Flow Meter

Flow Meter Specifications:

Full Scale (FS)=	25 scfm	(max flow rate measurable)
Flow Rate Repeatability =	2% of FS	(min flow rate measurable)
Required Supply Pressure =	50 psig	-
Outlet Pressure =	0 psig	-
I/O	4 – 20 mA	-

General Notes

Controller On/Off:

- Controller is ready to use immediately after system power is restored.
- Flow meter has zero flow when system is powered down.

Important Precautions:

- **Always make sure column gas exit is clear**; there should be no obstruction for gas to escape the column in order to avoid damage to the glass.
- Ball valve between gas manifold and flow meter should remain closed when flow meter is not in use.
    - Flow meter is not meant to be on/off control valve when powered on; Small amount of gas will continue to flow when SP = 0.0 flow rate.
- **NEVER** open ball valve between gas manifold and flow meter quickly (slug of gas can cause permanent damage to instrument).
    - Best practice is to barely open the valve in such a way that gas goes to the flow meter **as slowly as possible**.
    - Once the flow meter supply pressure is equalized to the gas manifold pressure, the valve can be fully opened (do not leave the valve in a throttling position).
- It is recommended to "ramp-up" the SP to "high" values
    - The flow meter is not programmed to ramp open; no ramping will result in a slug of gas through the flow meter which can cause damage to flow meter or system components.

Flow Meter Start-Up/Operation

Starting with system powered down:

1. Press "Start [Home]" to restore power.
2. Check manifold and gas supply.

1. Open all valves of selected cylinder bank to supply gas to the manifold.
2. Set supply pressure from gas manifold at ~50 psig with the pressure regulator that is inside the gas manifold.

3. Open valve between manifold and flow meter (see "Important Precautions" above).
    - Assure supply pressure stabilizes at 50 psig.
4. On controller screen:
    1. Press "SET POINT" (right arrow) button.
    2. Use up-down and right-left arrows to set the desired SP.
    3. Press "[ENTER] MENU" to send SP signal to flow meter.
    4. Press "SRART [HOME]" to return to home screen and view SP and PV flow rates.
    5. To change SP: press "SET POINT" (right arrow) button.
    6. Use up-down and right-left arrows to set the desired SP.
    7. Press "[ENTER] MENU" to send new SP signal to flow meter.

Flow Meter Shut-Down

Starting from normal flow meter operation:

1. From home screen:
    1. Press "Set Point" (left arrow) button.
    2. Use up-down and left-right arrows to specify SP to 0.0 flow rate.
    3. Press "[ENTER] MENU" to send SP signal to controller.
2. Close all cylinder valves of selected bank.
3. Wait for supply pressure to the flow meter to reach 0 psig and then disengage pressure regulator (supply pressure = 0 psig).
4. Close the valve between gas manifold and flow meter.
5. Press and hold "Stop [VOR]" to power down the system.

Flow Meter Emergency Shut-Down

- In case of emergency **TURN OFF** device by holding "STOP [VOR]" button for 3 seconds.
    - The previous set point value will be maintained when the controller is power on.
- *Alternative* Valve Over Ride (VOR) close
    - Press "Stop [VOR]" button once.
    - Use the up-down arrows to set the "Valve Over Ride" from "NORMAL" to "**CLOSED**."
    - The valve will be fully closed (absolutely zero flow) and the SP has no I/O control.
    - VOR must be set to "NORMAL" to give specified SP value control.

Gas Chromatograph

Operation

1. Ensure that the Helium supply to the GC is on continuously and the GC power switch is on.
2. Open EZ IQ and EZ Reporter software on the computer.
3. The GC should be in the standby mode when not in operation.

4. Click on “File”, “Methods”, “Open”, “OSU Quant.”
5. Click on “Control” in the main tab, and then “Download Method.”
6. The GC columns will start heating up to the set temperatures for measurements. This can be seen on the GC status window. When the GC columns are heated to the appropriate temperatures, the yellow window saying “Not Ready” will turn green saying “Ready.” This process will take roughly 20-30 minutes. The GC is now ready for measurement.
7. Start the vacuum pump connecting the spray column gas connections to the GC via the knockout condenser and the desiccant tubes.
8. Click on “Single Run” (play button icon), select input vial number as 2 (or another input connection desired), and injection volume of 3µl (3 minutes).
9. The GC will start taking the reading after 3 minutes of sample gas injection. The GC pump will come on (noticeable noise), and after pulling the sample in, the GC will start analyzing the gas composition.
10. After completion of the analysis, the EZ Reporter window pops up with the number values for the gas composition. Look up the raw value of CO_2 (and not the normalized value).

Calibration

1. Connect the calibration bottle to the GC directly.
2. Run the sample through the GC as an unknown sample following the procedure outlined above.
3. After the run gets completed, click on “Single Level Calibration” from the Analysis tab.
4. Select the corresponding run name of the unknown sample in step 2. Check the box next to “Calibrate Single Level.” Input level 1 in the box and click calibrate.
5. Calibrated values will be displayed in the EZ Reporter window.

APPENDIX H – VENDOR LIST

Company	Equipment Procured	Contact Person	Contact Email	Contact Phone
Allied Products Co.	S.S. Tanks	*Pat Pajerski*	ppajerski@alloyproductscorp.com	262-832-8432
Alloy and Stainless	Large piping	Rob Shepherd	rob.shepherd@alloyandstanless.net	405-942-0601
Artium	PDI system	Chad Sipperley	csipperley@artium.com	772-214-4888
Atlantic	Blower	Sam Laidler	sam@atlanticblowers.com	214-233-0280
Bete	Nozzles	Don Helfers	donhh@donhelfers.com	636-458-3013
Brooks Instruments	CO2 flow meter	Gary Heyer	gary.heyer@brooksinstrument.com	215-362-3792
Custom Machining	Misc.	Mike Lucas	mike.lucas@okstate.edu	405-744-5820
EHS (OkState)	Waste removal	Justin Eubanks	jeeuban@okstate.edu	405-744-3028
Emerson-Rosemont	Vortex meter	Cole Bowen	cole.bowen@emerson.com	405 550 3921
Harris Products Group	Gas Manifold	David Gailey	david_gailey@lincolnelectric.com	678-928-3801
H.S. Martin	Column Glass + piping	Jack Kontes	jack.kontes@hsmartin.com	856-692-8700
Horiba	TIC VIA-510	Atsushi Yamamoto	atsushi.yamamoto@horiba.com	281-482-4334
Inficon	Micro GC	Debbie Hutt	debbie.hutt@inficon.com	(315) 657-5205
Jim Finley	Custom Glass	Jim Finley	jfinley@glassworks.com	918-335-9775
Laser Safety (OkState)	Laser Inspection	Brandi Simmons	brandi.simmons@okstate.edu	405-744-3474
Lechler	Nozzles	Roderick Hamblen	roderickhamblen@lechlerusa.com	1 630 845 6827
Pegasus	Column Glass	Jessica Hare	jhare@pegasus-glass.com	519.620.7991 ext.34
Spraying Systems	Nozzles	Kyle Bade Darrell Sympson	kyle.bade@spray.com darrell.simpson@spray.com	630-517-1231 630-517-1934
Stillwater Steel	Gas Cylinders	Jessie	-	405-377-5550
Swagelok	Small piping	David Flournoy Ruben Martinez	david.flournoy@swagelok.com ruben.martinez@swagelok.com	405-833-6706 918-258-8661
VWR	Lab Supplies Chemicals	Jessica Boyd	jessica_boyd@vwr.com	918-729-6274
Air Liquide	Calibration gas	David Crofoot	david.crofoot@airliquide.com	(713) 624-8000

VITA

Yash Sharadchandra Tamhankar

Candidate for the Degree of

Doctor of Philosophy

Thesis: DYNAMIC ASPECTS OF SPRAYS FOR ABSORPTION APPLICATIONS

Major Field: Chemical Engineering

Biographical:

Personal:
Born in Pune, India to Sharadchandra Tamhankar and Ketaki Tamhankar on August 7, 1984.
Accepted a full time position with Phillips 66 in Bartlesville, Oklahoma beginning February 16, 2015.

Education:
Completed the requirements for the Doctor of Philosophy in Chemical Engineering at Oklahoma State University, Stillwater, Oklahoma in May, 2015.

Completed the requirements for the Master of Science in Chemical Engineering at Oklahoma State University, Stillwater, Oklahoma in December, 2010.

Completed the requirements for the Bachelor of Engineering in Chemical Engineering at University of Pune, Pune, Maharashtra, India in May, 2006.

Experience:
Research Assistant, School of Chemical Engineering, Oklahoma State University, Stillwater, Oklahoma: January 2011 – February 2015

Teaching Assistant, School of Chemical Engineering, Oklahoma State University, Stillwater, Oklahoma: August 2008 – May 2010

Commissioning Engineer, Praj Industries Ltd., Pune, Maharashtra, India: November 2006 – July 2008

Professional Memberships:
American Institute of Chemical Engineers (AIChE), Institute of Liquid Atomization and Spray Systems (ILASS), International Society of Automation (ISA)

Honor Societies:
Phi Kappa Phi, Golden Key, Omega Chi Epsilon